AN ANALOGUE MODEL STUDY OF ELECTROMAGNETIC INDUCTION IN THE NEWFOUNDLAND REGION

by

DAVID LAWRENCE HEBERT
B. Sc., Dalhousie University, 1980

A THESIS SUBMITTED IN PARTIAL FULFILLMENT

OF THE REQUIREMENTS FOR THE DEGREE OF

MASTER OF SCIENCE

in the Department
of
Physics

We accept this thesis as conforming to the reguired standard

(H. W. Dosso) (J. T. Weaver)

(R. E. Horita) (P. van den Driessche)

(G. R. Branton)

UNIVERSITY OF VICTORIA

AUGUST, 1982

Supervisor: Dr. H. W. Dosso

ABSTRACT

In this thesis, electromagnetic induction in the Newfoundland region was studied using scaled laboratory analogue model and field station measurements. Contour diagrams of the in-phase and quadrature-phase parts of the model magnetic field are used to show the field response to the bathymetry and complex coastlines in this region.

The results indicate a large enhancement in the magnetic field occurs over the straits. This is due to the induced current being restricted to the strait. The maximum anomalous magnetic field produced at the straits, found in analogue and numerical results, occurs when the depth of the strait is approximately 0.14 skin-depths. Magnetic field measurements show the deflection of induced current around capes which results in a large horizontal field seaward of the cape and a large vertical field at the cape coastline. An anomalous magnetic field is observed over the continental shelf edge for long periods, such as 900s; but not for short periods such as 100s.

Comparison of single station and inter-station induction arrows shows that the difference between the two types of arrows occurs when an anomalous horizontal field is present. Over the ocean and at the coastlines, the single station in-

phase arrows are smaller than the inter-station in-phase arrows, while just inland the single station in-phase arrows are larger than the inter-station in-phase arrows. The in-phase arrows point towards the nearest and largest current density. The quadrature arrows reverse direction at the coastline for short periods, but this reversal is not evident for long periods.

The model and field results differ considerably in the central region of Newfoundland. In this region, difference arrows, obtained by vector subtraction of model arrows from field arrows, point towards the major faults in the region. Model and field results also lead to the hypothesis of a horizontal conductivity contrast at depth in the central Newfoundland region.

[redacted]

H. W. Dosso J. T. Weaver

[redacted]

R. E. Horita P. van den Driessche

[redacted]

G. R. Branton

TABLE OF CONTENTS

page

page

LIST OF FIGURES

page

page

page

page

page

page

LIST OF TABLES

ACKNOWLEDGEMENTS

I wish to thank Dr. H.W. Dosso for the support and encouragement he has supplied throughout my research work. Also many useful and stimulating discussions with Dr. Dosso have been a source of guidance.

I like to thank Dr. J.A. Wright for his hospitality during my stay at Memorial University of Newfoundland. The many field station results supplied by Dr. Wright are also greatly appreciated.

I would like to thank Dr. W. Nienaber, Dr. J.T. Weaver, and Mr. G. Heard for many useful discussions. I would like to thank Mr. L. Friesen for assistance in using the finite-difference computer program of Brewitt-Taylor and Weaver.

I wish to acknowledge financial support from N.S.E.R.C. in the form of a postgraduate scholarship.

CHAPTER 1

INTRODUCTION

1.1 Electromagnetic Induction in the Earth

The study of time-varying magnetic fields at the surface of the earth continues to be of interest to geophysicists. The time-varying geomagnetic field at the surface consists of an external inducing field and a field due to induced earth currents. The external inducing field is due to ionospheric and magnetospheric current systems which result from the interaction of the solar wind with the earth's magnetosphere. The inducing field is composed of geomagnetic variations with periods from a fraction of a second to several days. According to Faraday's law of induction, the external field induces currents in the earth which produce a secondary time-varying electromagnetic field at the surface of the earth.

The observed electric and magnetic field variations at the surface of the earth depend upon the distribution of electric conductivity within the earth and the nature of the

inducing field. The period of the inducing field is of interest since the depth of penetration of the inducing field (skin-depth) is a function of the period of the inducing field. Thus electromagnetic induction allows probing of the earth's conductivity structure. Numerous attempts have been made to infer the complex conductivity structure of the earth from analysis of observed field variations on the surface. Electromagnetic induction studies of the earth can be divided into two major groups (Price, 1964): global studies, concerning the nature of the earth as a whole, and local studies, concerning the distribution of the electrical conductivity in the earth near the surface.

1.2 Global Induction Studies

In global induction studies, the electrical conductivity, σ, is often treated as a function of spherical polar coordinates (r, θ, φ). The induction problem then can be solved in terms of spherical harmonics giving the external and internal current sources.

Early global induction studies consisted of finding the lower order spherical harmonic terms for regular long period variations. Schuster(1889) separated the diurnal varying magnetic field into its components of internal and external origin. Chapman(1919) studied the diurnal and lunar

variations by spherical harmonic analysis. Chapman and Whitehead(1922) and Lahiri and Price(1939) calculated the inductive response of a sphere with σ as a function of only r, the distance from the centre of the sphere, and compared their results to the magnetic field observed at the surface of the earth.

Rikitake(1973) shows modern modelled results of the earth's conductivity as a function of the radial distance r. It may be reasonable to assume that within the interior of the earth, that the conductivity is mainly a function of r but in the earth's crust, the conductivity is also a function θ and φ. For example, the conductivity of the ocean is several orders of magnitude greater than that of the land massses. thus the effect of tne ocean must be included. Recent work of Fainbeg and Zinger(1981) has attacked the problem of global induction with a real near-surface conductivity distribution.

1.3 Local Induction Studies

Local induction studies are concerned with regions of the earth where the curvature of the earth can be neglected. The size of the region depends on the extent and period of the inducing field. In these studies, the earth can be represented by a semi-infinite half-space with some variable conductivity distribution. The conductivity distribution may

be one-dimensional (i.e. a function of depth only) or two- or three-dimensional.

Local induction problems have been studied by many methods. Weaver(1963) has solved analytically the problem of induction in two-quarter spaces with different conductivities. Induction in layered half-spaces with different source fields have also been solved analytically (eg. Price, 1950; Weaver, 1973). More complicated models are very difficult to solve analytically.

Numerical methods have also played an important role in studying local induction problems. Finite difference methods, calculating the magnetic or electric field over a grid of mesh points, have been developed by many authors (eg. Lines and Jones, 1973; Weidelt, 1975; Brewitt-Taylor and Weaver, 1976; Hermance, 1982). Zhdanov et al.(1982) give an excellent review of finite difference methods. Another numerical method used in induction problems uses thin sheets. Highly conductive layers are replaced by a single infinitesimally thin layer having an associated conductance. The induction problem is solved by treating the thin layers as currents sheets. Only simple two- and three-dimensional problems have been solved to date (Green and Weaver, 1978; Weaver, 1978; Weaver, 1979; Fischer, 1979; Dawson et al., 1979).

Since analytical and numerical methods are limited for solving complex three-dimensional structures, analogue models are often used. The magnetic and electric fields of simple three-dimensional analogue models such as cylinders (Ramaswamy and Dosso, 1977) and spheres (Ogunade et al., 1974; Ogunade and Dosso, 1977) have been studied. Induction in simple island-continent problems has been studied by Nienaber et al.(1976, 1977a, 1977b). Chan et al.(1981) studied electromagnetic induction for capes and bays using analogue models.

These simple models can serve as an aid in interpreting field results in areas such as the Rhinegraben (Babour and Mosnier, 1979; Dupis and Thera, 1982) and the Pyrenees (Babour et al., 1976). Such simple models cannot successfully represent some regions studied such as the British Isles (Edwards et al., 1971), Australia (Parkinson, 1959, 1964; Everett and Hyndman, 1967a, 1967b) and Japan (Rikitaki and Honkura, 1973). Due to the complexity of these regions and others, analogue models representing the known conductivity structure are often constructed to aid in determining the total conductivity structure of the region. An example of this is to use the analogue model in determining the well-known coast effect of the region. Then the field and model results can be used to determine the underlying conductivity structure not modelled. Analogue

models of regions such as Japan (Roden, 1963), Iceland (Hermance, 1968), Vancouver Island (Nienaber et al., 1979), the British Isles (Dosso et al., 1980a), the east coast of North America (Dosso et al., 1980b) and the Queen Charlotte Islands (Chan et al., 1981) have been used in studying the coast effect at these regions.

1.4 Electromagnetic Induction in Eastern Canada

Many electromagnetic induction studies have been carried out in eastern Canada. Srivastava(1971) and Srivastava and White(1971) have studied the time-varying magnetic field over an area from central New Brunswick through Nova Scotia to the continental shelf edge. Srivastava and Folinsbee(1975) examined the total field measured on a buoy off Nova Scotia at the continental shelf edge and compared the results to data measured in Dartmouth, Nova Scotia.

Extensive magnetotelluric measurements over eastern Canada were made by Hyndman and Cochrane(1971) and Bailey et al.(1974). Further analysis of the measurements to determine the conductivity structure of the region was made by Cochrane and Hyndman(1974) and Kurtz and Garland(1976). A review of some of the results for eastern North America is given by Greenhouse and Bailey(1981). An analogue model of the eastern coastal region of North America constructed by Dosso

et al.(1980b) was used to study the coast effect in this region.

There is geological evidence in the Newfoundland region suggesting that an ancient plate boundary could be present in this region (Church and Stevens, 1971; Dewey and Bird, 1971; Karson and Dewey, 1978; McKerrow and Cocks, 1978). Law and Riddihough(1971) have suggested that geomagnetic anomalies in stable tectonic areas are associated with geological boundaries marking ancient plate margins. Geomagnetic sounding in Newfoundland (Cochrane and Wright, 1977; Wright and Cochrane, 1980) was used in an attempt to determine whether an ancient plate margin exists in the region. Geomagnetic anomalies due to the sea-land conductivity contrast in the Newfoundland region could conceal any anomalies due to plate margins therefore an analogue model of the Newfoundland region was constructed to determined the scope of the coast effect. The model results serve as an aid in interpreting field results in this area.

1.5 Summary of the Work Covered in this Thesis

In this thesis electromagnetic induction, in the period range 100s to 1800s, in the Newfoundland region is studied using scaled analogue model measurements and field station measurements. The behavior of the magnetic field over the analogue model is studied for geomagnetic variations with

simulated periods of 100s, 300s, 900s, and 1800s and two perpendicular orientations of a uniform horizontal inducing source field, with the electric field of the inducing field i) roughly parallel to the continental shelf south of Nova Scotia and ii) roughly parallel to the Labrador Sea-mainland coastline.

The behavior of the magnetic field at straits, capes, and the continental shelf edge is discussed. Contour diagrams of the in-phase and quadrature-phase parts of the three magnetic field components for both polarizations are used to show the responses of these geographic features. The frequency dependence of the magnetic field at these regions is also discussed.

Detailed inter-station and single station induction arrows were calculated for the model magnetic field measurements. Comparison of these two types of induction arrows are discussed. The frequency dependence of model single station induction arrows are also investigated.

Results from fifteen field stations located in the Newfoundland region are compared to model results for the same geographic area. An attempt is made to explain differences between field and model results in relationship to geological structures in the region.

CHAPTER 2

MAXWELL'S EQUATIONS

Maxwell's equations are used to describe all classical electromagnetic phenomena. Two aspects of these equations discussed in this chapter will be electromagnetic induction for geophysical problems and electromagnetic scaling. For this work, the magnetic flux density ($\underline{B}$) will be referred to as the magnetic field and the electric field strength ($\underline{E}$), the electric field.

2.1 Electromagnetic Induction

Electromagnetic induction is a specific case of Maxwell's equations. Maxwell's equations, in Système Internationale, are

$$\nabla \times \underline{E} = -\frac{\partial \underline{B}}{\partial t} \qquad (2.1.1)$$

$$\nabla \times \underline{B} = \mu\epsilon\frac{\partial \underline{E}}{\partial t} + \mu \underline{J} \qquad (2.1.2)$$

$$\nabla \cdot \underline{E} = \rho/\epsilon \qquad (2.1.3)$$

$$\nabla \cdot \underline{B} = 0 \qquad (2.1.4)$$

Ohm's law gives the relationship

$$\underline{J} = \sigma \underline{E} \quad , \tag{2.1.5}$$

and the equation of continuity is

$$\nabla \cdot \underline{J} = -\frac{\partial \rho}{\partial t} \tag{2.1.6}$$

Taking the divergence of (2.1.2) and using (2.1.5), we obtain

$$\sigma (\nabla \cdot \underline{E}) + \epsilon \nabla \cdot \left(\frac{\partial \underline{E}}{\partial t} \right) = 0 \tag{2.1.7}$$

Using (2.1.3), (2.1.7) can be rewritten as

$$\frac{\sigma \rho}{\epsilon} + \frac{\partial \rho}{\partial t} = 0 \tag{2.1.8}$$

The solution to (2.1.8) is

$$\rho = \rho_o \, e^{-(\sigma/\epsilon)t} \quad . \tag{2.1.9}$$

This equation shows that any initial volume charge distribution (ρ_o) in a conductor will disperse at a rate which does not depend on the electromagnetic field. Inside a uniform conductor the volume charge can be neglected if the relaxation time constant satisfies the condition

$$\sigma/\epsilon \gg 1 \quad . \tag{2.1.10}$$

This condition is satisfied for geophysical problems ($\sigma/\epsilon \approx 10^{11}$/s). Therefore (2.1.3) can be replaced by

$$\nabla \cdot \underline{E} = 0 \quad . \tag{2.1.11}$$

If the electric and magnetic fields are sinusoidal with time ($e^{-i\omega t}$), which is the case for the model fields, then

$$\frac{\partial \underline{E}}{\partial t} = -i\omega \underline{E} \tag{2.1.12}$$

and

$$\frac{\partial \underline{B}}{\partial t} = -i\omega \underline{B} \tag{2.1.13}$$

Using (2.1.5) and (2.1.12), (2.1.2) can be rewitten as

$$\nabla \times \underline{B} = \mu(-i\omega\epsilon + \sigma) \underline{E} \quad . \tag{2.1.14}$$

Taking the curl of (2.1.1) and using (2.1.11) and (2.1.13)

$$\nabla^2 \underline{E} = -i\omega \nabla \times \underline{B} \quad . \tag{2.1.15}$$

Substituting (2.1.14) into (2.1.15)

$$\nabla^2 \underline{E} = -\mu\omega (\omega\epsilon + i\sigma) \underline{E} \quad . \tag{2.1.16}$$

Similarly, for the magnetic field

$$\nabla^2 \underline{B} = -\mu\omega (\omega\epsilon + i\sigma) \underline{B} \quad . \tag{2.1.17}$$

For geophysical problems, the permittivity of rock is $\epsilon/\epsilon_o \approx 9$ and for water, $\epsilon/\epsilon_o \approx 81$ (Grant and West,1965). Since the conductivity for rocks is of the order of 10^{-5}S/m and the highest frequency studied in this work is .01Hz, then

$$\omega\epsilon \ll \sigma \quad . \tag{2.1.18}$$

Therefore (2.1.16) and (2.1.17) can be written as

$$\nabla^2 \underline{E} = -i\omega\mu\sigma \underline{E} \tag{2.1.19}$$

and

$$\nabla^2 \underline{B} = -i\omega\mu\sigma \underline{B} \quad . \tag{2.1.20}$$

These equations are the ones used in solving for the electromagnetic fields in conductors for geophysical induction problems.

2.2 Electromagnetic Scaling

Since Maxwell's equations are linear differential equations, linear transformations of parameters can be applied. For electromagnetic scaling, the parameters are multiplied by a scale factor and certain relationships arise for these scale factors. The analogue model parameters are scaled values of their geophysical counterparts. For completeness, the scaling relationships are derived directly from Maxwell's equations. Two of Maxwell's equations (for geophysical induction problems) for the geophysical system

are

$$\nabla_g \times \underline{E}_g = i\omega_g \underline{B}_g \quad , \qquad (2.2.1)$$

$$\nabla_g \times \underline{B}_g = \mu_g \sigma_g \underline{E}_g \quad , \qquad (2.2.2)$$

and in the analogue model system are

$$\nabla_m \times \underline{E}_m = i\omega_m \underline{B}_m \quad , \qquad (2.2.3)$$

$$\nabla_m \times \underline{B}_m = \mu_m \sigma_m \underline{E}_m \quad . \qquad (2.2.3)$$

The subscripts g and m are used to denote the geophysical and model parameters, respectively. The other two Maxwell's equations contribute no more information on the transformations.

The parameters for the two systems are related by

$$\underline{E}_g = K_E \underline{E}_m \quad , \qquad (2.2.5)$$

$$\underline{B}_g = K_B \underline{B}_m \quad , \qquad (2.2.6)$$

$$\nabla_g = (1/K_L) \nabla_m \quad , \quad L_g = K_L L_m \quad , \qquad (2.2.7)$$

$$\omega_g = K_f \omega_m \quad , \quad f_g = K_f f_m \quad , \qquad (2.2.8)$$

$$\sigma_g = K_\sigma \sigma_m \quad , \qquad (2.2.9)$$

$$\mu_g = K_\mu \mu_m \quad , \qquad (2.2.10)$$

where K_E, K_B, K_L, K_f, K_σ, and K_μ are the scale factors for the electric field, magnetic field, length, frequency, conductivity, and permeability, respectively.

Substituting equations (2.2.5) to (2.2.10) into (2.2.1)

and (2.2.2), we obtain

$$\frac{K_E}{K_L}(\nabla_m \times \underline{E}_m) = K_f K_B (i\omega_m \underline{B}_m) \qquad (2.2.11)$$

$$\frac{K_B}{K_L}(\nabla_m \times \underline{B}_m) = K_\mu K_\sigma K_E (\mu_m \sigma_m \underline{E}_m) \qquad (2.2.12)$$

For (2.2.11) and (2.2.12) to be equivalent to (2.2.3) and (2.2.4), respectively, the relationships

$$\frac{K_E}{K_L K_f K_B} = 1 \qquad (2.2.13)$$

and

$$\frac{K_B}{K_L K_\mu K_\sigma K_E} = 1 \qquad (2.2.14)$$

must be satisfied.

For the two cases, geophysical and model, the permeabilities of the media are approximately the permeability of vacuum, therefore, $K_\mu = 1$. Equations (2.2.13) and (2.2.14) show that separately scaling the electric and magnetic fields is not necessary but their ratio must be scaled. Let k represent the impedance scale factor (K_E/K_B). Rewriting (2.2.13) and (2.2.14) using (2.2.7), (2.2.8), and (2.2.9),

$$\left(\frac{L_g}{L_m}\right)\left(\frac{f_g}{f_m}\right) = k = \left(\frac{L_m}{L_g}\right)\left(\frac{\sigma_m}{\sigma_g}\right) \qquad (2.2.15)$$

or

$$\left(\frac{L_g}{L_m}\right)^2\left(\frac{f_g}{f_m}\right)\left(\frac{\sigma_g}{\sigma_m}\right) = 1 \qquad (2.2.16)$$

must be satisfied for the analogue model to represent the geophysical problem. Maxwell's equations in non-dimensional form allow laboratory analogue models to be used to represent geophysical electromagnetic problems.

CHAPTER 3

LABORATORY ANALOGUE MODEL

The laboratory analogue model facilty in this work is used as an aid in studying the effects on electromagnetic induction by coastlines and bathymetry. An electromagnetically scaled model of a geographical area of interest is placed in a uniform horizontal inducing electromagnetic field. Electric and magnetic fields are measured over the surface of the model.

3.1 Apparatus Description

The analogue model facility used in this study is similar to that described by Dosso(1973) and Nienaber et al.(1976). It includes a plywood tank 2.44m by 1.68m and .76m deep filled to a height of .63m with a concentrated salt (NaCl) solution (Fig. 3.1.1). To minimize the effect of the concrete floor beneath the tank, the bottom of the tank is lined with a 5cm thick layer of graphite. A moderately uniform horizontal inducing field is provided by geometrically parallel line currents connected electrically

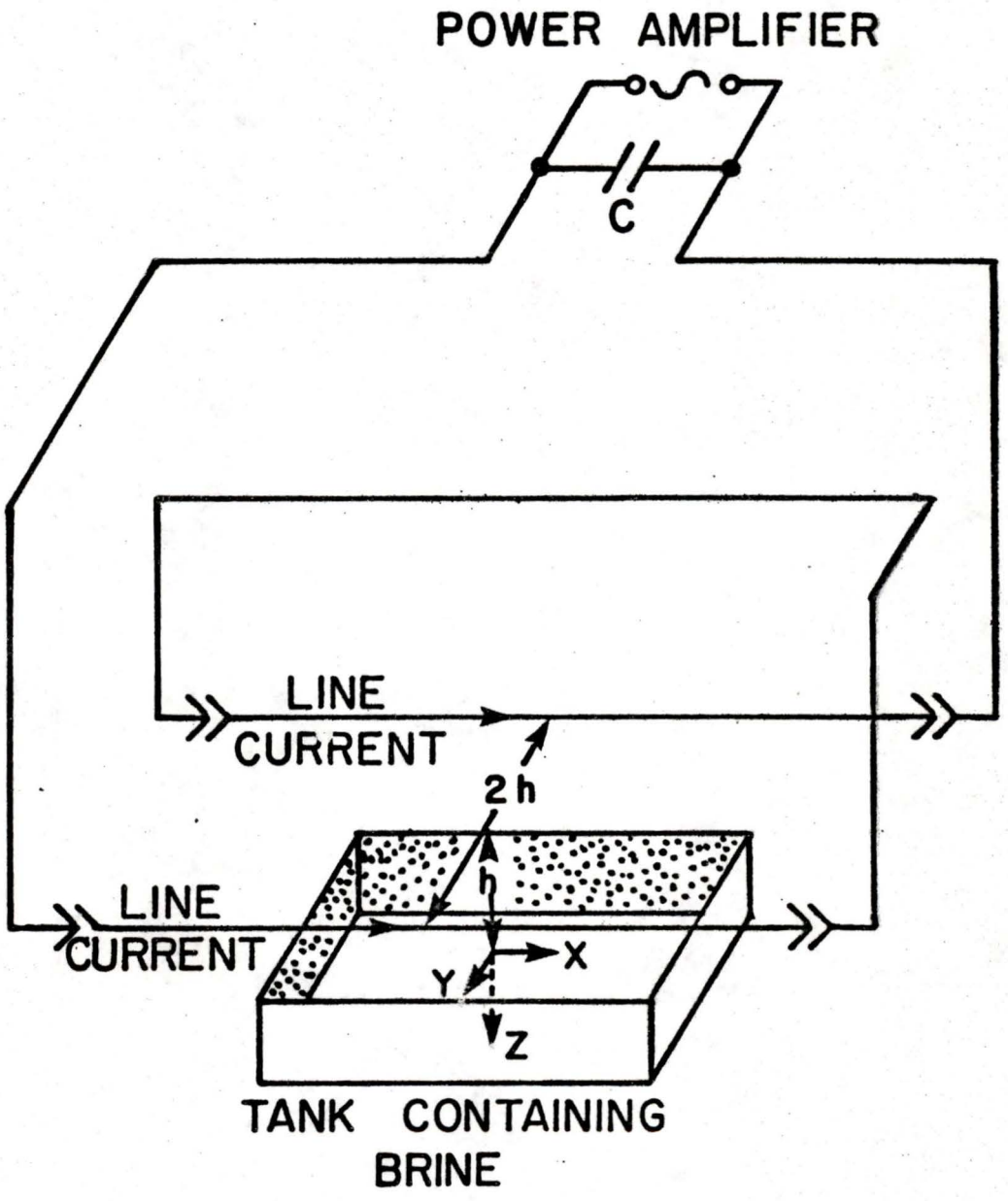

FIGURE 3.1.1 The laboratory analogue model facility

in series located 1.2m (h in Fig. 3.1.1) above the tank and separated by 2.4m. Connecting the line currents in series ensures the same field strength from both line currents. The line currents are supplied by a 1000W Savage power amplifier (for frequencies 8.33kHz and 16.67kHz) and a 150W McIntosh power amplifier (for frequencies of 50kHz and 150kHz). A variable capacitor connected in parallel with the amplifier is used to tune the circuit for resonance. The current is monitored to ensure a stable source field. The two walls of the tank perpendicular to the inducing electric field are lined with stainless steel plates. These two plates are connected by a heavy copper wire outside the tank. This allows electrical currents induced in the brine to flow parallel to the inducing electric field right to the ends of the tank reducing the end effects due to the finite size of the tank.

The two magnetic field detectors, for the horizontal and vertical field components, are similar in design. The detectors are 1mm long air core coils with 250 turns of #42 wire. The inside diameter of the coils is 2.35mm and the outside diameter, 6.35mm. The coils are encased in lucite tubes. The coil centre of the horizontal field probe is 3.8mm from the end of the lucite tube while the coil centre of the vertical field probe is located 1mm from the end of the lucite tube. While making measurements these probes are

placed just above the surface of the brine in the tank.

The horizontal electric field probe consists of three equally spaced electrodes in a straight line with the two outer electrodes separated by 1.48cm. The electrodes protrude through the sealed end of the lucite tube to make contact with the salt solution. The probe is designed to measure the average electric field between the two outer electrodes.

To measure a particular field component the appropriate probe is placed in the motor driven carriage which moves on a horizontal beam over the tank. The signal from the probe is fed through a differential amplifier to analyzing and recording equipment shown in Fig. 3.1.2. The lock-in analyzer compares the probe signal with a reference signal and produces a voltage proportional to the in phase and quadrature phase parts of the probe signal. These data are digitized and recorded on floppy disks by the IMS 8000 microcomputer for later analysis on the University of Victoria's main frame computer.

3.2 Analogue Model Description

The analogue model in this work is used in studying the electromagnetic effect of coastlines for induction in the earth. The region of interest is the area surrounding

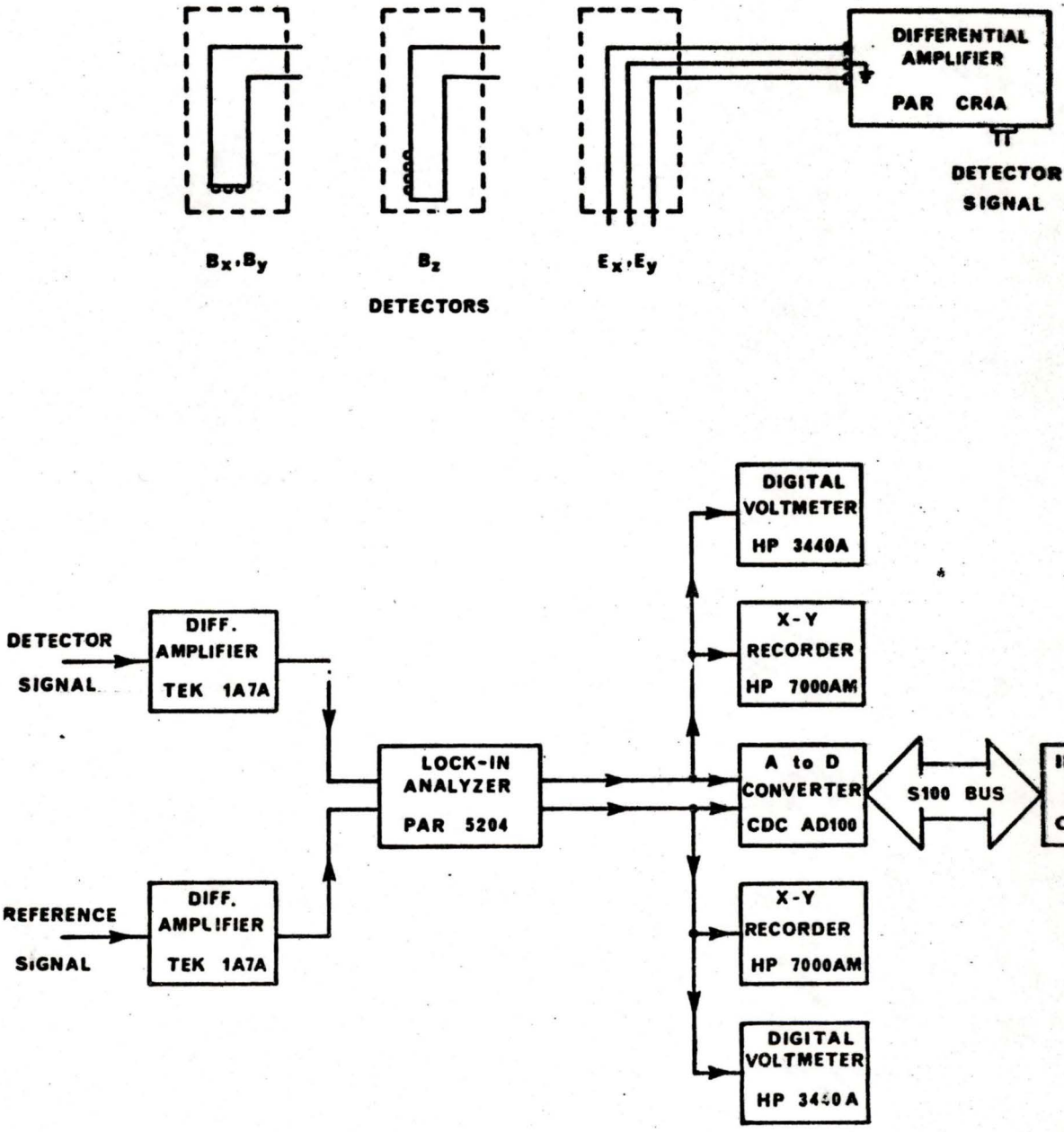

FIGURE 3.1.2 Magnetic and electric field detectors and analyzing and recording equipment

Newfoundland, an island on the east coast of Canada (Fig. 3.2.1). This map was composed from maps 801, 802, and 803 of the Geoscience map series (Canadian Hydrographic Service) with only coastlines and selected bathymetric contours traced. For the construction of this analogue model the coastlines and bathymetry were simplified and shown in Fig. 3.2.2. The coordinate system used is the standard geophysical system, a right-handed coordinate system with z downwards. The orientation of the coordinates on the map is the same as for the analogue model work of Dosso et al.(1980b) for the eastern coastal region of North America. This allows comparisons between the results of the two models without requiring coordinate transformations.

The electromagnetic scaling relationships derived in Section 2.2 show the conditions on the choice of scale factors. The size of the area of interest and the size of the tank facility determine the length scale factor. For this work, $K_L = L_g/L_m = 10^6$. The choice of model materials determines the conductivity scale factor. The use of brine to represent land, and graphite to represent ocean and sediment gives a scale factor $K_\sigma = \sigma_g/\sigma_m = 1.5\text{x}10^5$. From these two scale factors, the frequency scale factor is determined using eq. (2.2.16), giving $K_f = f_g/f_m = 1/(1.5\text{x}10^7)$. The impedance scale factor becomes $k = 1/15$. Figure 3.2.3 shows the relation between the different

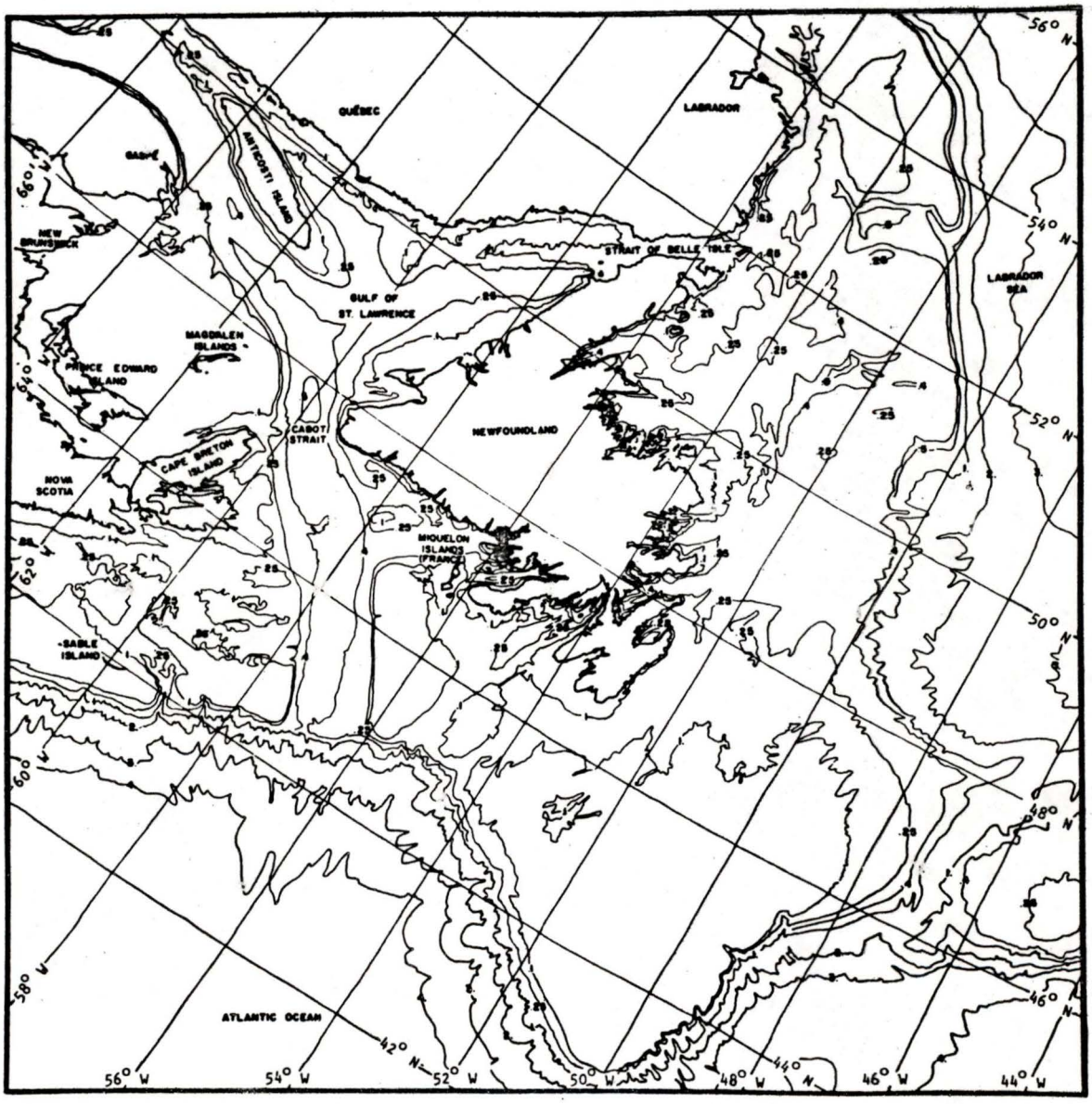

FIGURE 3.2.1 Map of Newfoundland region with coastlines and selected bathymetry contours (contours are in km)

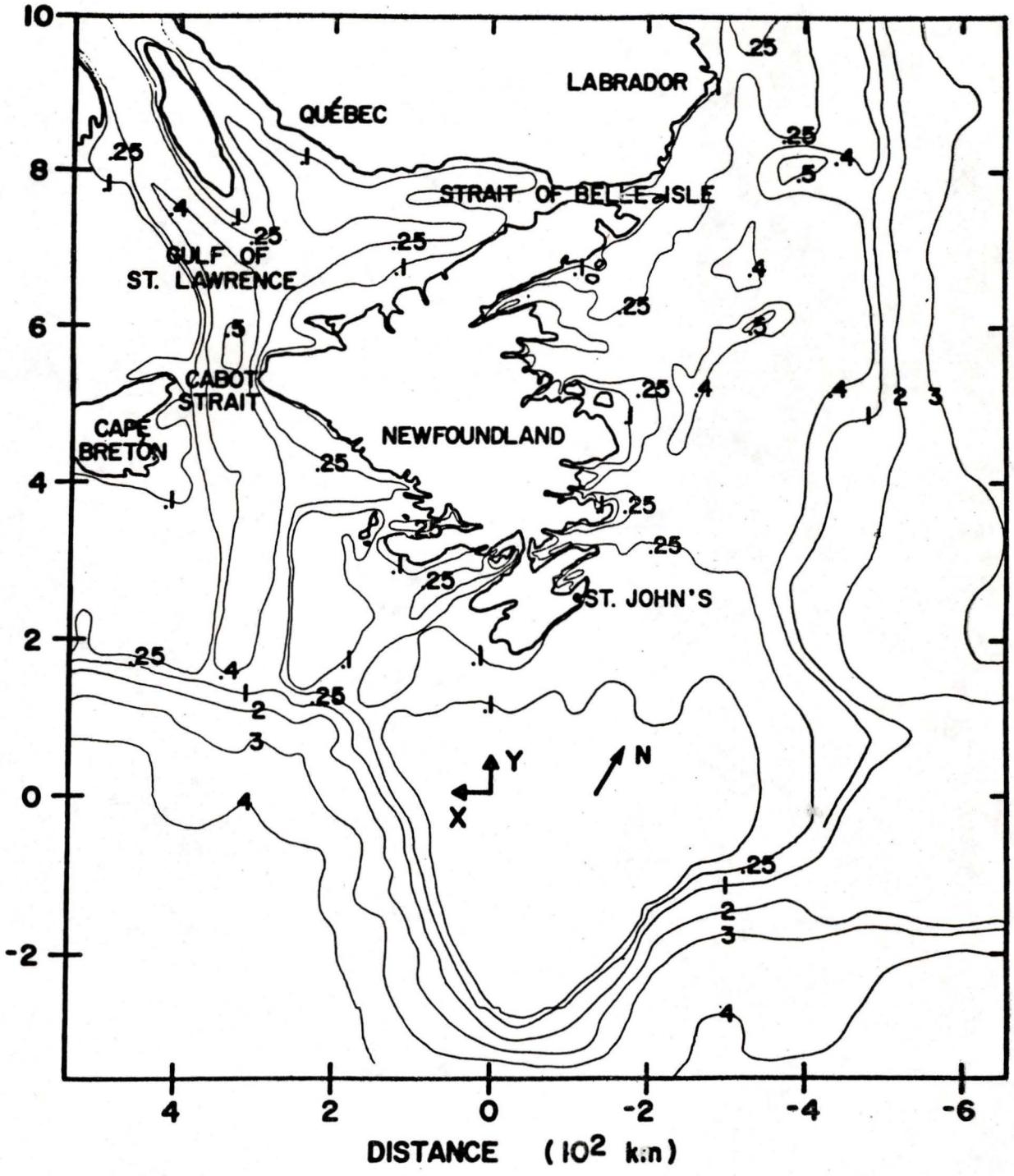

FIGURE 3.2.2 Simplified map of the Newfoundland region (bathymetric contours are in km)

NEWFOUNDLAND MODEL SCALING CONDITIONS

CONDUCTIVITY $\sigma_g/\sigma_m = 1.5 \times 10^{-5}$

	geophysical	model
σ_{land}	3.2×10^{-4} S/m	21 S/m
σ_{ocean}	3.0 S/m	1.2×10^5 S/m$^\Psi$
$\sigma_{sediments}$	0.1 S/m	

$^\Psi$ integrated conductivity

LENGTH $L_g/L_m = 1.0 \times 10^6$

geophysical	model
1 km	1 mm

FREQUENCY $f_g/f_m = 1/(1.5 \times 10^7)$

geophysical	model
100 s	150 kHz
300 s	50.0 kHz
900 s	16.7 kHz
1800 s	8.33 kHz

FIGURE 3.2.3 Scale factors for the analogue model of the Newfoundland region

geophysical and model parameters used in the analogue model study of the Newfoundland region.

The graphite is used to represent an integrated conductivity of the sea water and highly conductive sediments. The conductivity of the sediments was chosen to be 0.1S/m based on resistivity logs made on the continental shelf kindly supplied by Esso Resources Canada Limited and Shell Canada Resources Limited. The thickness of sediments was based on the results of several authors. Sheridan and Drake's(1968) data were used for the sediment thickness in the Gulf of St. Lawrence. The results of Fenwick et al.(1968) and Keen and Barrett(1981) were used for the sediment thickness on the continental shelf and in the deep ocean off the continental shelf. The conductivity of sea water was taken to be 3.0S/m based on temperature-salinity results in the Gulf of St. Lawrence complied by Forrester(1964) and measurements near St. John's by Huyer and Verney(1975). The low sea water conductivity is due to the large amounts of fresh water present in the Gulf of St. Lawrence and near land. The thickness of graphite (in the geophysical scale) representing the integrated conductivity for the ocean depth and thickness of sediment for each bathymetric contour in the simplified map is shown in Table 3.2.1. The thicknesses of sediments listed in Table 3.2.1 for ocean depths greater than 1000m are greater than values

OCEAN DEPTH	SEDIMENT THICKNESS	GRAPHITE THICKNESS (IN GEOPHYSICAL SCALE)
100 m	1572 m	254 m
250 m	1644 m	508 m
400 m	4002 m	889 m
500 m	5574 m	1143 m
1000 m	4290 m	1905 m
2000 m	8580 m	3810 m
3000 m	12870 m	5715 m
4000 m	17160 m	7620 m
5000 m	21450 m	9525 m

TABLE 3.2.1 Depth of ocean and thickness of sediments and the corresponding thickness of equivalent integrated conductivity of graphite for each bathymetric contour used in the contruction of the analogue model.

stated by Fenwick et al.(1968) but the conductivity of sea water in these regions is greater than 3.0S/m. Therefore the increased conductivity of the sea water being replaced by the greater depth of sediments should be a good approximation for our model study. Since the graphite is representing two layers with different conductivities, numerical model calculations were done. The surface fields of a two-dimensional numerical model of sediment and ocean layers were compared to the surface fields of a single layer with an equivalent integrated conductivity. A comparison of the fields at the surface of two models is given in Appendix A. The results showed that there was little difference in the response of the two numerical models for the periods of interest; thus the graphite can be used to represent the integrated conductivity of the ocean and sediment layers.

The ocean of the analogue model was constructed using graphite plate and "Grafoil", a Union Carbide product. Grafoil is laminated graphite foil available in sheets 24 inches wide and from .010 inches to .025 inches thick. The simplified map (Fig. 3.1.2) was used as a template. The first sheet of Grafoil .010 inches thick represented the integrated conductivity of 100m of ocean and 1572m of sediments. Layers of Grafoil representing the different bathymetries (Table 3.2.1) were laminated to the bottom of the previous layer. A suitably shaped graphite plate

representing the deep ocean in the southern region of the area was cemented to the bottom of the Grafoil. Constructing the model in this manner ensures a flat top surface for the model. The graphite was sanded to give a smoothed depth profile over all of the model.

The analogue model is supported on a wooden frame covered with a fibreglass screen. The screen is used to support the graphite model since the model is very thin and flexible over most of its area. The wooden frame also supports a graphite plate 1.5cm thick located 17.5cm below the upper surface of the model. This plate represents a highly conductive layer deduced in earlier field studies in the region of interest (Hyndman and Cochrane, 1971; Bailey et al., 1974; Cochrane and Hyndman, 1974; Kurtz and Garland, 1976). A discussion of representing the conductive layer by a graphite plate can be found in Appendix B. This layer will be called the (geomagnetic) mantle in this thesis.

The analogue model was placed in the tank containing the salt solution. Two perpendicular polarizations of the source field, E-polarization and B-polarization, were used. For E-polarization, the electric field of the source is in the x-direction while for B-polarization, the electric field of the source is in the y-direction. For E-polarization, the electric field of the source is roughly parallel to the

continental shelf on the east coast of North America and for B-polarization, the electric field of the source is roughly parallel to the Labrador Sea- mainland coastline. For both polarizations the edges of the graphite, representing the deep ocean, perpendicular to the electric field of the source were connected to the the stainless steel plates at the ends of the tank. This was done to minimize any effects due to the finite size of the deep ocean in the model.

3.3 Reference Field Measurements

The electric and magnetic fields at the surface of the brine (in the absence of the ocean of the analogue model) were measured for the four periods used in this study. These field measurements are referred to as the reference fields. The spatial variation in each field component of the reference fields was found to be small for all periods. The reference fields for E-polarization and 100s period of a traverse along x=0 are shown in Fig.3.3.1. This figure shows the in-phase and quadrature parts of each component of the electric and magnetic fields. The magnitude of the horizontal magnetic field (B_y for E-polarization) at a reference point in the tank is set to a value of 1.0 nT. All model field measurements are measured relative to this reference field component. This reference point is away from any effects due to the ocean of the analogue model.

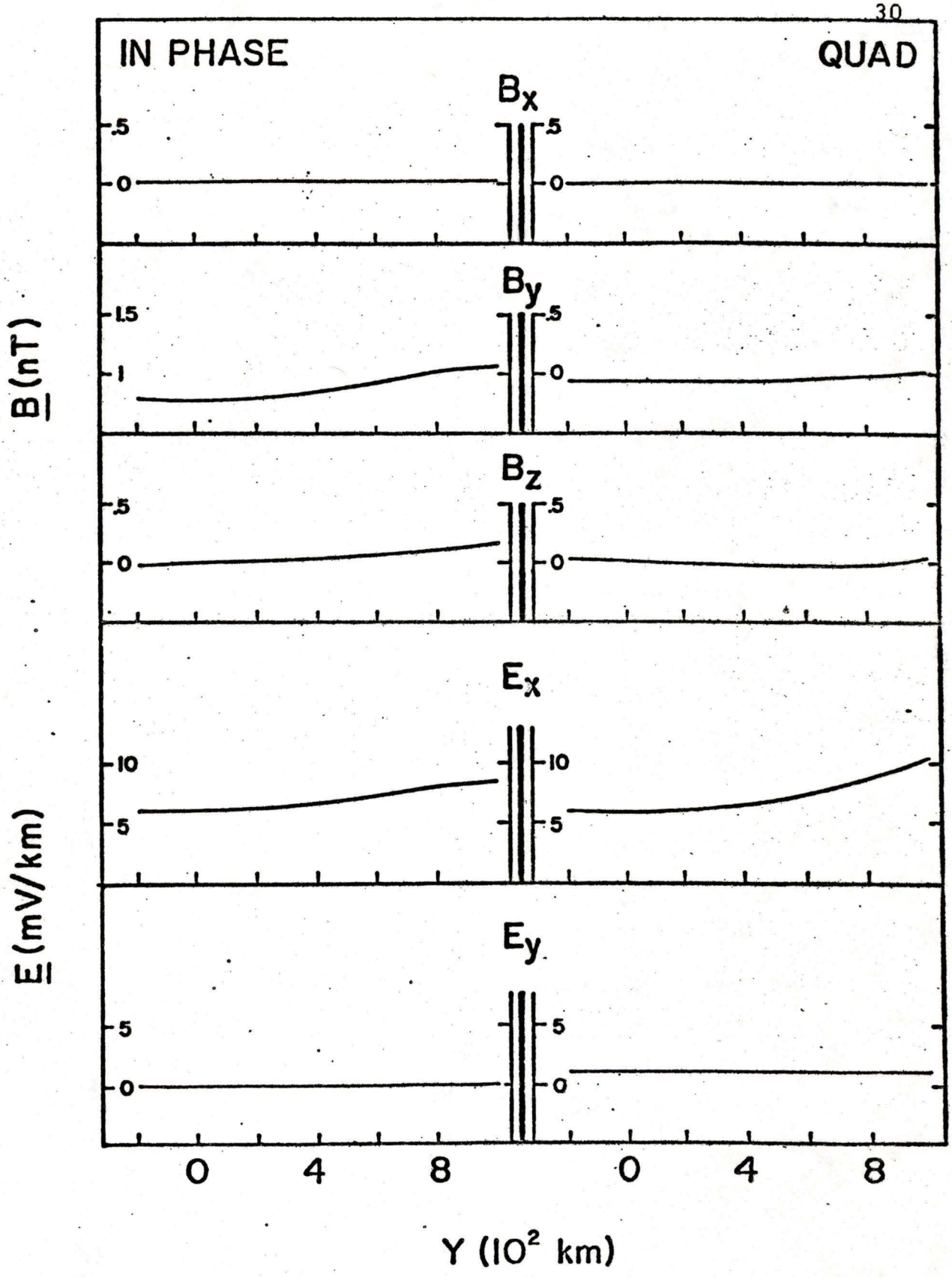

FIGURE 3.3.1 Reference fields for traverse along x=0 for a period of 100s and E-polarization

CHAPTER 4

MAGNETIC FIELD RESULTS

4.1 Introduction

The behavior of the magnetic field over the analogue model was studied for two perpendicular polarizations of the source, E-polarization and B-polarization. For E-polarization, the electric field of the source is in the x-direction, roughly parallel to the continental shelf on the east coast of North America. For B-polarization, the electric field of the source is in the y-direction, roughly parallel to the the Labrador Sea- mainland coastline.

The magnetic field components, B_x, B_y, and B_z, for the simulated periods of 100s, 300s, 900s, and 1800s, were measured over the surface of the model every 1cm (10km in the geophysical scale) in the x-direction and 0.5cm in the y-direction. The in-phase and quadrature-phase parts of each measurement of a field component were recorded relative to the reference field. For E-polarization, the reference field is B_y with in-phase B_y equal to 1.0 nT and quadrature B_y,

zero. For B-polarization, the reference field is B_x with in-phase B_x equal to -1.0 nT and quadrature B_x, zero. All field components measured are components of the anomalous field produced by the analogue model except B_y (E-pol) and B_x (B-pol) which have the reference (normal) field included in their in-phase part.

Contours of the in-phase and quadrature-phase parts of each magnetic field component for all four periods and both polarizations are examined. Contour diagrams for three magnetic field components, B_y, B_x, and B_z, for a period of 100s are shown in Figs. 4.1.1-4.1.3, respectively. For a period of 1800s, the contours of the magnetic field components are shown in Figs. 4.1.4-4.1.6. Contour diagrams of the magnetic field components for the 300s and 900s periods are shown in Appendix C.

4.2 The Behavior of the Magnetic Field at a Straight Coastline

For a straight coastline, an anomalous magnetic field occurs if the source field has a horizontal magnetic field component perpendicular to the coastline. There is an enhancement in this perpendicular magnetic field component and a vertical magnetic field component occurs as well. There is no enhancement in the horizontal magnetic field

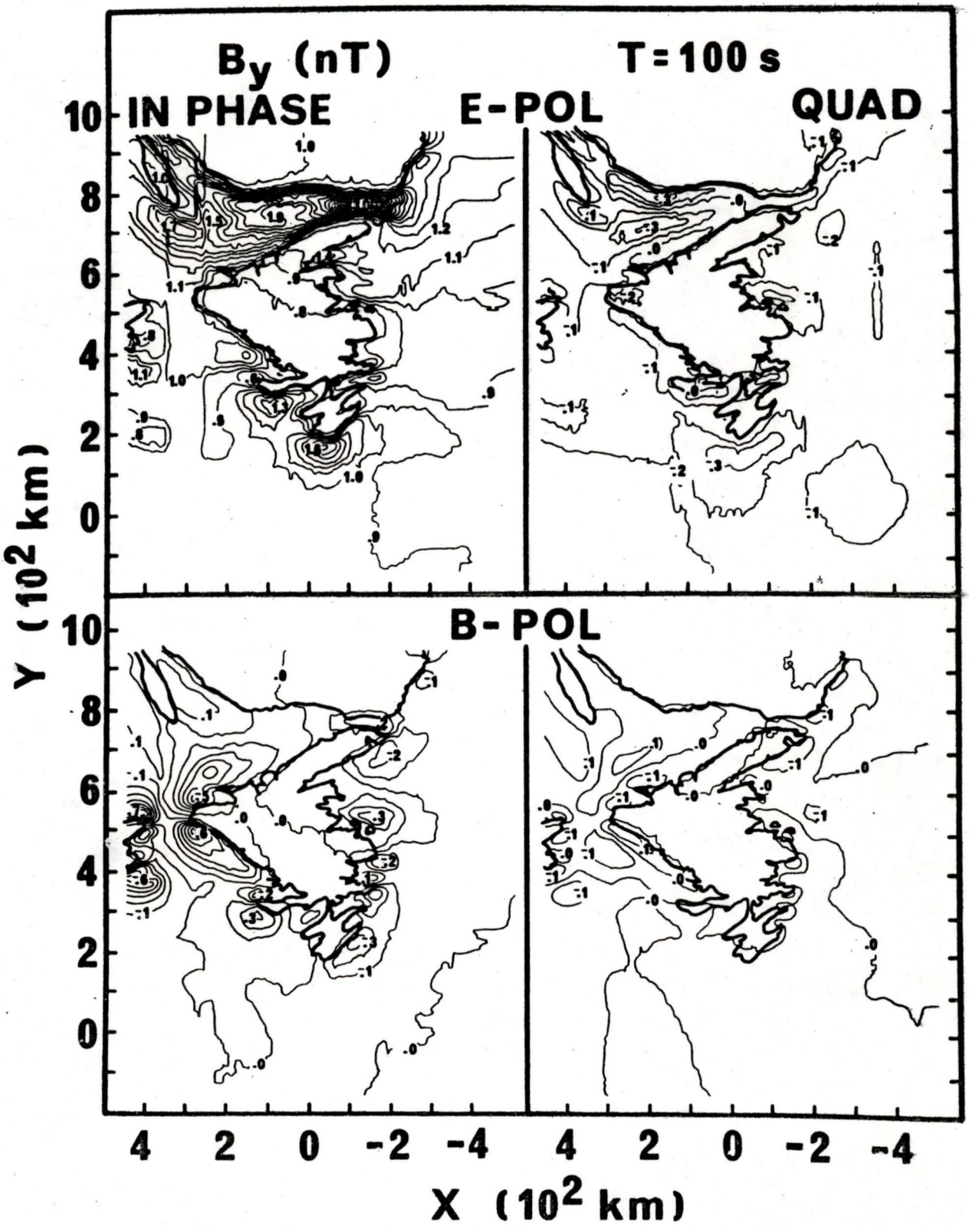

FIGURE 4.1.1 Contours of the in phase and quadrature phase parts of B_y for a period of 100s and both polarizations.

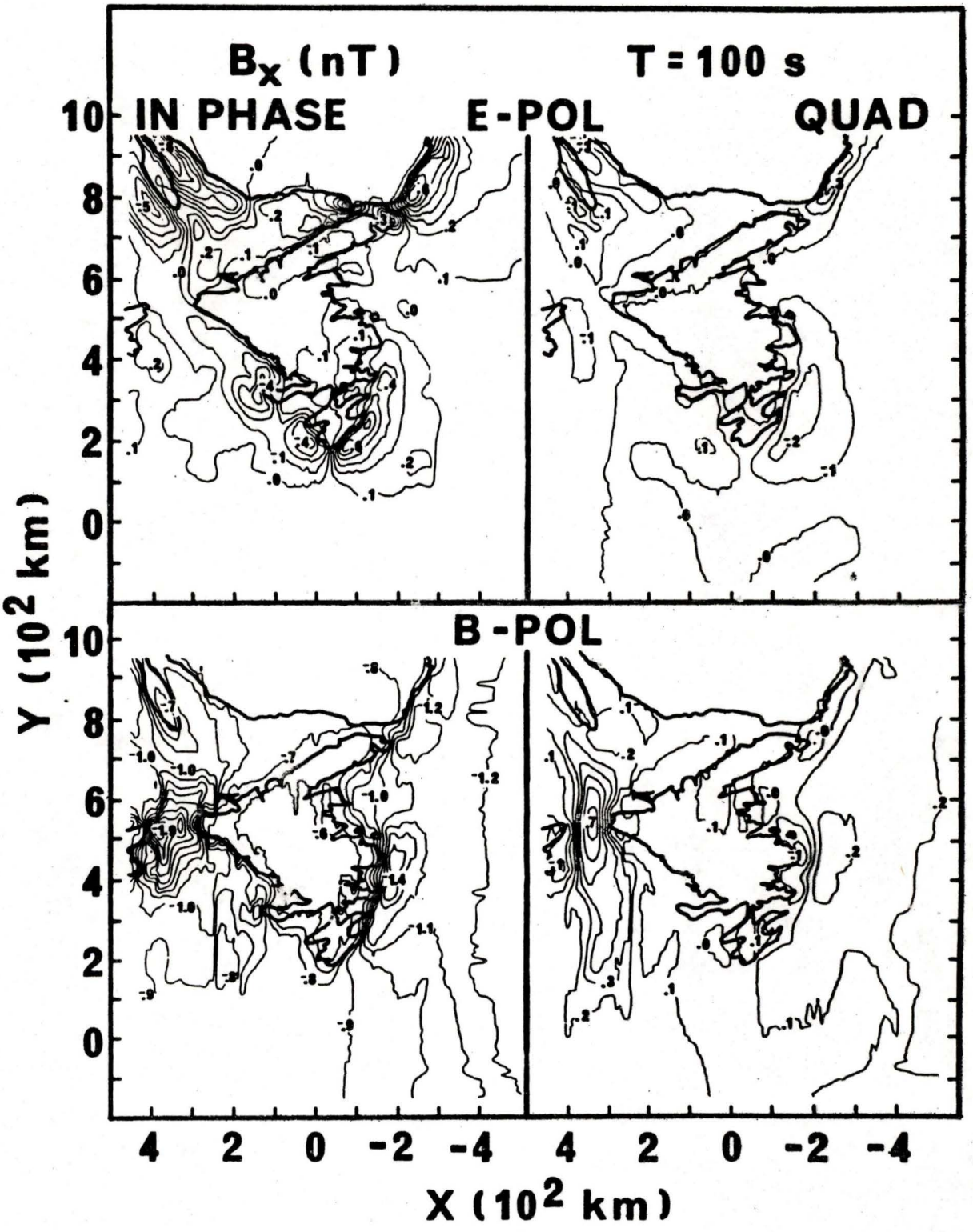

FIGURE 4.1.2 Contours of the in phase and quadrature phase parts of B_x for a period of 100s and both polarizations.

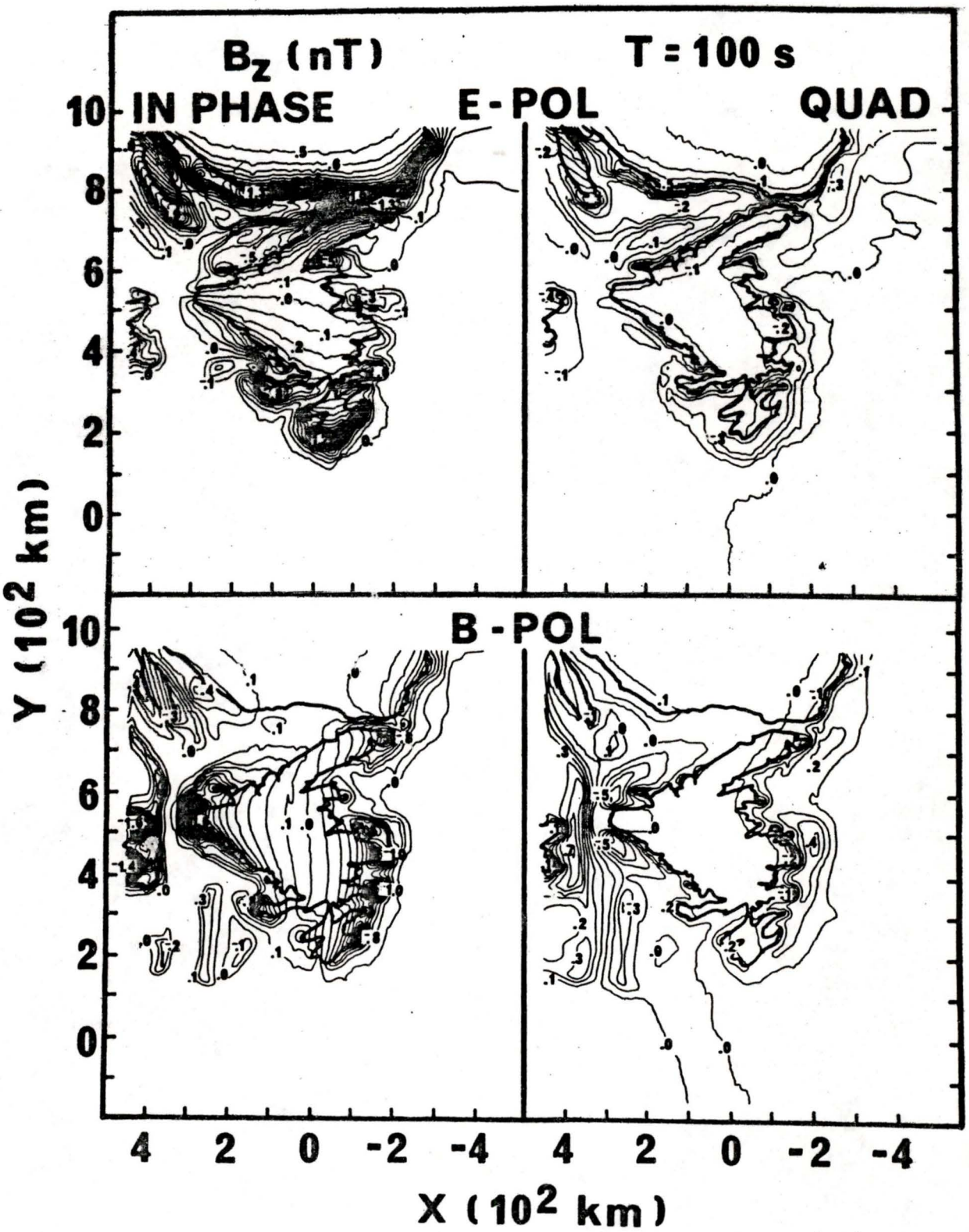

FIGURE 4.1.3 Contours of the in phase and quadrature phase parts of B_z for a period of 100s and both polarizations.

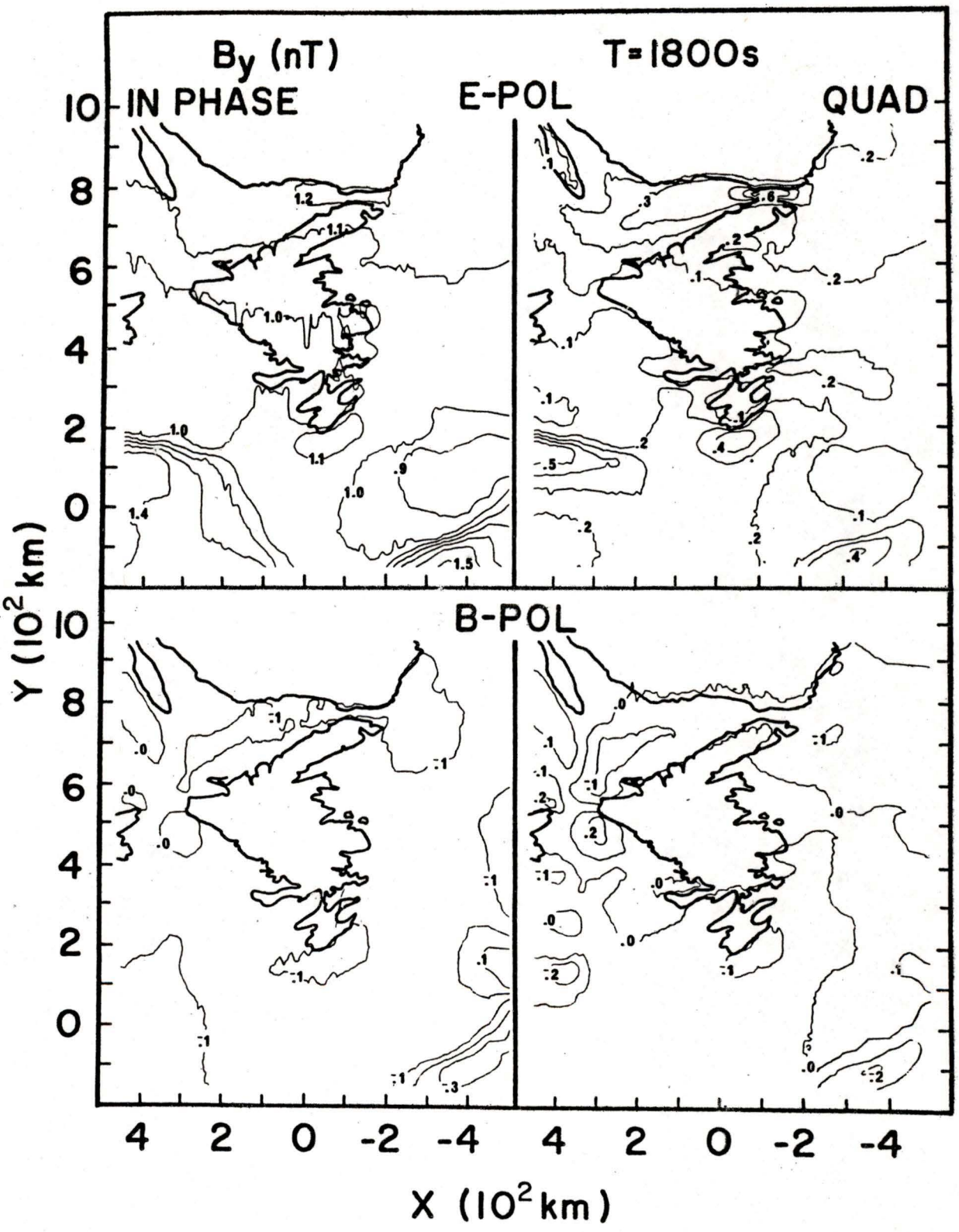

FIGURE 4.1.4 Contours of the in phase and quadrature phase parts of B_y for a period of 1800s and both polarizations.

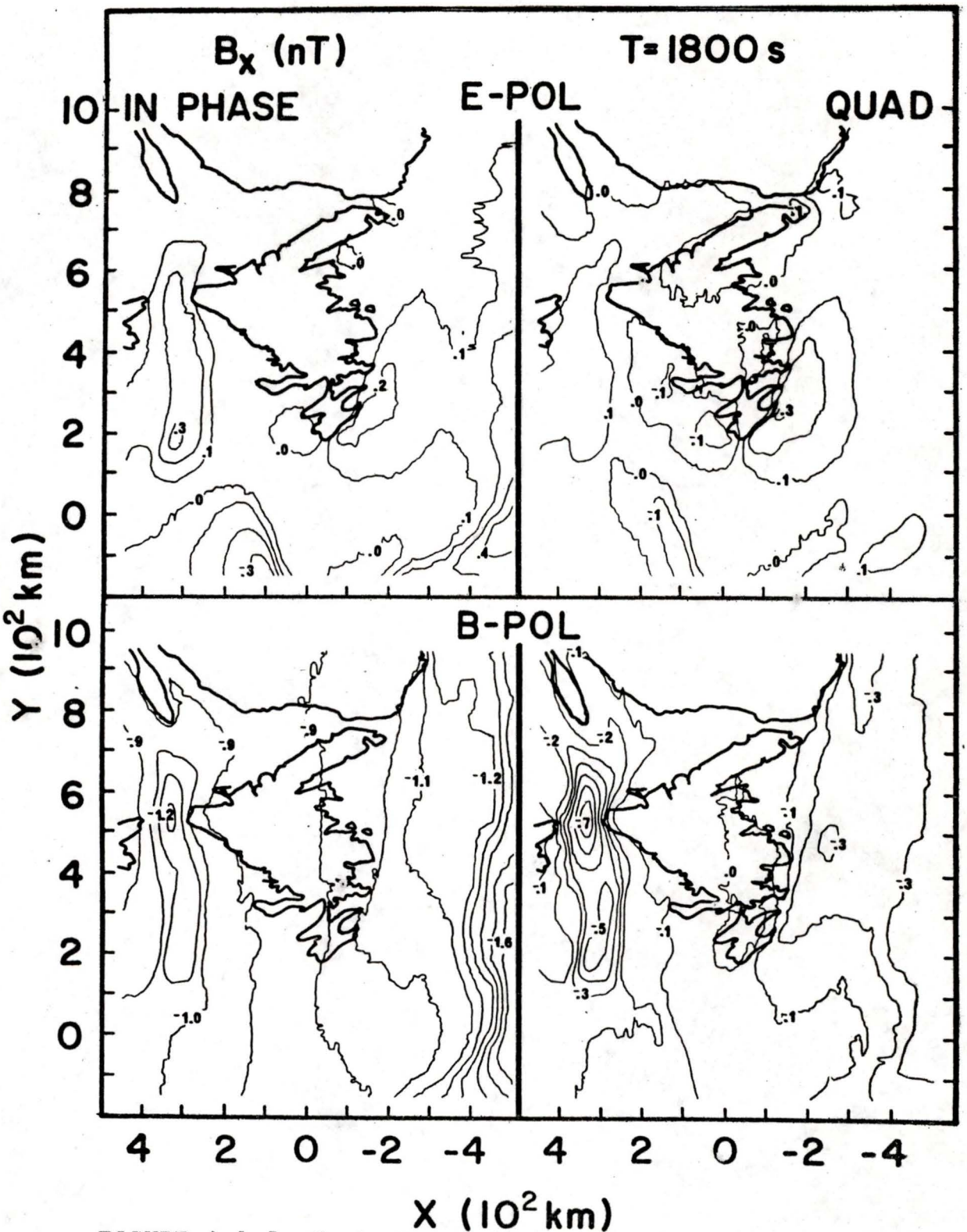

FIGURE 4.1.5 Contours of the in phase and quadrature phase parts of B_x for a period of 1800s and both polarizations.

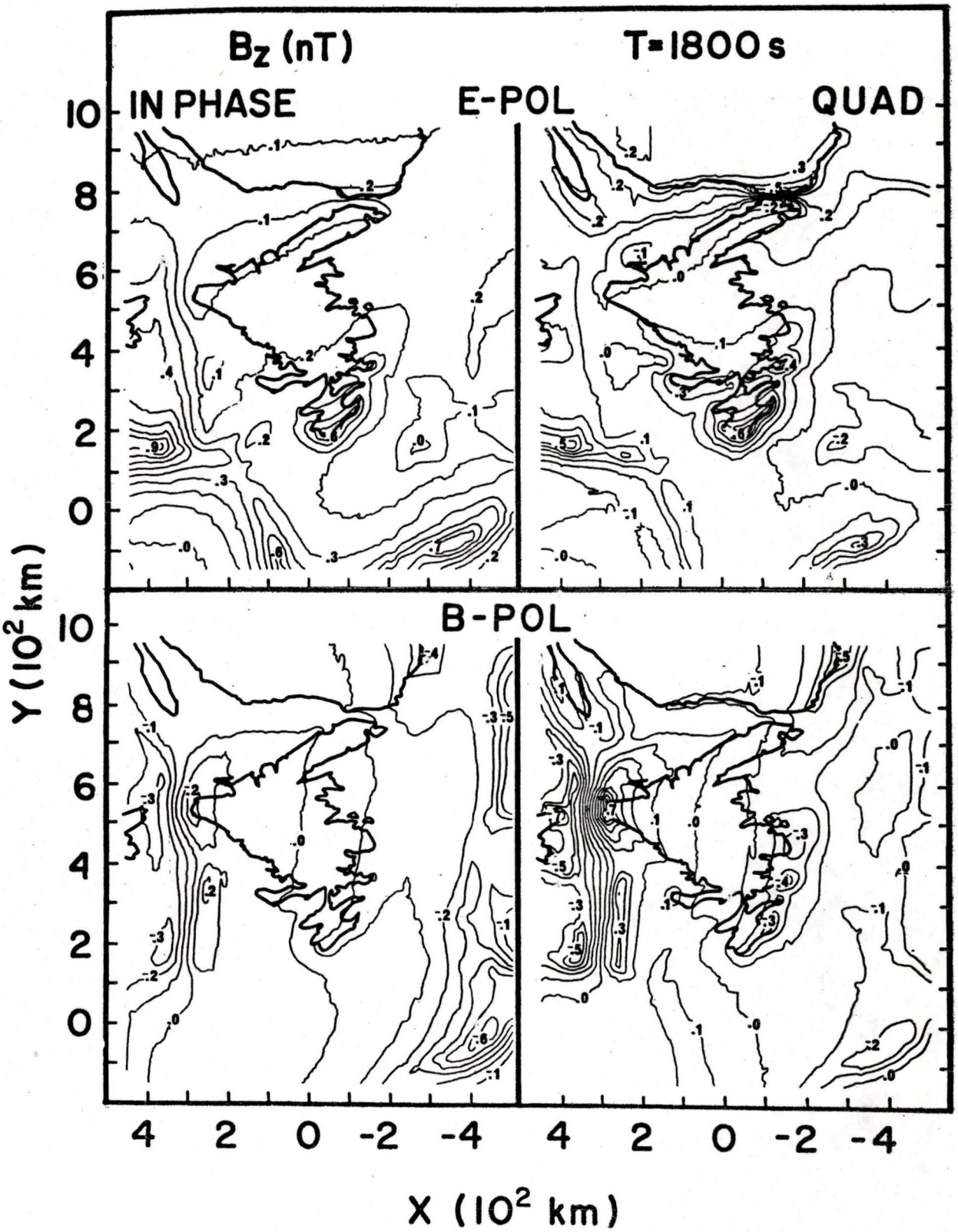

FIGURE 4.1.6 Contours of the in phase and quadrature phase parts of B_z for a period of 1800s and both polarizations.

component parallel to the coastline. The straight coastline effect is due to larger current induced in the ocean than in the less conducting land. This is the well known "coast effect".

A suitable location for examining the response of a straight coastline is the southern coast of Quebec and Labrador. Figure 4.1.1 shows that in-phase B_y (E-pol) reaches a maximum on the seaward side of the coastline for a period of 100s. In-phase B_y has a large spatial gradient near the coastline and approaches the value of the normal (reference) field a short distance landward. In-phase B_z(E-pol) in Fig. 4.1.3 reaches a maximum at the land-sea interface. Quadrature B_z also reaches a maximum at the coastline. B_x, for E-polarization (Fig. 4.1.2), and all three magnetic field components for B-polarization (Figs. 4.1.1-4.1.3) show no spatial variation at this coastline as expected for a straight coastline.

At the longer periods of 300s and 900s, the anomalous field near the Quebec and Labrador coastline is affected by the anomalous fields of other coastlines in the region. From Fig. 4.1.6 quadrature B_z (E-pol) shows a vertical field still present at the coastline for a period of 1800s. The anomalous magnetic field due to the conductivity contrast at the coastline is smaller for a period of 1800s than for the shorter periods. For increasing period, the magnitude of the

fields due to the coast effect decreases and the anomalous field changes from the in-phase to quadrature part for each field component.

4.3 The Behavior of the Magnetic Field at a Strait

The two straits present in the Newfoundland analogue model are the Strait of Belle Isle and Cabot Strait. The Strait of Belle Isle is a narrow shallow channel, which has a mainly two-dimensional structure, while Cabot Strait is a wider and deeper channel located between two capes.

For the 100s period, in-phase B_y for E-polarization in Fig. 4.1.1 reaches a maximum of 3.0 nT over the central region of the Strait of Belle Isle. Quadrature B_y is zero at this location. Figure 4.1.2 shows that the magnitude of B_x for B-polarization reaches a maximum over the central region of Cabot Strait with the anomalous field distributed equally in the in-phase and quadrature parts. When the horizontal magnetic field of the source is perpendicular to the direction of the strait, there is an enhancement in this horizontal component (eg. B_y for E-polarization for the Strait of Belle Isle). In Fig. 4.1.3, for E-polarization, in-phase B_z is -1.3 nT and 1.9 nT and quadrature B_z is -0.2 nT and 0.2 nT at the coastlines of the Strait of Belle Isle. For B-polarization, in-phase B_z is -1.6 nT and 1.6 nT

and quadrature B_z is 0.7 nT and -0.5 nT at the coastlines of Cabot Strait. The magnitude of the vertical field reaches a maximum at both coastlines of the straits depending on the polarization. Thus the vertical field undergoes approximately a 180^{o} phase shift from one coastline to the other.

The current induced in the straits can be visualized as a simple line current in the direction of the straits. The horizontal magnetic field component perpendicular to the direction of the line current reaches a maximum over the centre of the line current. The vertical magnetic field reaches a maximum at either side of the line current. There is a 180^{o} phase difference between the vertical field at the sides of the line current. The difference in the responses of the Strait of Belle Isle and Cabot Strait is due to the different geometry of the straits. Cabot Strait is approximately five times deeper and three times wider than the Strait of Belle Isle. Current induced in the deeper section of Cabot Strait will introduce a quadrature part of the anomalous field while current induced in the shallow Strait of Belle Isle will produce a smaller quadrature part. Cabot Strait is located between two capes which further affects the phase of the induced currents.

For the 1800s period, B_y (E-pol) in Fig. 4.1.4 shows that the enhancement of this component over the central

region of the Strait of Belle Isle is mainly in the quadrature part. Figure 4.1.5 shows that the enhancement of B_x (B-pol) over Cabot Strait is also mainly in the quadrature part. As for the 100s results, when the horizontal magnetic field of the source is perpendicular to the direction of the strait, there is an enhancement in this magnetic field component. Although not obvious from Fig. 4.1.6, the magnitude of B_z for 1800s is greater on one coastline of the strait than the other coastline. For the Strait of Belle Isle, the magnitude of B_z is larger on the Labrador coast than on the Newfoundland coast for E-polarization. Similarly for Cabot Strait, the magnitude of B_z is greater on the Cape Breton coastline than on the Newfoundland coastline. For the 100s period results, the magnitude of B_z is approximately equal on both sides of the straits. For the 1800s period, the vertical magnetic field undergoes an approximate 90^o phase shift across the straits, not the 180^o phase shift seen in the 100s results. Results of B_z for periods of 300s and 900s show that the difference in the magnitude of B_z at the coastlines increases with increasing period from 100s to 1800s. Similarly the phase shift of B_z over the strait decreases from 180^o at a period of 100s to 90^o at the 1800s period.

The frequency response of B_z at the straits can be

explained by induced current in the deep ocean. As described for the 100s results, the induced current in the strait can be represented as a line current. A second line current parallel to the first represents the induced current in the deep ocean. For the 100s period, the deep ocean line current is approximately zero compared with the strait line current. For increasing period, the deep ocean current increases relative to the strait current, producing a difference in the magnitude of B_z on the sides of the strait line current as observed in the model results. If the two line currents are slightly out of phase, the phase shift of B_z over the straits observed in the model can be explained by the frequency response of line currents described.

The two straits, Cabot Strait and the Strait of Belle Isle, show slightly different frequency responses for the magnetic field components. The magnitude of the anomalous field over the Strait of Belle Isle decreases with increasing period while, for Cabot Strait, the magnitude of the anomalous field reaches a maximum at the 300s period and then decreases with increasing period. Results of Dosso et al.(1980b) for a period of 3600s show that the response of the fields over both straits continue to decrease with period. All field components show the anomalous part of each component changing from the in-phase part to the quadrature part with increasing period.

4.4 The Behavior of the Magnetic Field at a Cape

The southern tip of Newfoundland can be considered as a single cape for the period range studied. Figure 4.1.1 shows a large enhancement in B_y (E-pol), mainly in the in-phase part, on the ocean side of the cape. In-phase and quadrature B_x (E-pol) in Fig. 4.1.2 show that the magnitude of B_x reaches a maximum on the sides of the cape but undergoes a 180^o phase shift over the cape. In Fig. 4.1.3 in-phase B_z reaches a maximum (1.2 nT) at the coastline of the southern tip of Newfoundland. Similarly a smaller maximum in quadrature B_z occurs at this coastline.

Similarly, in Fig. 4.1.1, the capes on either side of Cabot Strait show that in-phase and quadrature B_y (B-pol) have a similar response over the cape as in-phase and quadrature B_x (E-pol) have for the southern tip of Newfoundland. The two other components, B_x (B-pol) and B_z (B-pol), over Cabot Strait show the strait effect of Cabot Strait as well as the effect due to the capes, and thus the cape effect for the capes on Cabot Strait is less evident in these components.

The anomalous field components due to the capes are still evident at the 1800s period although smaller in magnitude than those for the 100s period results. For example, at the southern tip of Newfoundland, quadrature B_x

(E-pol) in Fig. 4.1.5 undergoes a 180° phase shift across the cape and both in-phase and quadrature B_z (E-pol) in Fig. 4.1.6 reach a maximum at the coastline. At this period, the ocean depth near the coastline is only approximately 0.07 skin-depths. Results for periods of 300s and 900s also show that the anomalous field due to the capes decreases with increasing period. As for the strait effect, the anomalous field changes from the in-phase part to the quadrature part in each field component with increasing period.

The cape effect observed in the model is expected from the results of Chan et al.(1981). Induced current deflected around a cape produces a horizontal magnetic field perpendicular to the sides of the cape (eg. B_x for E-polarization for the southern tip of Newfoundland). The induced current is deflected in one direction at the side of the cape and deflected in the opposite direction on the other side. Thus the horizontal field component perpendicular to the sides of the cape undergoes a 180° phase shift across the cape. The magnetic field component parallel to the coastline at the tip of the cape (eg. B_y for E-polarization for southern Newfoundland) reaches a maximum on the seaward side of the coastline which shows an increase in current density due to the deflection of current around the cape. This current density at the tip of the cape produces a larger

vertical field than expected for a straight coastline (Chan et al., 1981).

4.5 The Behavior of the Magnetic Field at the Continental Shelf

For the 100s period, there are no significant anomalous field components (greater than 0.1 nT) present over the continental shelf (Figs. 4.1.1-4.1.3). At this period, the depth of the shallow ocean near the shelf edge is approximately 0.15 skin-depths while the depth of the deep ocean is of the order of 1.5 skin-depths. Unlike the results for 100s, an anomalous magnetic field is observed at the shelf edge for the 1800s period. For E-polarization in Fig. 4.1.4, the anomalous part of B_y reaches a maximum in the deep ocean off the shelf edge south of Newfoundland and the magnitude of B_z (E-pol) in Fig. 4.1.6 reaches a maximum at this shelf edge. A smaller response is observed in B_x and B_z for B-polarization in Figs. 4.1.5 and 4.1.6 for the shelf edge in the eastern section of the model region. For the southern section of the shelf, the ocean depth varies from 250 m to 3000 m in a distance of 100 km, while for the eastern shelf edge, the ocean depth changes from 400 m to 3000 m in 200 km. The difference in the spatial gradient of the ocean depth at the shelf edge accounts for the difference in the magnitude of the response at the shelf edge.

The frequency response of the anomalous field at the continental shelf edge is different from that of the straits and capes. The maximum response at the shelf edge occurs at either 900s or 1800s in the model results. The results of Dosso et al.(1980b) show the response at the shelf edge for a period of 3600s is less than observed for the 1800s period results in the present model. For example, the magnitude of B_z for E-polarization at the shelf edge is approximately 0.4 nT for a period of 3600s (Dosso et al., 1980b). The magnitude of B_z in the Newfoundland model is approximately 0.9 nT for the 1800s period. The vertical field in the Newfoundland model at the shelf edge for a period of 3600s should be larger than that stated by Dosso et al.(1980b) since the ocean depth on the shelf was taken to be greater in the Dosso et al.(1980b) model, producing a smaller depth gradient at the shelf edge than found in the Newfoundland model. For periods greater than 1800s, the response of the shelf edge should decrease with increasing period. At long periods (> 900s) the continental shelf behaves as a coastline.

4.6 The Spatial Behavior of the Magnetic Field Over Land

The horizontal magnetic field components for both polarizations show little spatial variation over the land

away from the coastline for all four frequencies. The spatial variation of these components over the ocean depends on the location of currents induced as decribed earlier. The spatial variation in the vertical field over land decreases with increasing period. For example, in central Newfoundland for a period of 100s, in-phase B_z (E-pol) in Fig. 4.1.3 changes 0.1 nT over a distance of 50 km. For a period of 1800s in-phase B_z for E-polarization shown in Fig. 4.1.6 varies 0.1 nT over a distance of approximately 200 km in Newfoundland.

CHAPTER 5

ANALOGUE MODEL INDUCTION ARROWS

5.1 Introduction

The use of induction arrows (transfer function arrows) has become prevalent in geomagnetic studies. Parkinson(1959) and Wiese(1962) found that the vertical magnetic field could be correlated to the horizontal magnetic field. They were able to construct induction arrows in the horizontal plane which determined the location of conductive structures. Gregori and Lanzerotti(1980) presented a review of the different graphical methods used in calculating induction arrows and the relationship between the arrows produced by each method. Everett and Hyndman(1967) and Schmucker(1970) derived a mathematical basis to relate the anomalous magnetic field at a station to the magnetic field at a normal station using transfer functions.

For a horizontal inducing field in the model, Schmucker's(1970) equation 3.11 can be written as

$$B_z^E = a\, B_x^E + b\, B_y^E$$

$$B_z^B = a\, B_x^B + b\, B_y^B \qquad (5.1.1)$$

where B_z is the anomalous vertical field and B_x and B_y are the normal horizontal field components. The superscripts E and B signify the polarization of the source field. The complex constants a and b are obtained upon solving eq.(5.1.1). The in-phase arrow is the vector (-Re a, -Re b) and the quadrature arrow is the vector (-Im a, -Im b).

Two types of induction arrows, single station and inter-station arrows, are compared in this work. Single station induction arrows are commonly used in field studies. Since the horizontal field components at the station are assumed to have a small anomalous field part compared to the normal horizontal field, all three magnetic field components at the station are used in eq. (5.1.1). Inter-station induction arrows are calculated using the vertical magnetic field at a station and the horizontal field at a reference (normal) station in eq. (5.1.1).

5.2 Comparison of Single Station and Inter-station Induction Arrows

To compare the two types of arrows, inter-station and single station, these arrows were calculated for all four

periods. The normal station used in the inter-station arrow calculations was the reference station located away from the effects of the ocean. Since the differences between the two types of arrows are similar for all four periods, only a comparison of the two types of arrows for the 100s period is made here. Diagrams of the two types of arrows, inter-station and single station, for this period are shown in Figs. 5.2.1 and 5.2.2, respectively. The upper half of each diagram shows the contours of the magnitude of the induction arrows for the in- phase (left-hand side) and quadrature (right-hand side) arrows with a contour interval of 0.1. Below each contour diagram, the directions of the arrows are shown with the lengths of the arrows indicating relative magnitudes. Since the arrow direction does not vary quickly over the model, and to keep the direction and magnitude of the arrow visible, only the direction of every fourth arrow calculated is shown in the bottom half of each figure.

The inter-station induction arrows for 100s in Fig. 5.2.1 show that the magnitude of the in-phase arrow increases rapidly at the coastline. These arrows reach maxima in magnitude at the capes. The in-phase arrows decrease more slowly over land than over ocean. Figure 5.2.2 shows the same behavior for the single station in-phase arrows. The difference between the two types of arrows is the magnitude of the arrows at the coastline. The inter-station in-phase

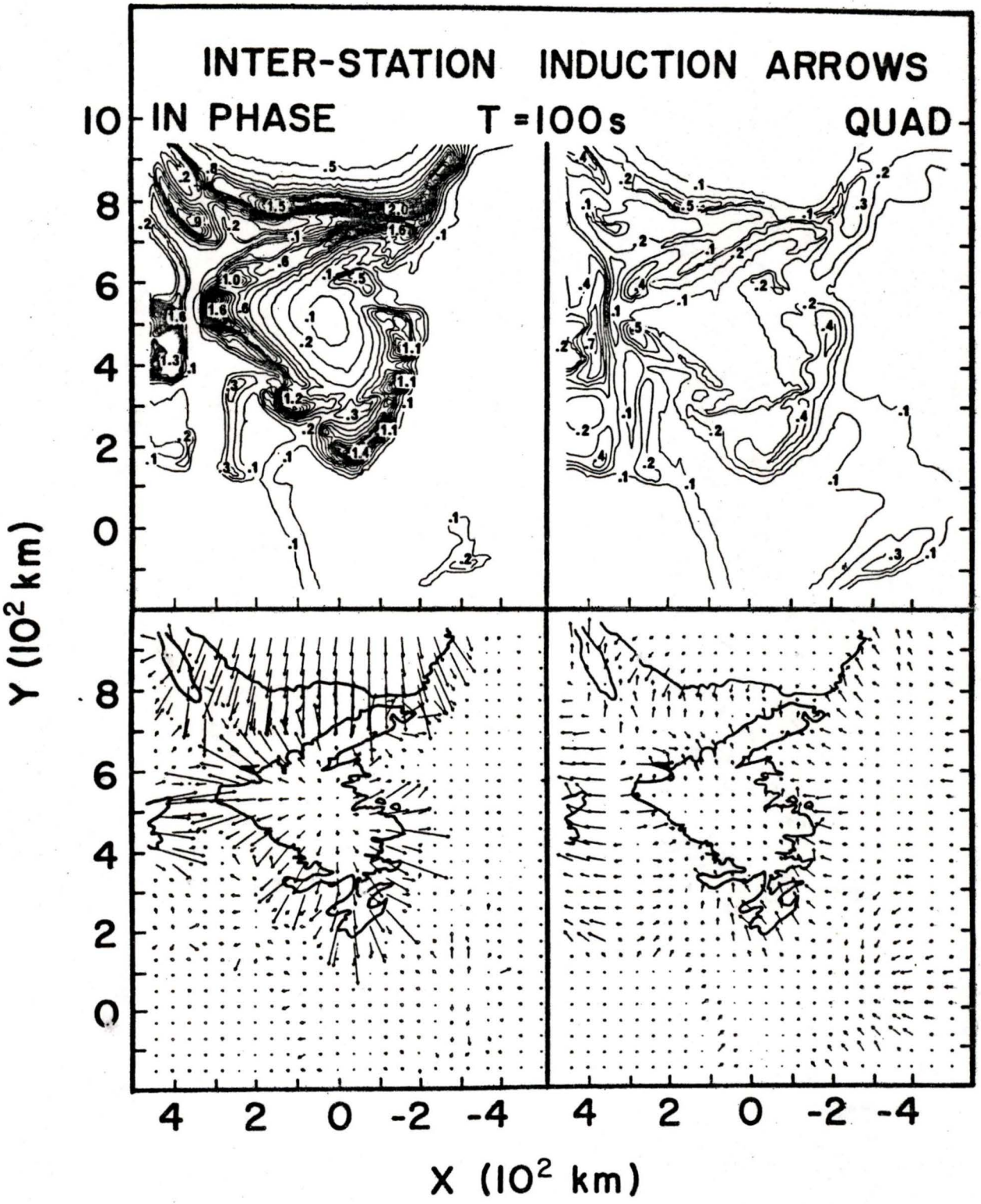

FIGURE 5.2.1 Inter-station induction arrows for a period of 100s

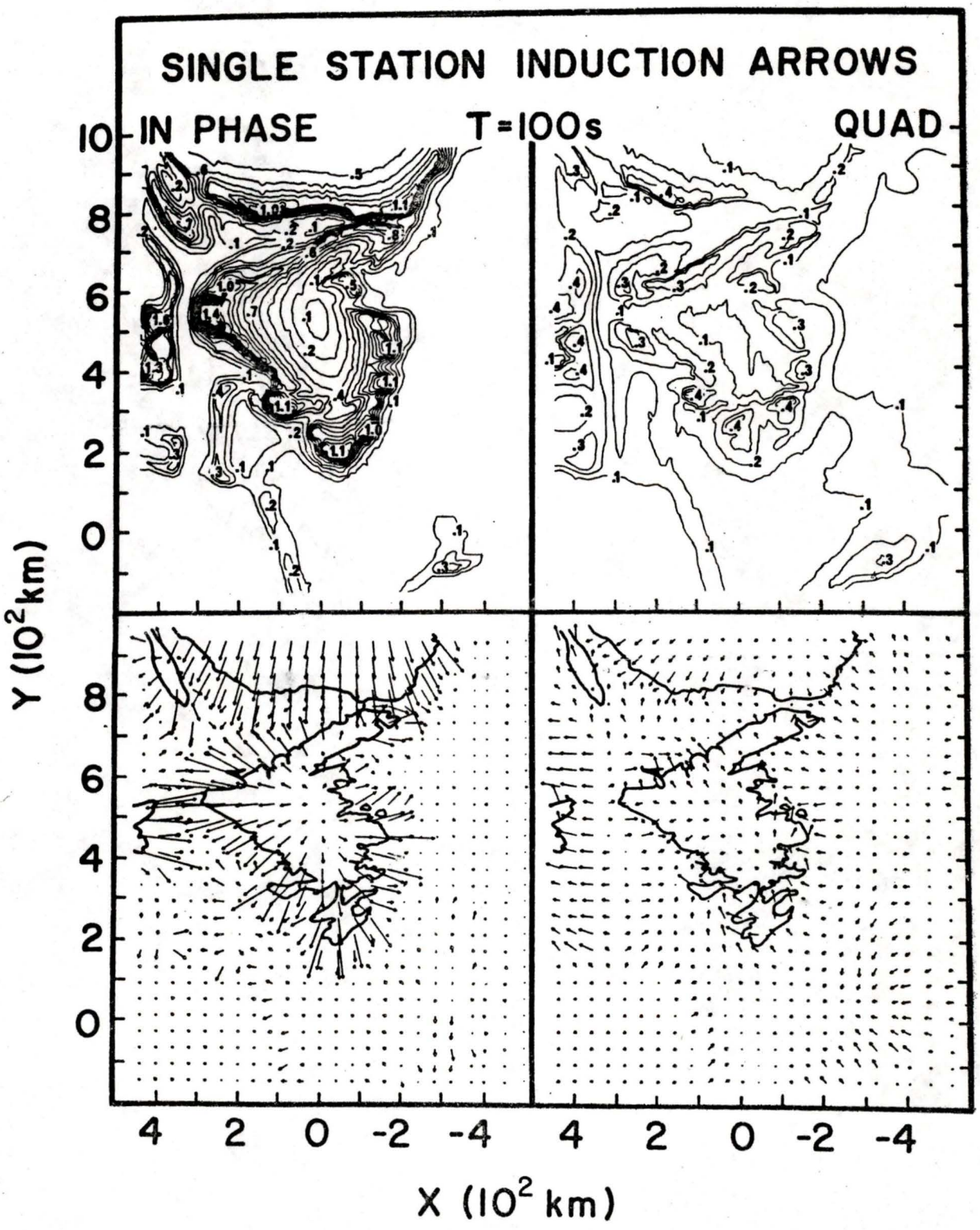

FIGURE 5.2.2 Single station induction arrows for a period of 100s

arrows are larger than the single station counterparts at the coastlines of the Strait of Belle Isle and Cabot Strait and at a few of the capes. The magnitude of the single station in-phase arrows decreases more slowly inland than the magnitude of the inter-station arrows. For example, in Fig.5.2.2, the magnitude of the single station arrow inland from Channel-Port aux Basques, Newfoundland (x=150km, y=500km) is 0.7, while the magnitude of the inter-station arrow (Fig. 5.2.1) is 0.3. The directions of the in-phase arrow for both types of induction arrows are approximately the same. A similar relationship is found between the two types of quadrature arrows. The inter-station quadrature arrows decrease more rapidly inland than the single station arrows. Over Cabot Strait the magnitude of the inter-station quadrature arrow is greater than the magnitude of the single station arrow at the same location. The directions of the two types of quadrature arrows are approximately the same for the same location. The difference in the magnitude of the single station and inter-station induction arrows for the 100s period can be explained by the presence of an anomalous horizontal magnetic field. The enhancement of the horizontal magnetic field over the straits and ocean near the coastline reduces the magnitude of the single station induction arrow at the coastline. The total horizontal field just inland of the coastline is smaller than the normal field. This

accounts for the single station induction arrows decreasing less rapidly landward than the inter-station arrows.

The inter-station induction arrows for periods of 300s, 900s, and 1800s are in Appendix D. The single station induction arrows for these periods are found in Section 5.3. As for the 100s period results, the difference between the two types of arrows, single station and inter-station, occurs where an anomalous horizontal magnetic field is present. Therefore the contour diagrams of the horizontal magnetic field components show where differences between the two types of arrows will occur. The difference between the two types of arrows for a location occurs only in the magnitude of the arrows. The direction of the arrows is approximately the same for both types of arrows. This is true for both the in-phase and quadrature arrows, but is more obvious for the in-phase arrows.

5.3 Frequency Response of Single Station Induction Arrows

As mentioned in the above section, the magnitude of the single station arrows for the 100s period in Fig. 5.2.2 reaches a maximum at the capes. In central Newfoundland, the in-phase arrow is zero since the net vertical field due to the induced currents in the ocean surrounding Newfoundland is zero. The in-phase arrows over Labrador decrease more

slowly inland than over Newfoundland. In Labrador, an in-phase arrow magnitude of 0.5 can be found more than 100km from the Strait of Belle Isle. The direction of the in-phase arrow is towards the nearest current density which is usually the nearest coastline for the 100s period. The quadrature arrow maximum occurs at the coastline. The magnitude of the quadrature arrow is usually less than the in-phase arrow magnitude at the same location. The direction of the quadrature arrow is toward the conductivity contrast. Therefore, the direction of the arrow reverses as the land-sea interface is crossed. The quadrature arrow is larger on the landward side of the interface. Both the in-phase and quadrature arrow contours delineate the continental shelf edge in the southern section of the model. The magnitude of the in-phase arrow is less at the shelf edge than at the coastline. The quadrature arrow magnitude is the same at the shelf edge as at the coastline.

Figure 5.3.1 shows the single station induction arrows for the 300s period. The in-phase arrow contours do not delineate the coastline as well as they did for the 100s period. The coastline for the northern half of Newfoundland is not as evident in the in-phase arrow contours for the 300s period as for the 100s period. The minimum in the magnitude of the in-phase arrows in Newfoundland for the 300s period is north of the location for the minimum found for the 100s

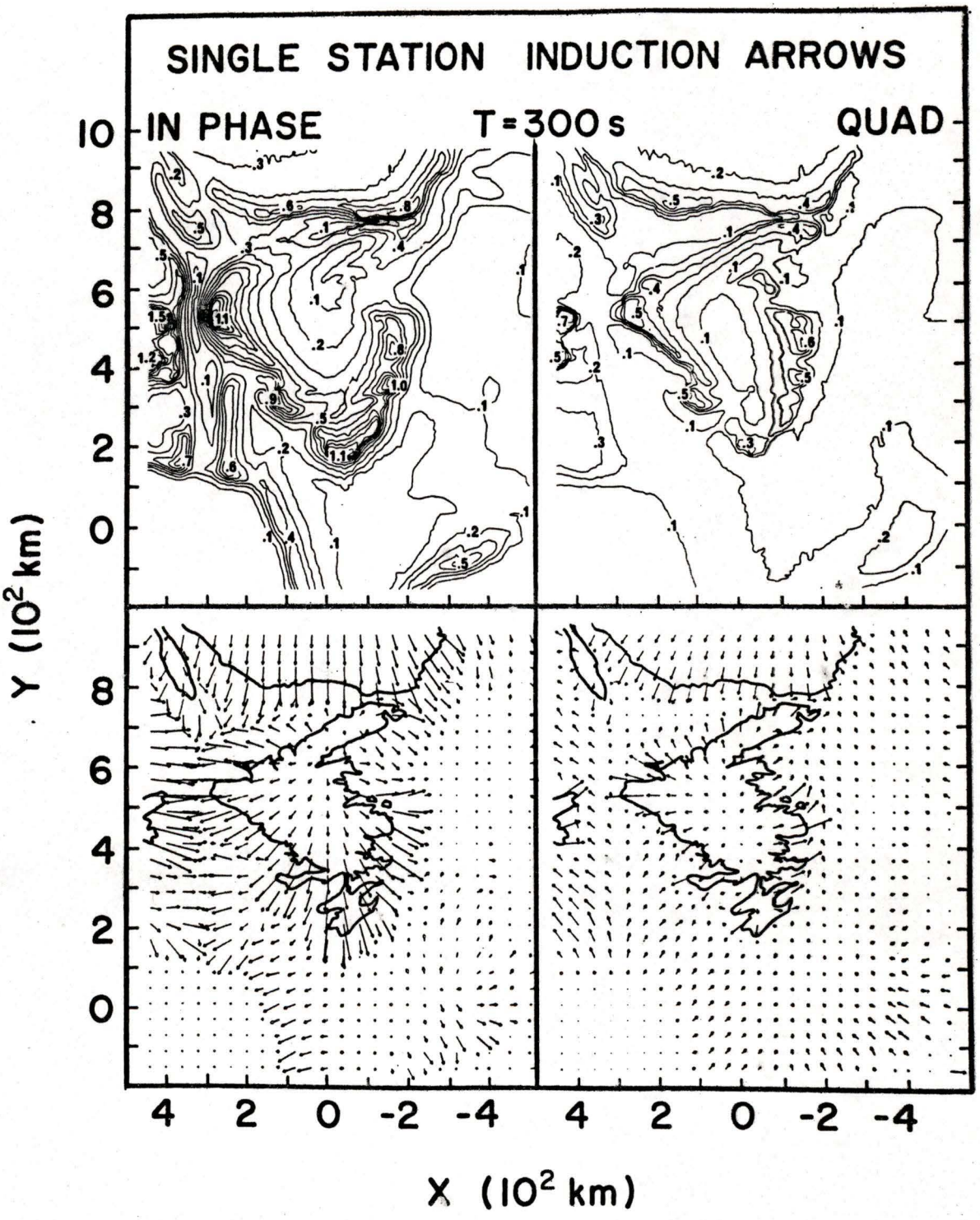

FIGURE 5.3.1 Single station induction arrows for a period of 300s

results. This is due to the relative increase in the current density in the deep ocean in the southern section of the model compared to the current density in the Strait of Belle Isle. The magnitude contours of the in-phase arrows for the 300s period delineate the southern edge of the shelf better than the magnitude contours of the in-phase arrows for a period of 100s. The arrow direction is towards the nearest current density, usually the nearest ocean. The direction of the arrow is rotated slightly to the deep ocean for certain locations. The quadrature arrows for the 300s period delineate the coastline better than the quadrature arrows for the 100s period. The quadrature arrow magnitude reaches a maximum at the capes. As for the 100s period, the quadrature arrows reverse direction over the land-sea interface but it is not as evident for the 300s period as for the 100s period. The quadrature arrows point away from the continental shelf towards the deep ocean. The in-phase and quadrature arrow magnitudes over the deep ocean are approximately zero.

The single station induction arrows for the 900s period are shown in Fig. 5.3.2. The coastlines are less evident in the in phase contour diagrams as for the shorter periods. The in-phase arrows show the location of a few capes and delineate the continental shelf. The direction of the in phase arrow is towards the deep ocean or Cabot Strait depending on the location. The quadrature arrow reaches a

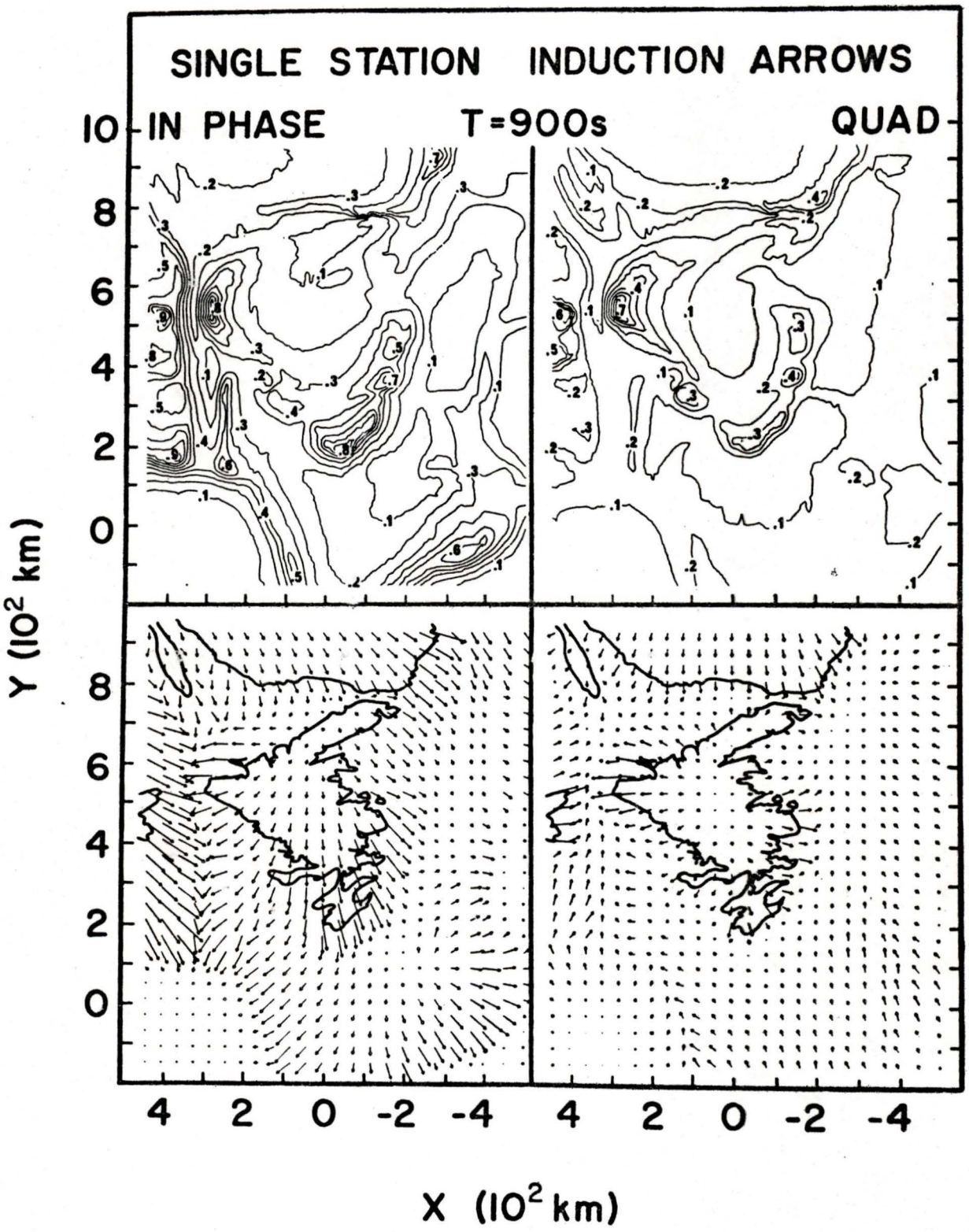

FIGURE 5.3.2 Single station induction arrows for a period of 900s

maximum at the capes on Cabot Strait. The continental shelf is not evident in the contour diagrams of the quadrature arrows. The quadrature arrows do not appear to reverse direction over the land-sea conductivity contrast as they did for periods of 100s and 300s.

For the 1800s period, the single station induction arrows are shown in Fig. 5.3.3. The in-phase arrows delineate the continental shelf but not the coastlines. Only a few capes are distinguishable as coastline features in the in-phase contour diagram. The in-phase arrows decrease less rapidly over the deep ocean for the 1800s period than the 900s in-phase arrows. As for the 900s period, the in-phase arrows point to either the deep ocean or are rotated towards Cabot Strait depending on the location. The quadrature arrow magnitude reaches a maximum at the capes. The quadrature arrows do not delineate the shelf edge. As for the 900s period, the quadrature arrows do not reverse direction at the coastline.

For increasing period, the location of the in-phase maximum changes from the coastlines for a period of 100s to the continental shelf at a period of 1800s. The direction of the in-phase arrow is towards the nearest current concentration. For the shorter periods, this direction is to the nearest conductor (ocean). As the period increases, the direction of the arrow is rotated to the deeper ocean. For

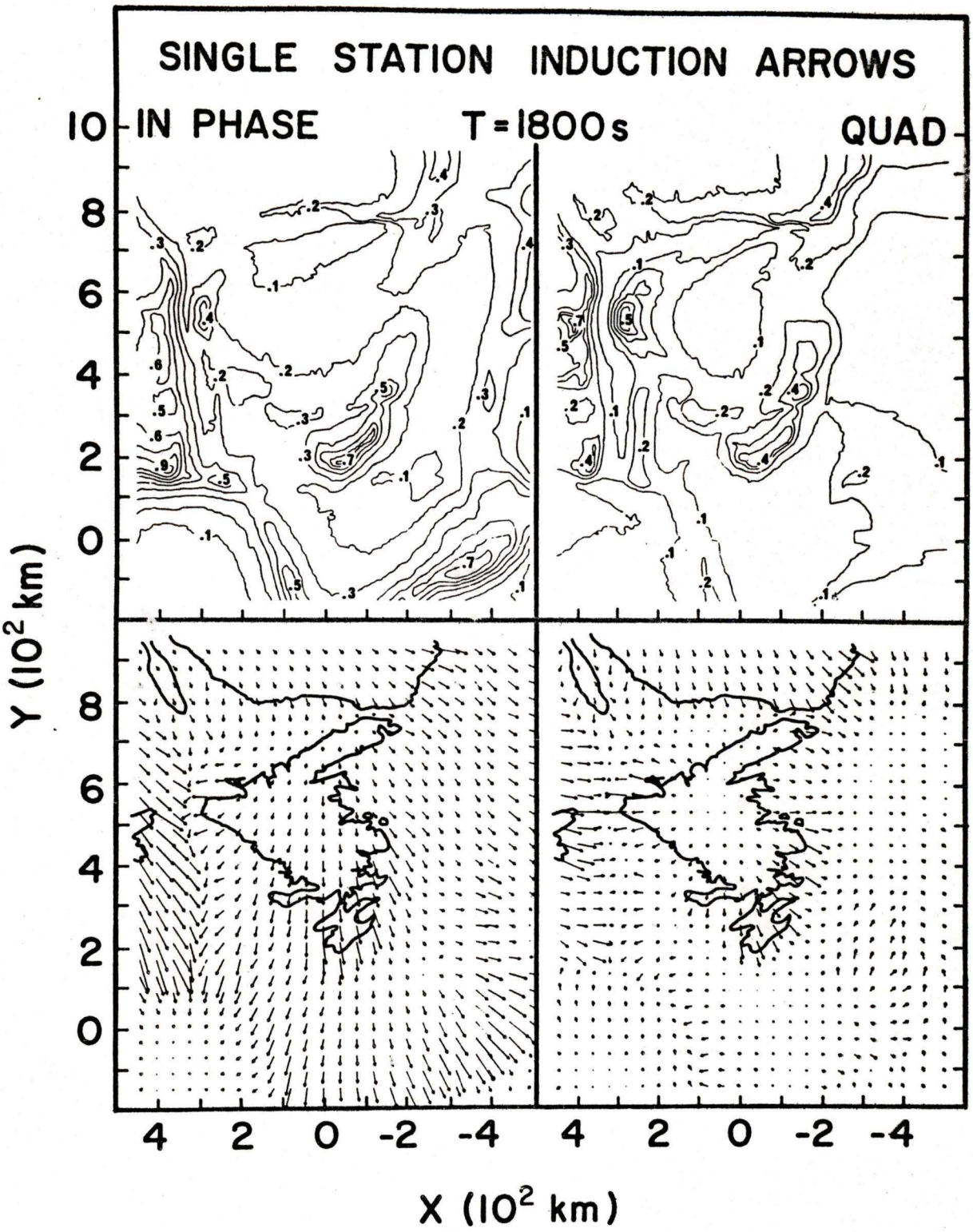

FIGURE 5.3.3 Single station induction arrows for a period of 1800s

the 900s period, the deeper ocean includes Cabot Strait. At a period of 1800s, the deep ocean off the shelf at the southern and eastern sections of the model region dominates and the effect of Cabot Strait decreases.

For the two shorter periods, 100s and 300s, the quadrature arrows reverse direction over the land-sea interface. For the two longer periods, 900s and 1800s, this reversal does not happen. The maximum in the magnitude of the quadrature arrows occurs at the capes. Over the frequency range studied, there is little variation in the size of the quadrature arrows . This is especially noticeable at the coastlines.

CHAPTER 6

COMPARISON OF FIELD AND MODEL RESULTS

6.1 Introduction

Field station results in the Newfoundland region were taken from the results of Hyndman and Cochrane(1971), Bailey et al.(1974), Cochrane and Wright(1977), and Wright(1981, private communication). The location and source of results for each of the fifteen field stations in the region studied are shown in Table 6.1.1. The induction arrows calculated at these stations are compared to model single station induction arrows for the same geographical area.

Magnetic field components at two field stations, Stephenville and Cape North, of Hyndman and Cochrane(1971) were obtained using three component flux-gate magnetometers and chart recorders. Transfer functions were calculated for periods between 120s and 7200s. The model results for the 100s period were compared to field results at a period of 120s. Comparisons of model and field station results for the other three periods were made at the appropiate periods.

STATION	LOCATION		SOURCE
	LATITUDE	LONGITUDE	
Bonavista (BNV)	48° 43'N	53° 06'W	A
Cape North (CN)	46° 53'N	60° 30'W	B
Deer Lake (DL)	49° 12'N	57° 17'W	C
Exploits (EXP)	48° 52'N	56° 18'W	A
Flowers Cove (FLC)	51° 18'N	56° 43'W	A
Green Point (GP)	49° 40'N	57° 56'W	D
Little Hearts Ease (LHE)	48° 01'N	53° 42'W	A
Marystown (MTN)	47° 10'N	55° 10'W	A
New World Island (NWI)	49° 29'N	54° 50'W	A
Northwest Gander (NWG)	48° 27'N	55° 27'W	D
Serpentine Lake (SL)	48° 55'N	58° 11'W	D
Stephenville (SV)	48° 20'N	58° 20'W	B
St. John's (STJ)	47° 35'N	52° 40'W	A
Trepassey (TRE)	46° 43'N	53° 24'W	A
Whalehead (WH)	50° 42'N	59° 20'W	C

TABLE 6.1.1 Location and source of each field station (A - Cochrane and Wright(1977), B - Hyndman and Cochrane(1971), C - Bailey et al.(1974), D - Wright(1981, private communication)

Three component flux-gate magnetometers were used by Bailey et al.(1974) in measuring the magnetic field at Whalehead and Deer Lake. Transfer functions calculated for Whalehead covered the range of periods studied for the analogue model while results for Deer Lake covered the period range from 120s to 3870s. As with the Hyndman and Cochrane(1971) results, the field results for the 120s period at Deer Lake were compared to the 100s model results. All other comparisons between field and model results are at the same periods.

The magnetic field measurements of Cochrane and Wright(1971) and Wright(1981, private communication) were taken from an EDA flux-gate magnetometer and then low pass filtered at a 200s period. Digital sampling of the field component was every 64s. The shortest usable period for the transfer function calculations is 128s but the field variations for periods shorter than 200s have been filtered. Therefore the transfer function results for the field stations were extrapolated to a period of 100s. All comparisons of field and model results were made at the periods simulated in the model.

The accuracy of a field station induction arrow depends on many factors such as the length of data obtained and the amount of activity present. The field station induction arrows shown in this thesis have an approximate uncertainity

of 0.05 in their magnitude and 30^{o} in their direction.

The fifteen stations in the Newfoundland region can be separated into two major groups. In Fig. 6.1.1 the stations, Green Point(GP), Serpentine Lake(SL), Stephenville(SV), Deer Lake(DL), Exploits(EXP), New World Island(NWI), and Northwest Gander(NWG) are located near the major faults in the central region of Newfoundland shown in Fig. 6.1.2. The remainder of the stations, Whalehead(WH), Flower Cover(FLC), Cape North(CN), Bonavista(BNV), Marystown(MTN), Little Hearts Ease(LHE), St. John's(STJ) and Trepassey(TRE) are located either south or north of the fault zone.

6.2 Stations Located in the Central Region of Newfoundland

At a period of 100s, the in-phase induction arrows in Fig. 6.2.1 for the seven field stations in the central region of Newfoundland show little agreement with model results. For example, at Serpentine Lake, the in-phase arrow from the field results points towards Cabot Strait while the in-phase arrow from the model results points to Gaspé and is larger. At the New World Island station, the in-phase induction arrow from the model results is approximately five times larger and perpendicular to the in-phase arrow from the field results.

If the anomalous field present at a station could be separated into the part due to the coast effect and the part

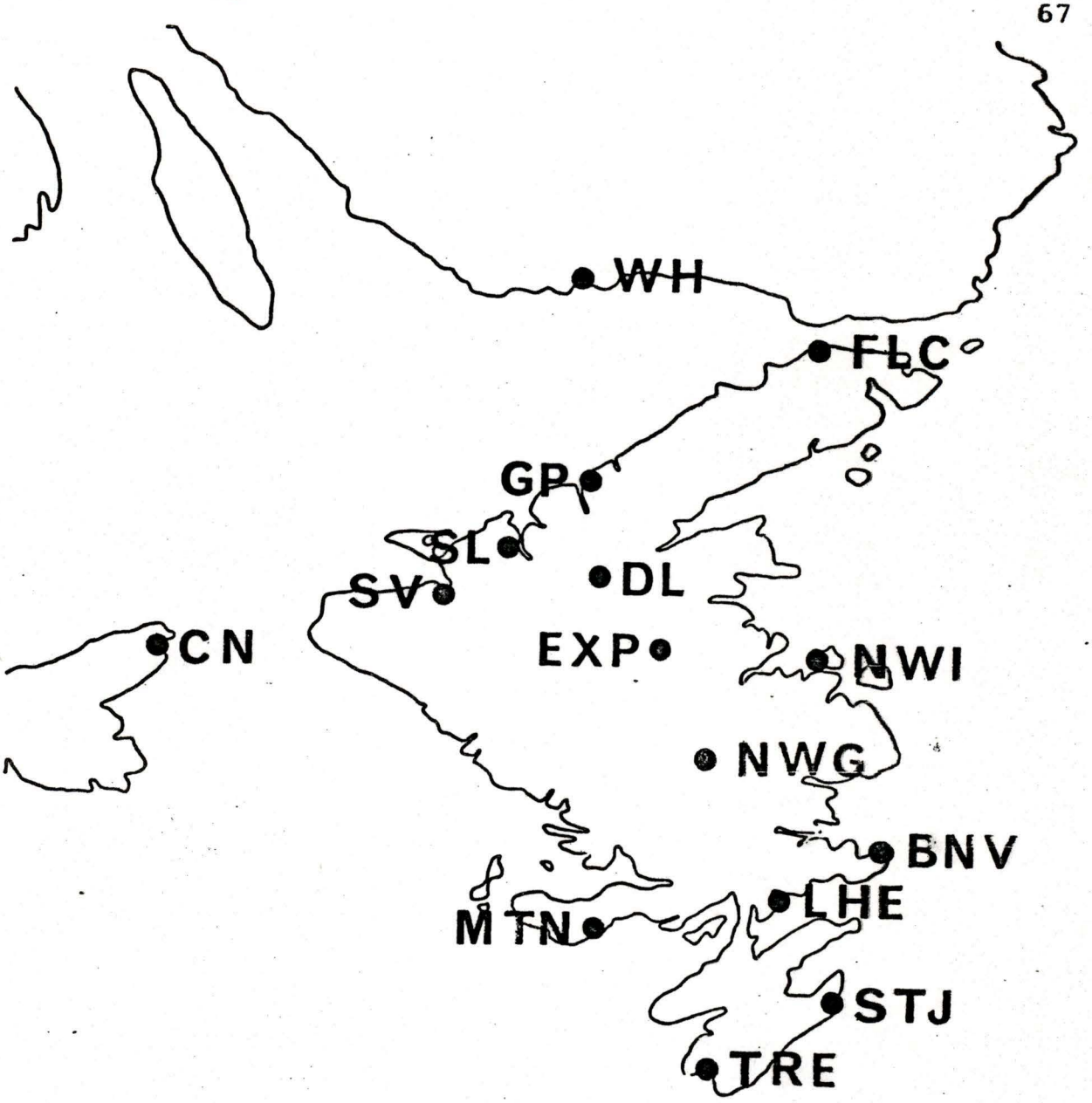

FIGURE 6.1.1 Location of field stations (WH -Whalehead, FLC -Flower Cove, GP -Green Point, SL -Serpentine Lake, DL -Deer Lake, SV -Stephenville, CN -Cape North, EXP -Exploits, NWI -New World Island, NWG - Northwest Gander, BNV -Bonavista, LHE -Little Hearts Ease, MTN -Marystown, STJ -St. John's, TRE - Trepassey)

FIGURE 6.1.2 Location of major faults in the Newfoundland region

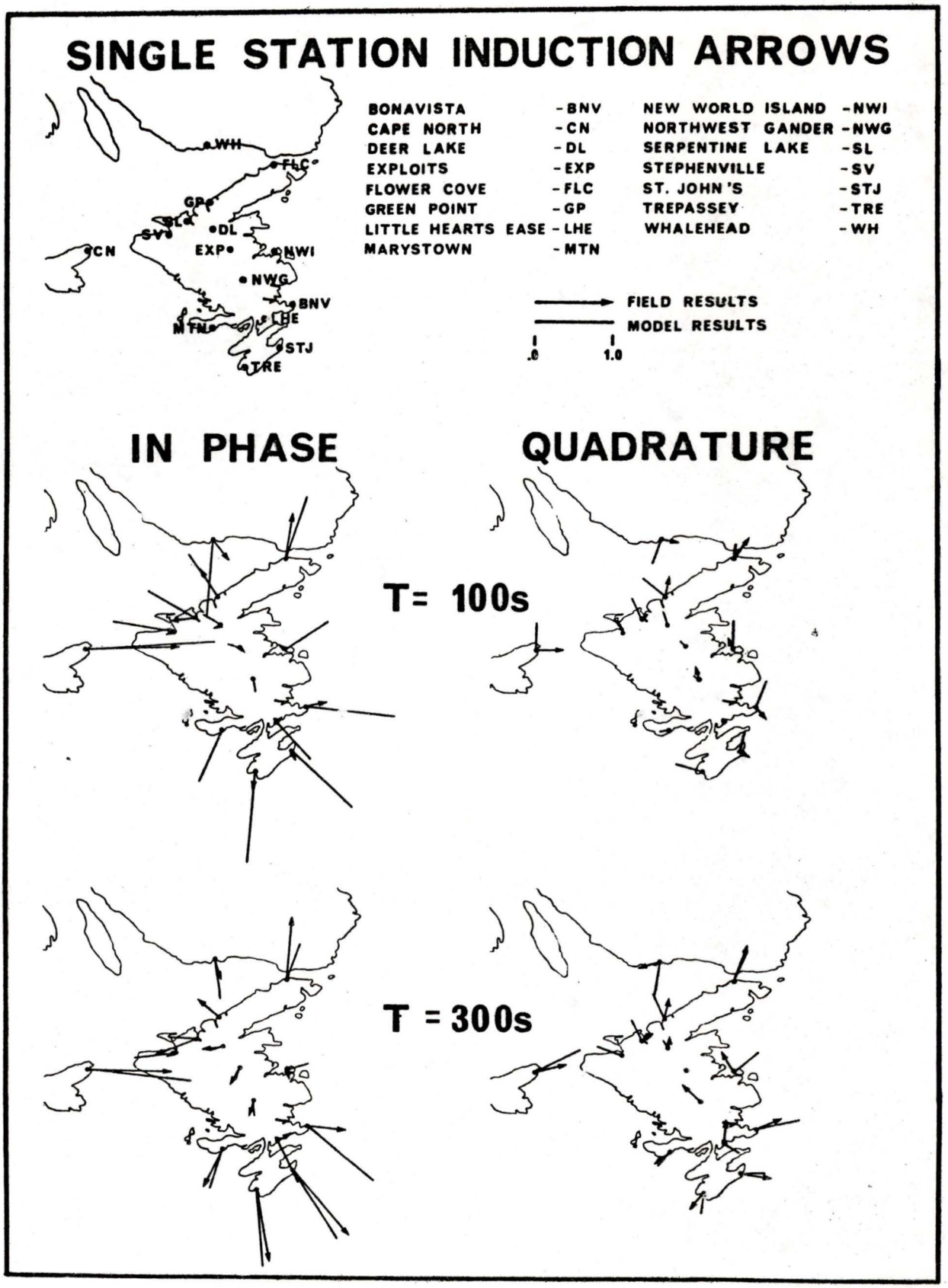

FIGURE 6.2.1 Field and model single station induction arrows for periods of 100s and 300s

due to the underlying structure, a simple vector subtraction of the model (coast effect) induction arrow from the field station (total) induction arrow would give an induction arrow due to the underlying structure (difference arrow). The anomalous field can be separated into these two parts if there is little or no interaction between the fields produced by the coast effect and the underlying structure which is assumed in this thesis.

An approximate vector subtraction of the model induction in-phase arrows from the field induction in-phase arrows for the station in this central region of Newfoundland shows that the resulting difference in-phase induction arrow points generally to the massive fault zone present in central Newfoundland. For example, a vector subtraction of model and field in-phase arrows for Deer Lake shows that the difference arrow points towards central Newfoundland.

The field station quadrature arrows for all stations in this region are very small and probably not significant except for the arrow at the Green Point station. A vector subtraction of field and model results for this location results in a difference arrow pointing towards the long fault running northward along the northern section of Newfoundland shown in Fig. 6.1.2.

The field station in-phase arrows for the 300s period in Fig. 6.2.1 show good agreement with model results for

stations in the centre and south of the major fault system, eg. Exploits. Stations north of the system, such as Serpentine Lake, show the effects due to both the fault and nearby coastline. The difference induction arrows are due to the underlying structure and generally point towards the fault system at this period.

The quadrature arrows for the field results at the 300s period are generally very small. The two main exceptions are at Green Point and New World Island. The difference induction arrows for these two stations again point towards the faults. The large quadrature arrow for field results at Northwest Gander also points towards the fault zone. This arrow is the difference arrow since there is a very small quadrature arrow present at this location in the model results; thus the field induction arrow must be due to the underlying structure in the region.

At the longer periods of 900s and 1800s, Fig. 6.2.2 shows that the field station in-phase induction arrows are larger than the model in-phase arrows. The directions of the field station induction arrows agree with the directions of model induction arrows. The general direction of these arrows is towards the deep ocean. A deep conducting layer that extends over the southern half of the Newfoundland region could produce this result. In the model study, the

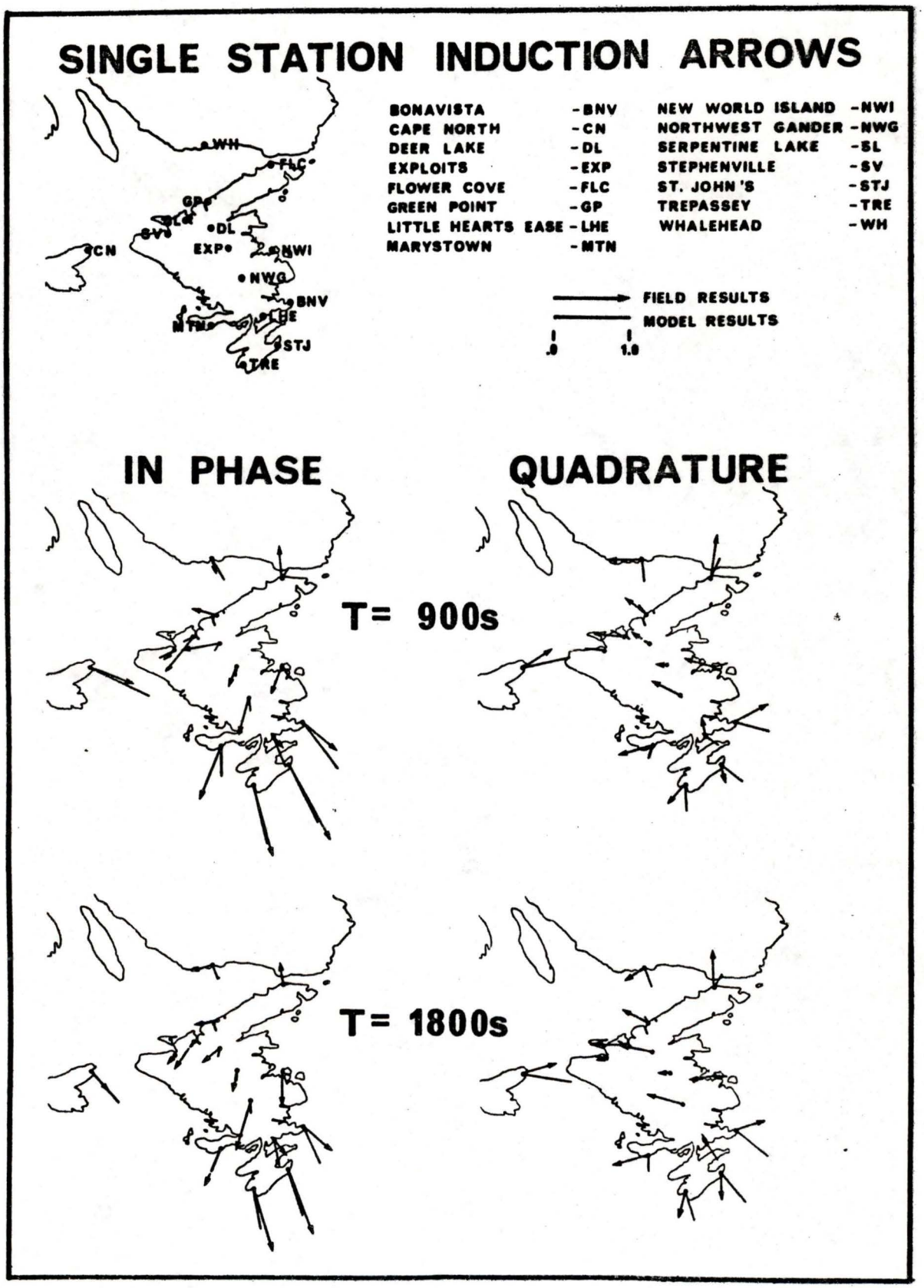

FIGURE 6.2.2 Field and model single station induction arrows for periods of 900s and 1800s

deep conductive layer was under the whole region thus not giving a conductivity contrast at depth in the horizontal direction. Cochrane and Hyndman(1971) proposed such a highly conductive layer from central Nova Scotia to the deep ocean for a two-dimensional numerical model based on their field results. This layer could extend to central Newfoundland.

The field station quadrature arrows for the 900s and 1800s period point towards the Cabot Strait region. There are no significant model quadrature arrows for these stations at these periods. It is difficult to determine what is producing this behavior in the quadrature arrows at the field stations.

6.3 Stations Located in the Northern and Southern Regions of Newfoundland

The two field stations, Whalehead(WH) and Flower Cove(FLC) in the northern section of the Newfoundland region are located away from the major faults in the modelled region. Similarly, the five southern stations, Cape North(CN), Bonavista(BNV), Little Hearts Ease(LHE), Marystown(MTN), St. John's(STJ), and Trepassey(TRE) are located away from the fault zone.

In Fig. 6.2.1 at Bonavista, Marystown, Little Hearts Ease, St. John's, and Trepassey, there is no agreement in the magnitude of model and field in-phase induction arrows at a

period of 100s. The model in-phase arrows are orders of magnitude larger than those of field results. Similarly there is little agreement between the model and field quadrature arrows for this period. Field results at these stations for this period are probably unreliable due to extrapolation of the transfer functions calculated. For the model results, the ocean depth of the model near the coastline is probably overestimated thus increasing the magnitude of the model arrows. These reasons could explain the difference between field and model results.

For the 100s period, the in-phase arrows at Cape North and Flower Cove, and the quadrature arrows at Flower Cove show agreement between field and model results. This demonstrates that the coast effect is the main effect at these stations for this period. The quadrature arrows at Cape North show that the arrows for the model and field results have the same magnitude but are perpendicular. No obvious explanation is apparent to explain this behavior.

At Whalehead, there is a difference between model and field results for both in-phase and quadrature arrows. Kurtz(1973) states that there is a fault located northeast of the Whalehead station. The in-phase and quadrature difference arrows point generally in this direction.

There is general agreement between field and model

results at the southern and northern stations for the 300s period. The only disagreement between the field and model results occurs at Little Hearts Ease, Bonavista, and Whalehead. At Whalehead, the poor agreement in the quadrature arrows can be explained by the fault in the region. The in-phase and quadrature difference arrows for Little Hearts Ease point towards central Newfoundland. This result could be explained by a buried conducting body located inland from Little Hearts Ease. At Bonavista, there is only disagreement in the model and field results for the in-phase arrow. The in-phase difference arrow at Bonavista points towards New World Island. This difference between model and field results at Bonavista could be explained by either the fault zone near New World Island or inadequate modelling of the ocean around this region.

There is general agreement of model and field in-phase induction arrows at the northern and southern stations for the 900s and 1800s periods as shown in Fig. 6.2.2. There is a greater difference between model and field results present for the quadrature arrows for these periods. It appears that the field station quadrature arrows are more sensitive to local conductivity anomalies than the in-phase arrows. This would explain the good agreement found in the in-phase arrows and poorer agreement in the quadrature arrows for field and model results. As discussed in Section 6.2, the difference

quadrature arrows could be due to the boundary of the conducting contrast speculated at depth from model and field results for stations in central Newfoundland, discussed in Section 6.2.

CHAPTER 7

SUMMARY AND CONCLUSIONS

The analogue model study of the Newfoundland region has brought out many interesting features. The well-known coast effect is evident for a straight coastlines, eg. the southern Labrador-Quebec coastline. The effect of the straits, capes, and the continental shelf is also evident in the model.

7.1 The Effect of a Strait

In the analogue model, there are two straits, Cabot Strait and the Strait of Belle Isle, which are of interest. The direction of Cabot Strait is perpendicular to the Strait of Belle Isle and parallel to the electric field of the source for B-polarization. From model results, an anomalous field arises over the strait only when the electric field of the source has a component parallel to the strait direction. For this case, the magnetic field component perpendicular to the direction of the strait reaches a maximum over the centre of the strait. This is evident for the Strait of Belle Isle where in-phase B_y (E-Pol) in Fig. 4.1.1 reaches a maximum of

3.0 nT. A large vertical field is present near the coastlines reaching a maximum at the land-sea interface. A line current representing the induced current in the strait can be used to determine the magnetic field components produced by induced current in the strait. The direction of the line current corresponds to the direction of the strait.

7.2 The Effect of a Cape

The southern tip of Newfoundland and the two capes on the sides of Cabot Strait were used in studying the effect of a cape. The magnetic field behavior at a cape was studied for the polarization with the electric field of the source parallel to the coastline of the cape tip. The magnetic field component perpendicular to the coastline at the end of the cape reaches a maximum just seaward of the cape tip. The magnetic field component parallel to the cape tip coastline reaches a maximum just seaward of the sides of the cape. This field component undergoes a 180^{o} phase shift across the cape. A vertical magnetic field is present at the cape coastline and reaches a maximum at the tip of the cape. The magnitude of the vertical field at the cape coastline is larger than the magnitude of the vertical field at a straight coastline as found by Chan et al.(1981). The cape effect demonstrates the deflection of current around the cape and

the increased current density in the ocean at the tip of the cape.

7.3 The Effect of a Continental Shelf

The edge of the continental shelf in the Newfoundland region is located a large distance from the coastline unlike the shelf edge on the west coast of Canada. This allows one to study the anomalous magnetic field produced over a continental shelf edge separately from the anomalous field produced at the coastline. For the short period studied, 100s, there was no significant anomalous magnetic field produced at the continental shelf edge. For long periods, such as 900s and 1800s, an anomalous magnetic field was produced at the shelf edge as if a coastline was present. There is an enhancement in the horizontal magnetic field component perpendicular to the shelf edge on the deep ocean side of the edge. A vertical magnetic field component is also observed at the edge of the continental shelf.

7.4 Frequency Dependence of the Magnetic Field

The four periods studied allow the frequency dependence of the anomalous field produced at straits, capes, and the continental shelf to be investigated. Figure 7.4.1 shows the locations of the anomalous horizontal magnetic field for the Strait of Belle Isle (A), Cabot Strait (B), the southern tip

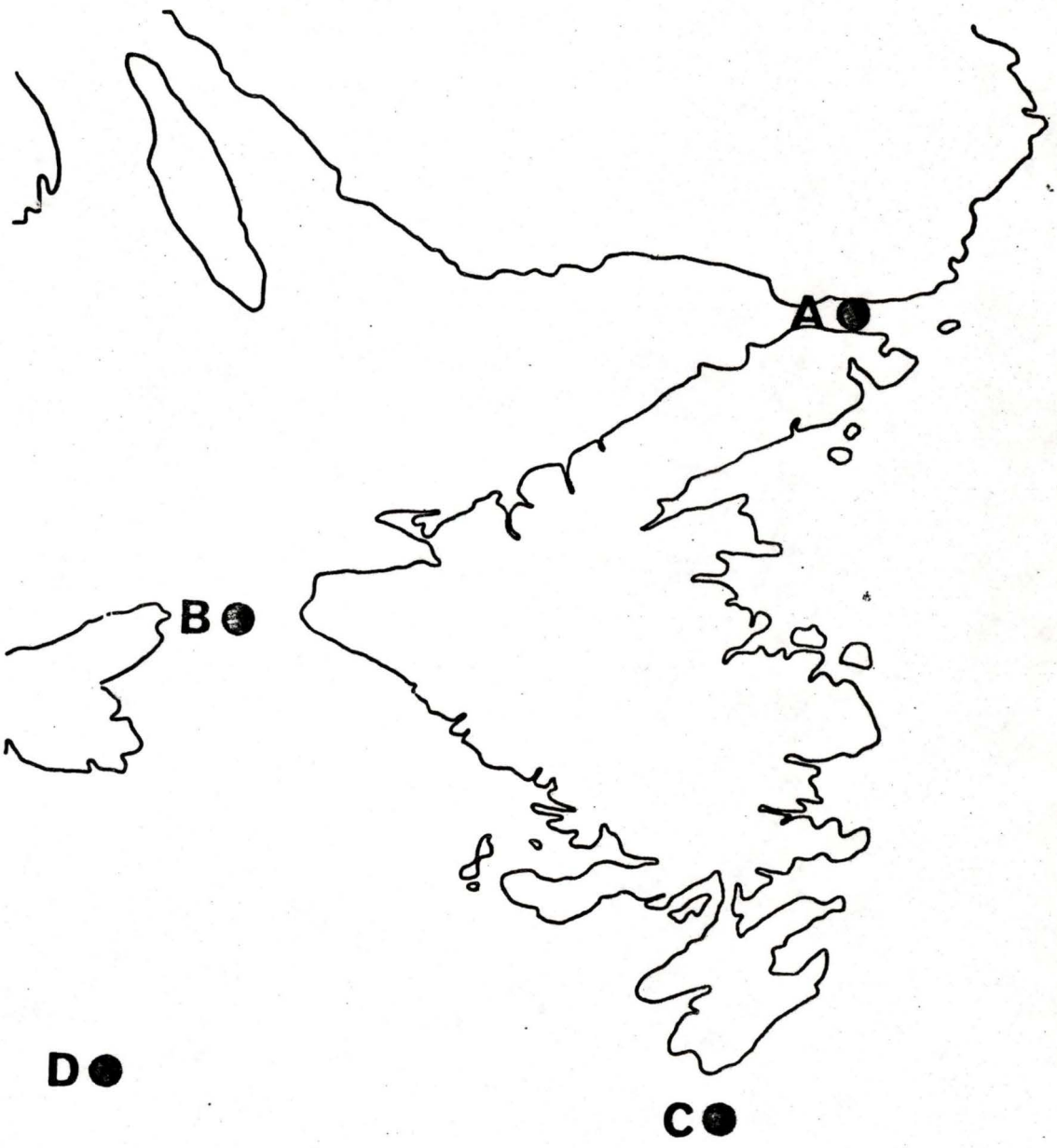

FIGURE 7.4.1 Locations of anomalous horizontal field measurements used for frequency response of straits, cape, and continent shelf edge

of Newfoundland as a cape (C), and the continental shelf edge (D) used in studying the frequency dependence of magnetic field. At these locations, the anomalous horizontal field reaches a maximum for the straits, cape, and shelf edge. The frequency dependence of the magnitude and phase of this magnetic field component for these locations is shown in Fig. 7.4.2. The phase of the anomalous field is relative to the reference station.

Figure 7.4.2 shows that the maximum response of the Strait of Belle Isle occurs at a period less than 100s. A two-dimensional model of the Strait of Belle Isle shows that the maximum in the horizontal field occurs around a period of 30s. For this period, the depth of the Strait of Belle Isle is 0.12 skin-depths. The maximum response of Cabot Strait occurs around a period of 300s when the depth of the strait is approximately 0.15 skin-depths. Thus the maximum response of the straits occurs when the depth of the strait is approximately 0.14 skin-depths.

The frequency response of a cape, shown by C in Fig. 7.4.2, shows that the effect due to a cape can be significant for long periods such as 1800s even for capes with shallow oceans. The magnitude of the cape effect decreases slowly with increasing period.

The maximum field for the continental shelf edge occurs between 900s and 1800s. In this period range, the ocean

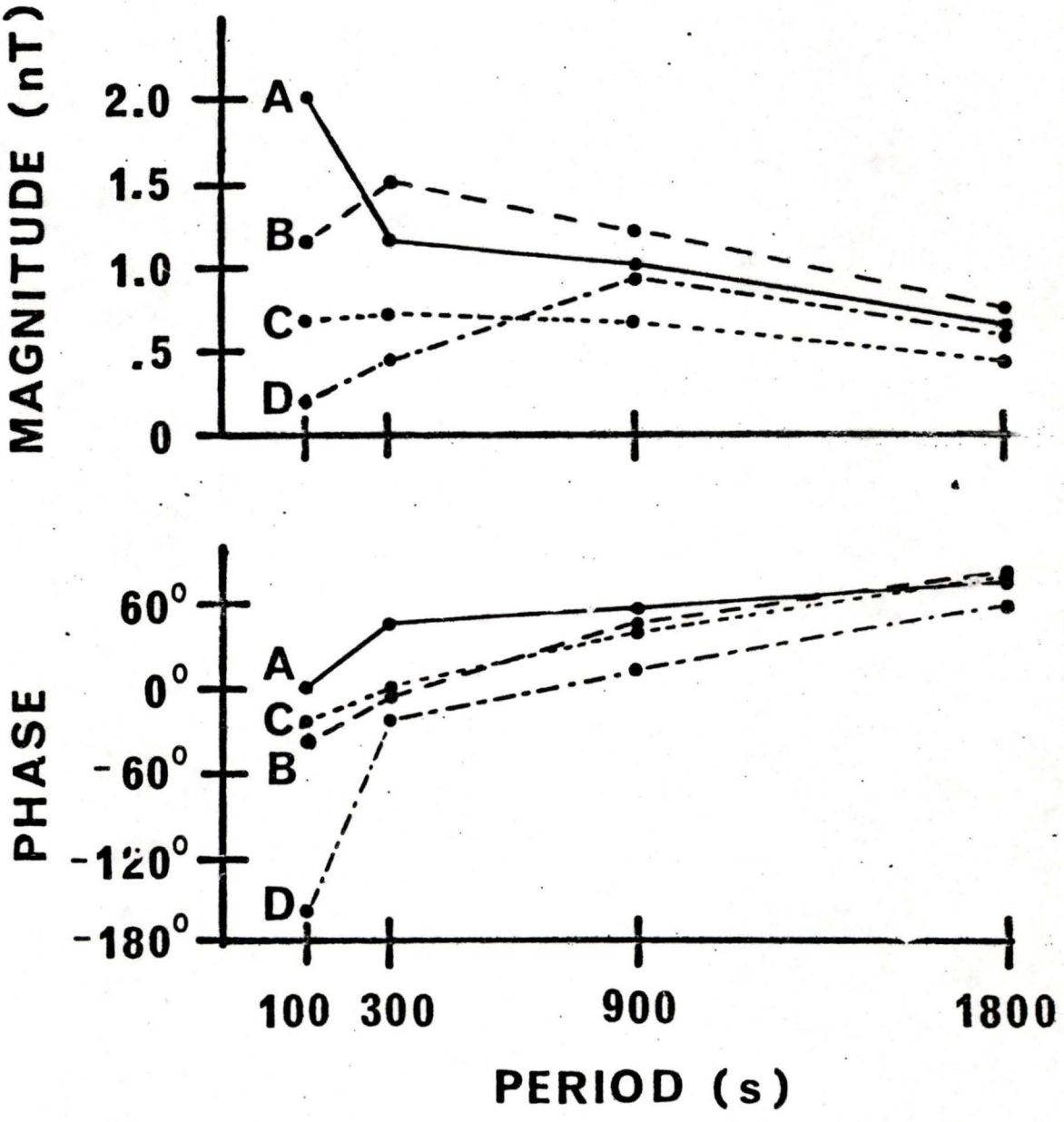

FIGURE 7.4.2 Magnitude and phase of the anomalous horizontal field for the Strait of Belle Isle (A), Cabot Strait (B), southern tip of Newfoundland (C), and the continental shelf edge (D)

depth on the shelf is approximately 0.04 skin-depths while the depth of the deep ocean is 0.4 skin-depths. For the 100s period, no anomalous field (greater than 0.2nT) occurs at the shelf edge. The ocean depth for the 100s period ranges from 0.15 to 1.5 skin-depths from the shelf to the deep ocean. If the conductor is very thin (less than 0.04 skin-depths) on one side of a thickness transition and thick (greater than 0.04 skin-depths) on the other side, an anomalous field should be produced by induction. Figures of the magnetic field components in Chapter 4 show the spatial gradient of the conductor thickness is also important, which is evident by comparing the anomalous field over the shelf edge for the southern and eastern sections of the model. The larger gradient over the shelf edge in the southern section produces a larger anomalous field than the thickness transition of the ocean for the eastern section of the region.

The phase of the anomalous field for all four locations shows that the phase lead of the anomalous field with respect to the reference field increases with increasing period. For very long periods, the phase lead appears to approach a limit. The reason for this behavior is not clear.

7.5 Comparison of Single Station and Inter-station Induction Arrows

The comparison of single station and inter-station induction arrows in Section 5.2 shows that the difference between the two types of arrows occurs when an anomalous horizontal field is present. An enhancement in the horizontal magnetic field produces the difference between the magnitude of the single station arrow and inter-station arrow at the same location. Thus the single station arrows are smaller than inter-station arrows over the ocean and at the coastlines and single station arrows are larger than inter-station arrows just inland from the coastline.

7.6 Frequency Dependence of Single Station Induction Arrows

The direction of the in-phase arrows for the short periods is towards the nearest ocean (conductor). As the period of the source field increases, the direction of the in-phase arrows rotates towards the deep ocean. Thus the in-phase arrows point towards the nearest and largest current density. The magnitude of the in-phase arrow reaches a maximum just landward of the land-sea interface.

The quadrature arrows reverse direction over the land-sea interface for short periods, for example, at 100s. At longer periods, this reversal is not evident. The magnitude

of the quadrature arrow reaches a maximum at the conductivity contrasts.

7.7 Comparison of Model and Field Results

A comparison of model and field results shows that the results from the stations can be divided into two groups. The results from stations located in the central region of Newfoundland greatly differ from model results. For vector subtraction of model arrows from field arrows, the resulting difference arrows point towards the faults in the region. The other stations show that the anomalous field at these stations is due mainly to the land-sea conductivity contrast.

Examining the relationship between model and field results for different periods, there could be a horizontal conductivity contrast at depth. The difference between field and model results for Newfoundland for long periods leads to the assumption of a highly conductive layer present under the southern section of the Newfoundland region.

7.8 Recommendations for Further Work

Recommended further work in studying electromagnetic induction in the Newfoundland region can be divided into three sections:

First, there is the unending desire for more and better field data. This is especially true for short periods such

as the 100s period studied. A line of station measurements should be made across the fault zone in central Newfoundland to investigate the region. It would be useful if simultaneous measurements could be taken to allow the calculation of difference fields and thus induction arrows using only the anomalous fields.

Second, the study of the behavior of in-phase and quadrature arrows for simple three-dimensional problems should be undertaken. The dependence of these arrows on different parameters, such as the depth of the conducting body, would aid in interpreting field and model results. A study should be made to test the difference arrow hypothesis. If the anomalous field from two conducting bodies can be separated thus allowing the calculation of difference arrows, it would be a great aid in determining the underlying structure in many regions.

Third, more measurements of the magnetic field over Newfoundland for different periods could be undertaken. For example, the maximum response of the Strait of Belle Isle for the model could be determined to check the numerical results. The graphite plate used for the conductive geomagnetic mantle could be placed under only the southern section of the Newfoundland region instead of under the whole model. This would allow testing the hypothesis of a conductivity contrast

at depth.

These three areas are probably the most promising to help determine the geological structure in the Newfoundland region using electromagnetic induction.

REFERENCES

Babour, K. and Mosnier, J. 1979. Differential geomagnetic sounding in the Rhinegraben, Geophys. J. R. astr. Soc., 58, 135-144.

Babour, K., Mosnier, J., Daignieres, M., Vasseur, G., Le Mouel, J. L. and Rossignol, J. C. 1976. A geomagnetic variation anomaly in the northern Pyrenees, Geophys. J. R. astr. Soc., 45, 583-600.

Bailey, R. C., Edwards, R. N., Garland, G. D., Kurtz, R. D. and Pitcher, D. 1974. Electrical conductivity studies over a tectonically active area in eastern Canada, J. Geomag. Geoelectr., 26, 125-146.

Brewitt-Taylor, C. R. 1976. A computer program for the solution of electromagnetic induction problems (revised 1977), Dept. of Physics, University of Victoria, Victoria, British Columbia.

Brewitt-Taylor, C. R. and Weaver, J. T. 1976. On the finite difference solution of two-dimensional induction

problems, Geophys. J.R. astr. Soc., 47, 375-396.

Chan, E., Dosso, H. W., and Law, L. K. 1981. An analogue model study of electromagnetic induction in the Queen Charlotte Islands region, J. Geomag. Geoelectr., 33, 587-605.

Chan, G. H., Dosso, H. W. and Law, L. K. 1981. An analogue model study of electromagnetic induction for cape and bay coastlines, Phys. Earth Planet. Int., 27, 167-176.

Chapman, S. 1919. The solar and lunar diurnal variations of terrestrial magnetism, Phil. Trans. Roy. Soc. (London) Ser. A, 218, 1-118.

Chapman, S. and Whitehead, T. T. 1922. The influence of electrically conducting material with the earth on various phenomena of terrestrial magnetism, Trans. Camb. Phil. Soc., 22, 463-482.

Church, W. R. and Stevens, R. K. 1971. Early Palezoic ophiolite complexes of the Newfoundland Appalachians as mantle-oceanic crust sequences, J. Geophys. Res., 76, 1460-1466.

Cochrane, N. A. and Hyndman, R. D. 1974. Magnetotelluric and magnetovariational studies in Atlantic Canada, Geophys. J. R. astr. Soc., 39, 385-406.

Cochrane, N. A. and Wright, J. A. 1977. Geomagnetic sounding near the nothern termination of the Appalachian system, Can. J. Earth Sci., 14, 2858-2864.

Conte, S. D. and de Boor, Carl 1972. Elementary Numerical Analysis: an alogorithmic approach, McGraw-Hill Book Company

Dawson, T. W., Weaver, J. T. and Raval, U. 1979. B-polarization induction in two generalized thin sheets at the surface of a conducting half-space, Geophys. J. R. astr. Soc., 69, 209-234.

Dewey, John F. and Bird, John M. 1971. Origin and emplacement of the ophiolite suite: Appalachian ophiolites in Newfoundland, J. Geophys. Res., 76, 3179-3206.

Dosso, H. W. 1966. Analytical and analogue methods of studying electromagnetic variations at the earth's surface, Ph.D. Thesis, University of British Columbia, Vancouver, British Columbia

Dosso, H. W. 1973. A review of analogue model studies of the coast effect, Phys. Earth Planet. Int., 7, 294-302.

Dosso, H. W., Nienaber, W. and Hutton, V. R. S. 1980a. An

analogue model study of electromagnetic induction in the British Isles region, Phys. Earth Planet. Int., 22, 68-85.

Dosso, H. W., Nienaber, W., Wright, J. A., Greenhouse, J. P. and Bailey, R. C. 1980b. An analogue model study of electromagnetic induction in the eastern coastal region of North America, Phys. Earth Planet. Int., 23, 13-30.

Dupis, A. and Thera, A. L. 1982. Natural electromagnetism in the Rhine Graben, Geophys. J. R. astr. Soc., 68, 547-557.

Edwards, R. N., Law, L. K., and White, A. 1971. Geomagnetic variations in the British Isles and their relation to electrical currents in the ocean and shallow seas, Phil. Trans. Roy. Soc. (London) Ser. A, 270, 289-323.

Everett, J. E. and Hyndman, R. D. 1967a. Geomagnetic variations and electrical conductivity structure in south-western Australia, Phys. Earth Planet. Int., 1, 24-34.

Everett, J. E. and Hyndman, R. D. 1967b. Magneto-telluric investigations in south-western Australia, Phys. Earth Planet. Int., 1, 49-54.

Fainberg, E. R. and Zinger, B. Sh. 1981. Electromagnetic induction in a spherical model of the earth with a real distribution of near surface conductivity, Phys. Earth Planet. Int., 25, 52-56.

Fenwick, D. K. B., Keen, M. J., Keen, Charlotte and Lambert, A. 1968. Geophysical studies of the continental margin northeast of Newfoundland, Can. J. Earth Sci., 5, 483-500.

Fischer, Gaston 1979. Electromagnetic induction effects at an ocean coast, Proc. IEEE, 67, 1050-1060.

Forrester, W. D. 1964. A quantitative temperature- salinity study of the Gulf of St. Lawrence (unpublished manuscript), Report B.I.O. 64-11, Bedford Inst. Oceanog., Dartmouth, NS, Canada.

Grant, F. S. and West, G. F. 1965. Interpretation Theory in Applied Geophysics, McGraw-Hill Book Company

Green, V. R. and Weaver, J. T. 1978. Two-dimensional induction in a thin sheet of variable integrated conductivity at the surface of a uniformly conducting earth, Geophys. J. R. astr. Soc., 55, 721-736.

Greenhouse, J. P. and Bailey, R. C. 1981. A review of geomagnetic variation measurements in the eastern United

States: Implications for continental tectonics, Can. J. Earth Sci., 18, 1268-1289.

Gregori, G. P. and Lanzerotti, L. J. 1980. Geomagnetic depth sounding by induction arrow representation: A review, Rev. Geophys. Space Physics, 18, 203-209.

Hermance, John F. 1982. Refined finite-difference simulations using local integral forms: Applications to telluric fields in two dimensions, Geophysics, 47, 825-831.

Huyer, Adriana & Verney, Andrew 1975. Temperature, salinity and Sigma- t at Station 27 (47° 33' N, 52° 35' W), 1950-1959, Marine Environment Data Service, Technical Report No. 3, Dept. of Environment, Ottawa, Canada.

Hyndman, R. D. and Cochrane, N. A. 1971. Electrical conductivity structure by geomagnetic induction at the continental margin of Atlantic Canada, Geophys. J.R. astr. Soc., 25, 425-446.

Karson, J. and Dewey, J. F. 1978. Coastal complex, western Newfoundland: An early Ordovician ocean fracture zone, Geol. Soc. Amer. Bull., 89, 1037-1049.

Keen, C. E. and Barrett, D. L. 1981. Thinned and subsided

continental crust on the rifted margin of Eastern Canada: Crustal structure, thermal evolution and subsidence history, Geophys. J.R. astr. Soc., 65, 443-465.

Kurtz, R. D. 1973. A magnetotelluric investigation of eastern Canada. Ph.D. Thesis, University of Toronto.

Kurtz, R. D. and Garland, G. D. 1976. Magnetotelluric measurements in eastern Canada, Geophys. J. R. astr. Soc., 45, 321-347.

Lahiri, B. N. and Price, A. T. 1939. Electromagnetic induction in non-uniform conductors, and the determination of the conductivity of the earth from terrestrial magnetic variations, Phil. Trans. Roy. Soc. (London) Ser. A, 237, 509-540.

Law, L. K. and Riddihough, R. P. 1971. A geographical relationship between geomagnetic variation anomalies and tectonics, Can. J. Earth Sci., 8, 1094-1106.

Lines, L. R. and Jones, F. W. 1973. The perturbation of alternating geomagnetic fields by three-dimensional island structures, Geophys. J. R. astr. Soc., 32, 133-154.

McKerrow, W. S. and Cocks, L. R. M. 1978. A lower Palezoic

trench-fill sequence, New World Island, Newfoundland, Geol. Soc. Amer. Bull., 89, 1121-1132.

Nienaber, W., Dosso, H. W. and Law, L. K. 1977a. Studies of electromagnetic induction for island-continent ocean channels with applications to Vancouver Island, Acta. Geodact., Geophys. et Monanist. Acad. Sci. Hung. Tomas, 12, 187-190.

Nienaber, W., Dosso, H. W., Law, L. K., Jones, F. W. and Ramaswamy, V. 1976. An analogue model study of electromagnetic induction for island- continent ocean channels, Phys. Earth Planet. Int., 13, 169-183.

Nienaber, W., Dosso, H. W., Law, L. K., Jones, F. W. and Ramaswamy, V. 1977b. An analogue model study of electromagnetic induction for island-continent ocean channels for H-polarization, Phys. Earth Planet. Int., 15, 69-76.

Nienaber, W., Dosso, H. W., Law, L. K., Jones, F. W. and Ramaswamy, V. 1979. An analogue model study of electromagnetic induction in the Vancouver Island region, J. Geomag. Geoelectr., 31, 115-132.

Nienaber, W., Dosso, H. W. & Hutton, V. R. S. 1981. Electromagnetic in the British Isles region: Analogue

model and field station results, Phys. Earth Planet. Int., 27, 122-132.

Ogunade, S. O. and Dosso, H. W. 1977. Subsurface electromagnetic response of a conducting sphere embedded in the lower layer of a two-layer earth, Acta. Geodact., Geophys. et Montanist. Acad. Sci. Hung. Tomas, 12, 311-314.

Ogunade, S. O., Ramaswamy, V. and Dosso, H. W. 1974. Electromagnetic response of a conducting sphere buried in a conducting earth, J. Geomag. Geoelectr., 26, 417-427.

Parkinson, W. D. 1959. Direction of rapid geomagnetic fluctuations, Geophys. J.R. astr. Soc., 2, 1-14.

Parkinson, W. D. 1964. Conductivity anomalies in Australia and the ocean effect, J. Geomag. Geoelectr., 15, 222-226.

Price, A. T. 1950. Electromagnetic induction in a semi-infinite conductor with a plane boundary, Quart. J. Mech. Appl. Math., 3, 385-410.

Price, A. T. 1964. A note on the interpretation of magnetic variations and mangetotelluric data, J. Geomag.

Geoelectr., 15, 241-248.

Ramaswamy, V. and Dosso, H. W. 1977. The response of a conducting cylinder to the inducing fields of various sources, J. Geomag. Geoelectr., 29, 181-189.

Rikitake, Tsuneji 1973. Global electric conductivity of the earth, Phys. Earth Planet. Int., 7, 245-250.

Rikitake, Tsuneji and Honkura, Yoshimori 1973. Recent Japanese studies on conductivity anomalies, Phys. Earth Planet. Int., 7, 203-212.

Roden, Robert B. 1963. The effect of an ocean on magnetic diurnal variations, Geophys. J. R. astr. Soc., 8, 375-388.

Schmucker, Ulrich 1970. Anomalies of geomagnetic variations in southwestern United States, Bull. Scripps Inst. Oceanog., 13, University of California Press.

Schuster, A. 1889. The diurnal variation of terrestrial magnetism, Phil. Trans. Roy. Soc. (London) Ser. A, 180, 467-518.

Sheridan, Robert E. and Drake, Charles L. 1968. Seaward extension of Canadian Appalachians, Can J. Earth Sci., 5, 337-373.

Srivastava, S. P. 1971. Diurnal variation of the total magnetic field along the east coast of Canada, Earth Planet. Sci. Letters, 10, 423-429.

Srivastava, S. P. and Folinsbee, R. A. 1975. Measurement of variations in the total geomagnetic field at sea off Nova Scotia, Can. J. Earth Sci., 12, 227-236.

Srivastava, S. P. and White, A. 1971. Inland, coastal, and offshore magnetotelluric measurements in eastern Canada, Can. J. Earth Sci., 8, 204-216.

Summers, D. M. 1971. Electromagnetic induction in a N-layered conducting half-space, M.Sc. Thesis, University of Victoria, Victoria, British Columbia

Weaver, J. T. 1963. The electromagnetic field within a discontinuous conductor with reference to geomagnetic micropulsations near a coastline, Can. J. Phys., 41, 484-495.

Weaver, J. T. 1973. Induction in a layered plane earth by uniform and non-uniform source fields, Phys. Earth Planet. Int., 7, 266-281.

Weaver, John T. 1979. Electromagnetic induction in a thin sheet conductivity anomalies at the surface of the

earth, Proc. IEEE, 67, 1044-1050.

Weaver, J. T. and Brewitt-Taylor, C. R. 1978. Improved boundary conditions for the numerical solution of E-polarization problems in geomagnetic induction, Geophys. J.R. astr. Soc., 54, 309-317.

Weidelt, P. 1975. Electromagnetic induction in three-dimensional structures, J. Geophys., 41, 85-109.

Wiese, H. 1962. Geomagnetische Tiefentellurik Teil II: Die Streichrichtung der Untergrundstrukturen des elektrischen Widerstandes, erschlossen aus geomagnetischen Variationen, Geofis. Pura Appl., 52, 82-103.

Wright, J. A. and Cochrane, N. A. 1980. Geomagnetic sounding of an ancient plate margin in the Canadian Appalachians, J. Geomag. Geoelectr., 32, Suppl I, SI 133- SI 140.

Zhdanov, M. S., Golubev, N. G., Spichak, V. V. and Varentsov, Im. M. 1982. The construction of effective methods for electromagnetic modelling, Geophys. J. R. astr. Soc., 68, 598-607.

APPENDIX A

COMPARISON OF TWO-DIMENSIONAL NUMERICAL MODELS:
1) OCEAN AND SEDIMENT LAYERS, AND
2) A SINGLE LAYER OF EQUIVALENT CONDUCTANCE

The region of ocean surrounding Newfoundland has highly conductive sediments beneath it. Since there are a limited number of materials with the proper conductivity available for use in an analogue model, it was proposed to replace the two conductive layers by a single layer of the same conductance. To examine the validity, two-dimensional numerical model calculations were done.

The computer program used was written by C.R. Brewitt-Taylor(1976). The program is based on a finite difference method described by Brewitt-Taylor and Weaver(1976) and Weaver and Brewitt-Taylor(1978).

A.1 Calculations and Results

The two-dimensional models are simple approximations to a cross-section of the area of interest. The models

represent the conductivity structure in the y-z plane with the z-direction representing increasing depth. A shallow layer representing the ocean over the continental shelf and a deep ocean are present in both models. Two periods (100s and 1000s) were tested. The results for the two perpendicular polarizations were calculated. For the polarization with the inducing electric field perpendicular to the coastline, the only spatial varying field component at the surface was E_y (the electric field component perpendicular to the coastline). For the two periods studied, only the magnitude of this component at the land-sea interface was different for the two models. The results for this polarization are not shown. The results for the polarization with the inducing electric field parallel to the coastine are shown in Figs. A.2.1 - A.2.4. These figures show the magnitude of the field components B_y, B_z, and E_x and their respective phase Φ_y, Φ_z, and Ψ_x at the surface of each model. These figures show little difference in the surface fields for the two models for periods of 100s and 1000s.

A.2 Conclusions

For the field component E_y the size of the electric field probe used in the model measurements will average the electric field over the land-sea interfaces. Therefore this field component discrepancy at the interfaces can be ignored.

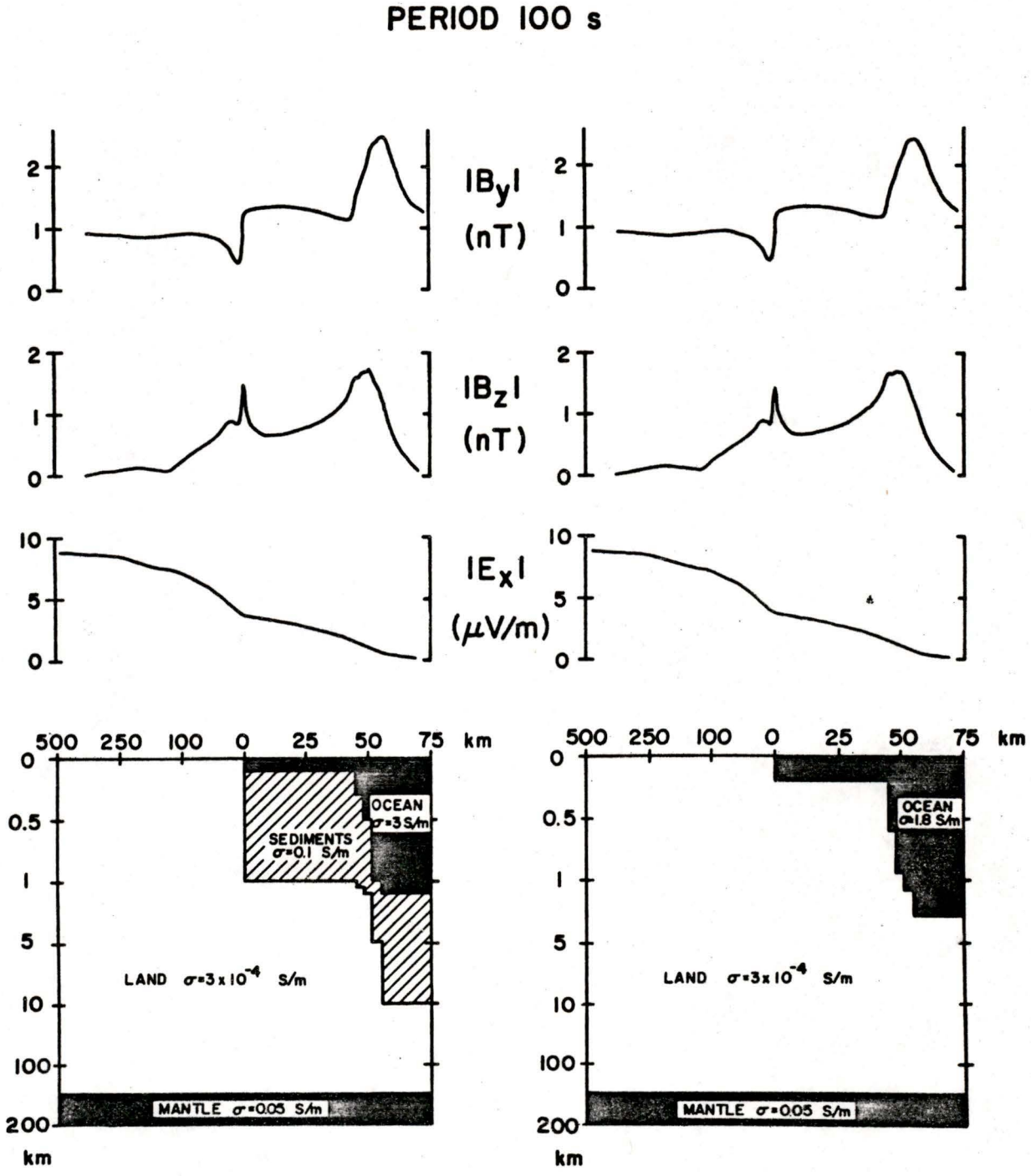

FIGURE A.2.1 Magnitudes of the field components of the two numerical models for a period of 100s with the inducing electric field parallel to the coastline.

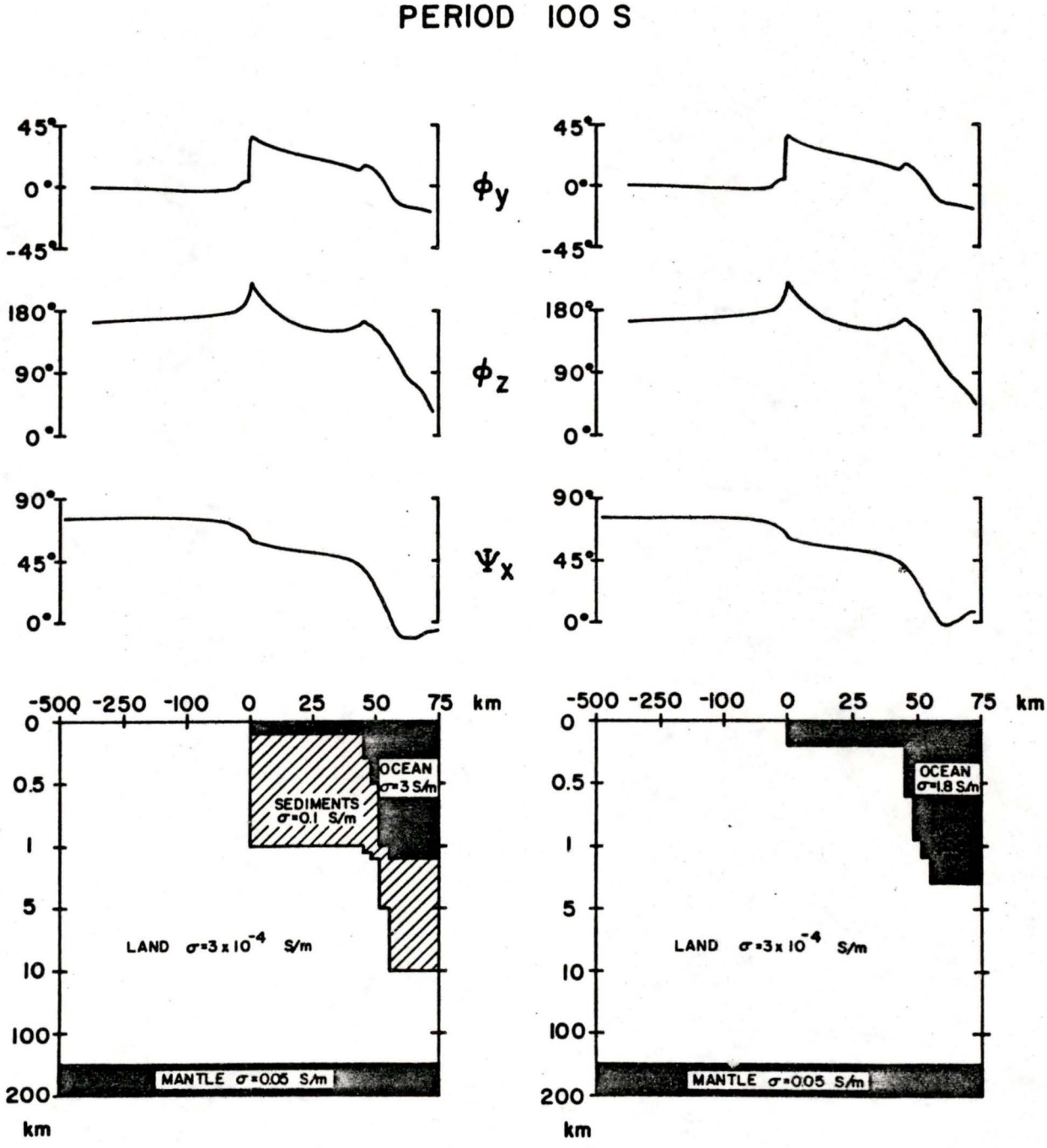

FIGURE A.2.2 Phase of the field components of the two numerical models for a period of 100s with the inducing electric field parallel to the coastline.

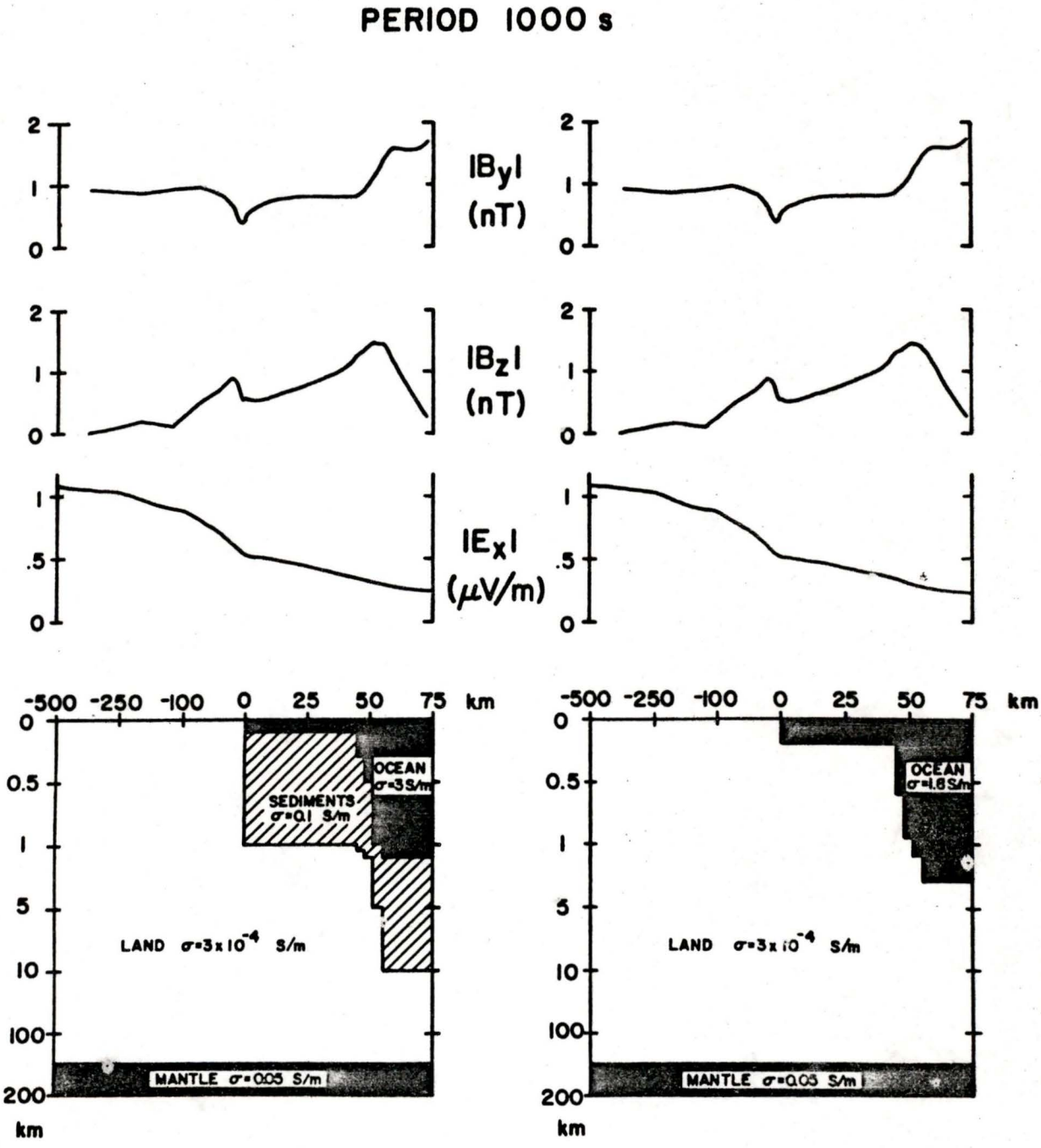

FIGURE A.2.3 Magnitudes of the field components of the two numerical models for a period of 1000s with the inducing electric field parallel to the coastline.

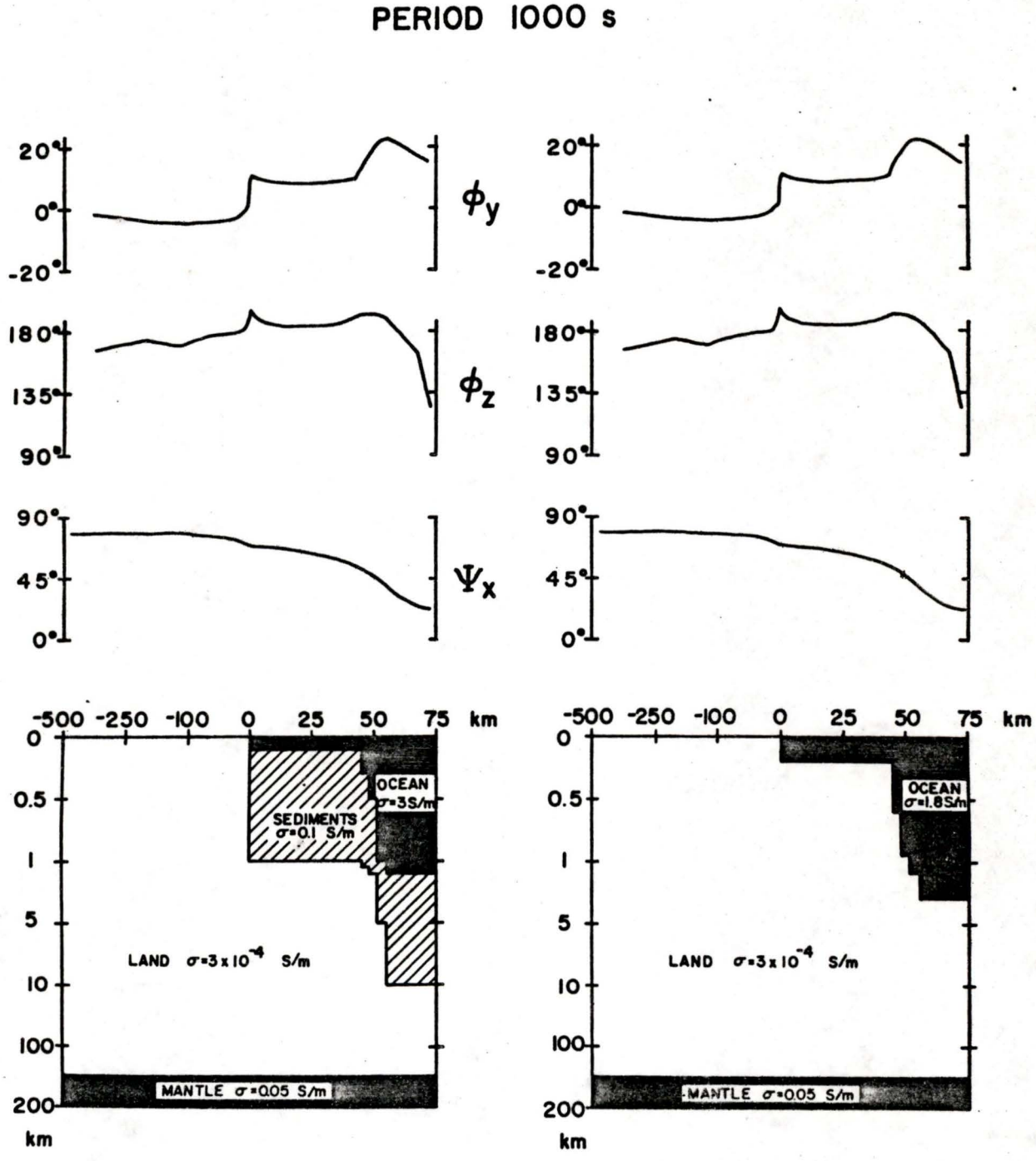

FIGURE A.2.4 Phases of the field components of the two numerical models for a period of 1000s with the inducing electric field parallel to the coastline.

There is good agreement between the models for all other field components. The results from the numerical models show that the replacement of a ocean and sediment layers with a single layer of equivalent conductance is permitted for the periods studied in this thesis.

APPENDIX B

CALCULATION OF MODEL GEOMAGNETIC MANTLE DEPTH

B.1 Introduction

Magnetotelluric measurements on the eastern coast of Canada by several authors (including Hyndman and Cochrane, 1971; Bailey et al., 1974; Cochrane and Hyndman, 1974; Kurtz and Garland, 1976) have shown that a deep highly conductive layer (geomagnetic mantle) must be present in the Newfoundland region. A graphite plate 1.5cm thick was used to simulate this layer in our laboratory analogue model. The conductivity that the graphite plate represented in the geophysical system was greater than the conductivity of the geomagnetic mantle. Therefore it was necessary to calculate the depth of the graphite plate in the model to simulate adequately the effect of the mantle.

Since the depth of the graphite plate representing the geomagnetic mantle depends on frequency, and the depth and conductivity of the mantle are not exactly determined, a

simple one-dimensional layered mathematical model is used to determine the required depth of the plate in the analogue model. The inducing field used in the mathematical model is a normal incident plane wave. The solution for a plane wave incident at an arbitrary angle for a layered earth has been discussed by Kurtz(1973), Dosso(1966), and Summers(1971). Weaver(1973) has solved the layered earth problem for uniform and non-uniform source fields.

B.2 One-dimensional Models

The solution for a normal incident electromagnetic wave on a two- or a three- layer model is well known. The wave equation for fields in conductors are derived from Maxwell's equations. (See Section 2.1.) The one-dimensional wave equation for a horizontal electric field (for example, $\underline{E} = E\,\underline{n}$) travelling in the z-direction is

$$\frac{\partial^2 \underline{E}}{\partial z^2} = -\mu\omega(\omega\epsilon+i\sigma)\,\underline{E} \quad . \qquad \text{(B.2.1)}$$

For geophysical problems ($\sigma >> \omega\epsilon$) the wave equation reduces to

$$\frac{\partial^2 \underline{E}}{\partial z^2} = -i\mu\omega\sigma\, \underline{E} = -k^2\, \underline{E} \qquad \text{(B.2.2)}$$

where

$$k = (1+i)\sqrt{\frac{\mu\omega\sigma}{2}} \quad . \qquad \text{(B.2.3)}$$

The general solution to the differential equation is

$$\underline{E} = E\, \underline{n} = (A\, e^{ikz} + B\, e^{-ikz})\, e^{-i\omega t}\, \underline{n}. \qquad \text{(B.2.4)}$$

The constants A and B are determined by the boundary conditions. The electric field in each layer of the two- and three-layer models can be written as shown in Fig. B.2.1.

According to the boundary conditions the horizontal electric field and its first derivative in the z-direction must be continuous across the layer boundaries. In the bottom layer of each model the electric field approaches zero as z approaches infinity.

B.3 Two-layer Case

Since the horizontal electric field and its derivative with respect to z must be continuous at z=h

$$\begin{aligned} A\, e^{ik_1 h} + B\, e^{-ik_1 h} &= C\, e^{ik_2 h} \quad , \\ k_1 A\, e^{ik_1 h} - k_1 B\, e^{-ik_1 h} &= k_2 C\, e^{ik_2 h} \quad . \end{aligned} \qquad \text{(B.3.1)}$$

TWO-LAYER MODEL

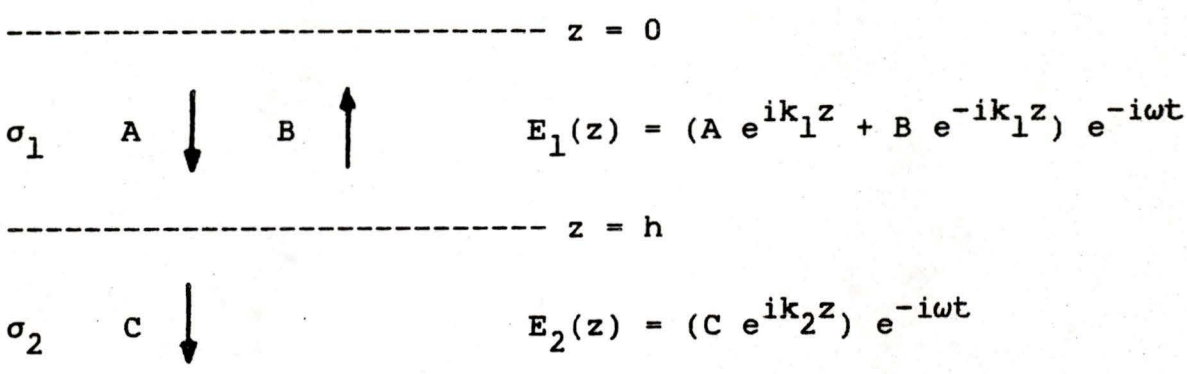

THREE-LAYER MODEL

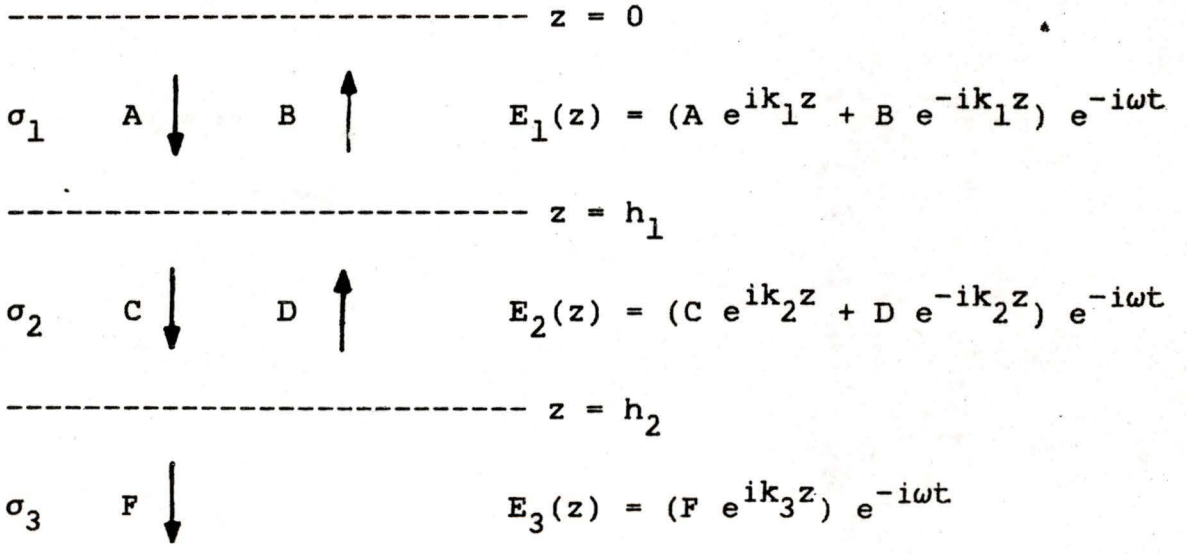

FIGURE B.2.1 Electric field in each layer of the two-layer and three-layer models

If we let the incoming wave in the first layer be of unit strength, then

$$A = 1$$

and

$$B = \left(\frac{(k_1-k_2)}{(k_1+k_2)}\right) e^{i2k_1h} \quad . \tag{B.3.2}$$

The electric field at the surface (z=0) is

$$E_1(0) = (A+B)\, e^{-i\omega t} = \left[1 + \left(\frac{(k_1-k_2)}{(k_1+k_2)}\right) e^{i2k_1h}\right] e^{-i\omega t} \quad . \tag{B.3.3}$$

B.4 Three-layer Case

The electric field and its derivative in the z-direction must be continuous. Therefor

$$\begin{aligned}
A\, e^{ik_1h_1} + B\, e^{-ik_1h_1} &= C\, e^{ik_2h_1} + D\, e^{-ik_2h_1} \quad , \\
k_1 A\, e^{ik_1h_1} - k_1 B\, e^{-ik_1h_1} &= k_2 C\, e^{ik_2h_1} - k_2 D\, e^{-ik_2h_1} \quad , \\
C\, e^{ik_2h_2} + D\, e^{-ik_2h_2} &= F\, e^{ik_3h_2} \quad , \\
k_2 C\, e^{ik_2h_2} - k_2 D\, e^{-ik_2h_2} &= k_3 F\, e^{ik_3h_2} \quad .
\end{aligned} \tag{B.4.1}$$

Solving the above equations for the electric field at the surface and allowing the incoming inducing field to be of unit strength,

$$A = 1$$

and

(B.4.2)

$$B = \left[\frac{(k_2+k_3)(k_1-k_2)e^{ik_2h_1} + (k_1+k_2)(k_2-k_3)e^{ik_2(2h_2-h_1)}}{(k_2+k_3)(k_1+k_2)e^{ik_2h_1} + (k_1-k_2)(k_2-k_3)e^{ik_2(2h_2-h_1)}}\right]e^{i2k_1h_1}.$$

The electric field at the surface (z=0) is

$$E_1(0) = (A+B)\,e^{-i\omega t} = \left[1 + \left(\frac{(k_2+k_3)(k_1-k_2)e^{ik_2h_1}+(k_1+k_2)(k_2-k_3)e^{ik_2(2h_2-h_1)}}{(k_2+k_3)(k_1+k_2)e^{ik_2h_1}+(k_1-k_2)(k_2-k_3)e^{ik_2(2h_2-h_1)}}\right) e^{i2k_1h_1}\right] e^{-i\omega t} \qquad (B.4.3)$$

B.5 Mantle Depth Calculation

To determine the required depth of the graphite plate, the electric field at the surface for the two- and three-layer model were compared. The geophysical case was represented by the two-layer model and the laboratory case, by the three-layer model.

The magnetotelluric results of Kurtz(1973) for the Deer Lake station in Newfoundland were used for the geophysical mantle parameters. The mantle conductivity and depth were .05S/m and 144km, respectively. The layer represented by the graphite plate had a conductivity of 1.8S/m and a thickness of 15km. The depth of this layer was the parameter desired. The parameters for the two models used in the computer program are shown in Table B.5.1. The geophysical depth of

TWO - LAYER MODEL

$\sigma_1 = 3.0 \times 10^{-4}$ S/m $h = 144$ km

$\sigma_2 = 0.05$ S/m

THREE - LAYER MODEL

$\sigma_1 = 3.0 \times 10^{-4}$ S/m $h_1 = ?$

$\sigma_2 = 1.8$ S/m $h_2 = h_1 + 15$ km

$\sigma_3 = 3.0 \times 10^{-4}$ S/m

TABLE B.5.1 Parameters used in the computer program for the calculation of the graphite plate depth

the graphite plate layer(h_1) was found using the bisection method. This method determined the value of h_1 in the three-layer model when the electric field at the surface in the two models are equal, that is, (B.3.3) equals (B.4.3). The computer program used is given in Section B.6.

For periods of 100s, 500s, and 1000s, the depth of the graphite plate was calculated to be 151.2km, 172.5km, and 188.3km, respectively. For the periods studied in this thesis, a 175km depth was taken as an appropiate value.

B.6 Program Listing

```
C                                                                       0010
C PROGRAMS TO CALCULATE DEPTH OF GRAPHITE PLATE BY FINDING WHEN EQ. B.3.3   0020
C EQUALS B.4.3, USING THE BISECTION METHOD                              0030
C SUBROUTINE BISECT FROM CONTE AND DE BOOR, ELEMENTARY NUMERICAL        0040
C ANALYSIS: AN ALGORITHMIC APPROACH, MCGRAW-HILL BOOK CO., 1972,        0050
C PAGE 35.                                                              0060
C                                                                       0070
      EXTERNAL FF                                                       0080
C                                                                       0090
C FUNCTION FF CONTAINS THE EQUATION ( B.3.3-B.4.3 )                     0100
C SET UPPER AND LOWER BOUNDS (A AND B) FOR THE PLATE'S DEPTH IN METRES  0110
C                                                                       0120
      A=1.                                                              0130
      B=500000.                                                         0140
      CALL BISECT(FF,A,B,1.E-6,IFLAG)                                   0150
      IF(IFLAG.GT.1) STOP                                               0160
      XI=(A+B)/2000.                                                    0170
      ERROR=ABS(A-B)/2000.                                              0180
      WRITE(8,600) XI,ERROR                                             0190
600   FORMAT('AT T=500S THE MANTLE DEPTH (KM) IS ',E15.7,' PLUS/MINUS ' 0200
     &,E15.7)                                                           0210
      STOP                                                              0220
      END                                                               0230
C                                                                       0240
C                                                                       0250
C                                                                       0260
      SUBROUTINE BISECT(F,A,B,XTOL,IFLAG)                               0270
      IFLAG=0                                                           0280
      N=-1                                                              0290
      FA=F(A)                                                           0300
C CHECK FOR SIGN CHANGE                                                 0310
      IF(FA*F(B).LE.0.) GOTO 5                                          0320
      IFLAG=2                                                           0330
      WRITE(8,601) A,B                                                  0340
601   FORMAT(' F(X) IS OF SAME SIGN AT THE TWO ENDPOINTS                0350
     *   ',2E15.7)                                                      0360
      RETURN                                                            0370
    5 ERROR=ABS(B-A)                                                    0380
    6 ERROR=ERROR/2.                                                    0390
C CHECK FOR SUFFICIENTLY SMALL INTERVAL                                 0400
      IF(ERROR.LE.XTOL)  RETURN                                         0410
      XM=(A+B)/2.                                                       0420
C CHECK FOR UNREASONABLE ERROR REQUIREMENT                              0430
      IF(XM+ERROR.EQ.XM)  GOTO 20                                       0440
      FM=F(XM)                                                          0450
C TEMPORARY PRINTOUT                                                    0460
      N=N+1                                                             0470
      WRITE(8,606) N,A,XM,B,FA,FM                                       0480
606   FORMAT(I3,' X-VALUES',3F15.7,/,3X,' F-VALUES',2E15.7,/)           0490
C CHANGE TO NEW INTERVAL                                                0500
      IF(FA*FM.LE.0.) GOTO 9                                            0510
      A=XM                                                              0520
      FA=FM                                                             0530
      GOTO 6                                                            0540
    9 B=XM                                                              0550
      GOTO 6                                                            0560
   20 IFLAG=1                                                           0570
      RETURN                                                            0580
      END                                                               0590
```

```
C                                                                       0610
C                                                                       0620
      FUNCTION FF(X)                                                    0630
      DOUBLE PRECISION S,K,T,S1M1,S2M1,S1M2,S2M2,S3M2,D,DD              0640
      COMPLEX*16 K1M1,K2M1,K1M2,K2M2,K3M2,MOD1,MOD2,MOD,SS              0650
C                                                                       0660
C SET PARAMETERS FOR TWO-LAYER MODEL (M1) AND THREE-LAYER               0670
C MODEL (M2)                                                            0680
C  PARAMETERS ARE:                                                      0690
C     CONDUCTIVITY OF ITH LAYER FOR JTH MODEL     SIMJ                  0700
C     DEPTH OF SECOND LAYER FOR M1                D                     0710
C     DEPTH OF SECOND LAYER FOR M2                X                     0720
C     THICKNESS OF SECOND LAYER FOR M2            DD                    0730
C     PERIOD OF EM WAVE                           T                     0740
C     WAVENUMBER OF ITH LAYER JTH MODEL           KIMJ                  0750
C                                                                       0760
      S1M1=3.D-4                                                        0770
      S2M1=.05                                                          0780
      D=144000.                                                         0790
      S1M2=3.D-4                                                        0800
      S2M2=1.8                                                          0810
      S3M2=3.D-4                                                        0820
      DD=15000.                                                         0830
      T=500.                                                            0840
      K=4.*1.E-7*3.14159**2/T                                           0850
      S=DSQRT(K*S1M1)                                                   0860
      K1M1=DCMPLX(S,S)                                                  0870
      S=DSQRT(K*S2M1)                                                   0880
      K2M1=DCMPLX(S,S)                                                  0890
      S=DSQRT(K*S1M2)                                                   0900
      K1M2=DCMPLX(S,S)                                                  0910
      S=DSQRT(K*S2M2)                                                   0920
      K2M2=DCMPLX(S,S)                                                  0930
      S=DSQRT(K*S3M2)                                                   0940
      K3M2=DCMPLX(S,S)                                                  0950
C                                                                       0960
C SS IS I (SQRT (-1.))                                                  0970
C                                                                       0980
      SS=DCMPLX(0.D0,1.D0)                                              0990
C                                                                       1000
C CALCULATE ELECTRIC FIELD AT SURFACE FOR TWO-LAYER MODEL (EQ. 8.3.3)   1010
C                                                                       1020
      MOD1=(K1M1-K2M1)*CDEXP(SS*2.*K1M1*D)/(K1M1+K2M1)                  1030
C                                                                       1040
C CALCULATE ELECTRIC FIELD AT SURFACE FOR THREE-LAYER MODEL (EQ.8.4.3)  1050
C                                                                       1060
      MOD2=(K2M2+K3M2)*(K1M2-K2M2)*CDEXP(SS*K2M2*X)+(K1M2+K2M2)*(K2M2-K3
     &M2)*CDEXP(SS*K2M2*(X+2*DD))                                       1080
      MOD2=MOD2/((K2M2+K3M2)*(K1M2+K2M2)*CDEXP(SS*K2M2*X)+(K1M2-K2M2)*(K
     &2M2-K3M2)*CDEXP(SS*K2M2*(X+2.*DD)))                               1100
      MOD2=MOD2*CDEXP(SS*2.*K1M2*X)                                     1110
C                                                                       1120
C CALCULATE DIFFERENCE OF 8.3.3 AND 8.4.3                               1130
C                                                                       1140
      MOD=MOD2-MOD1                                                     1150
C                                                                       1160
C  COMPARE EITHER THE REAL PART OR MAGNITUDE OF THE DIFFERENCE OF THE   1170
C  ELECTRIC FIELD                                                       1180
C                                                                       1190
C     FF=DREAL(MOD)                                                     1200
      FF=CDABS(MOD2)-CDABS(MOD1)                                        1210
      WRITE(8,1000) MOD1,MOD2                                           1220
1000  FORMAT(2D15.6,10X,2D15.6)                                         1230
      RETURN                                                            1240
      END                                                               1250
```

APPENDIX C

MAGNETIC FIELD RESULTS FOR PERIODS OF 300s AND 900s

Contours of the three magnetic field components, B_y, B_x, and B_z, for a period of 300s are shown in Figs. C.1 - C.3. Figures C.4 - C.6 show the contours of the magnetic field components for a period of 900s.

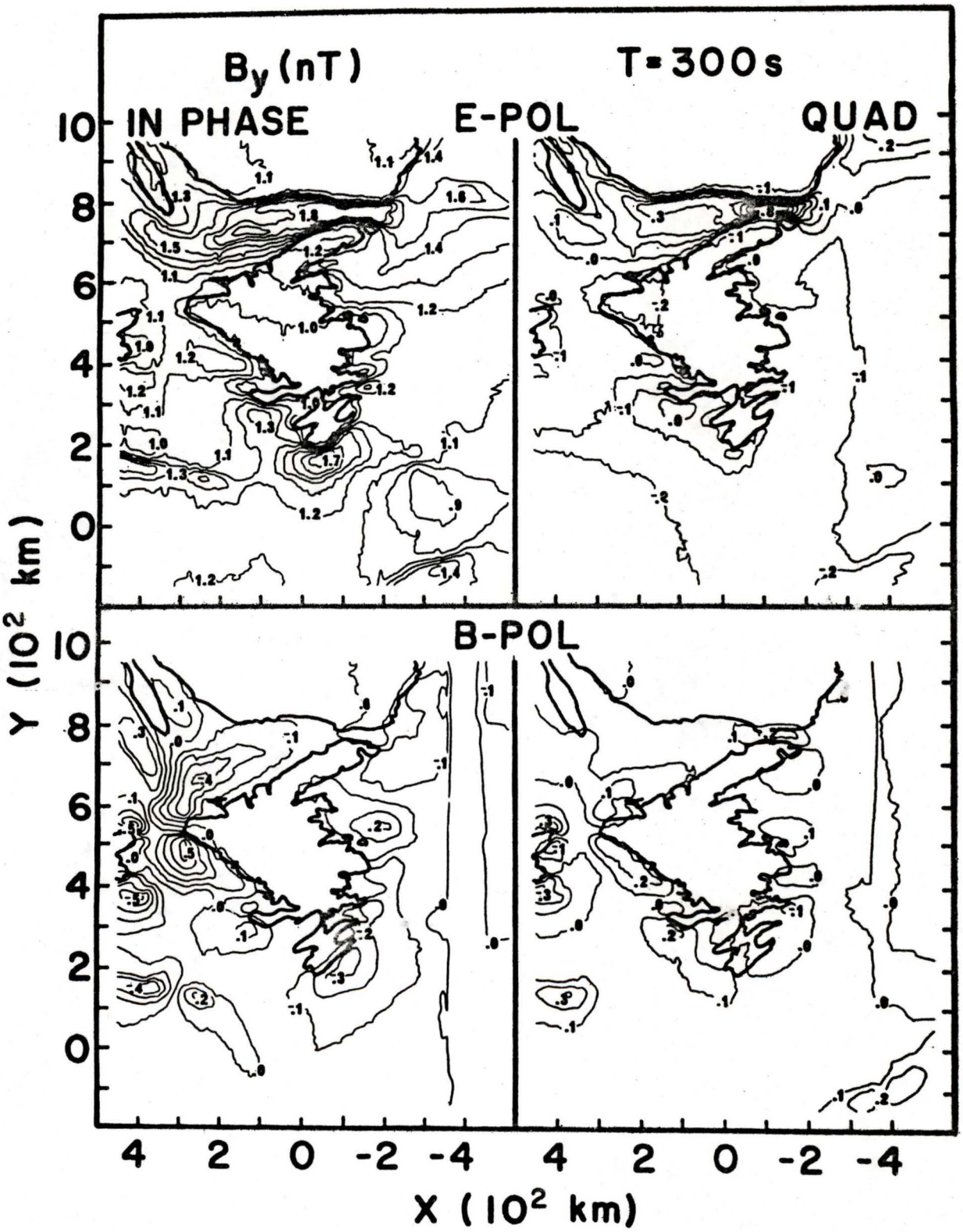

FIGURE C.1 Contours of the in phase and quadrature phase parts of B_y for a period of 300s and both polarizations.

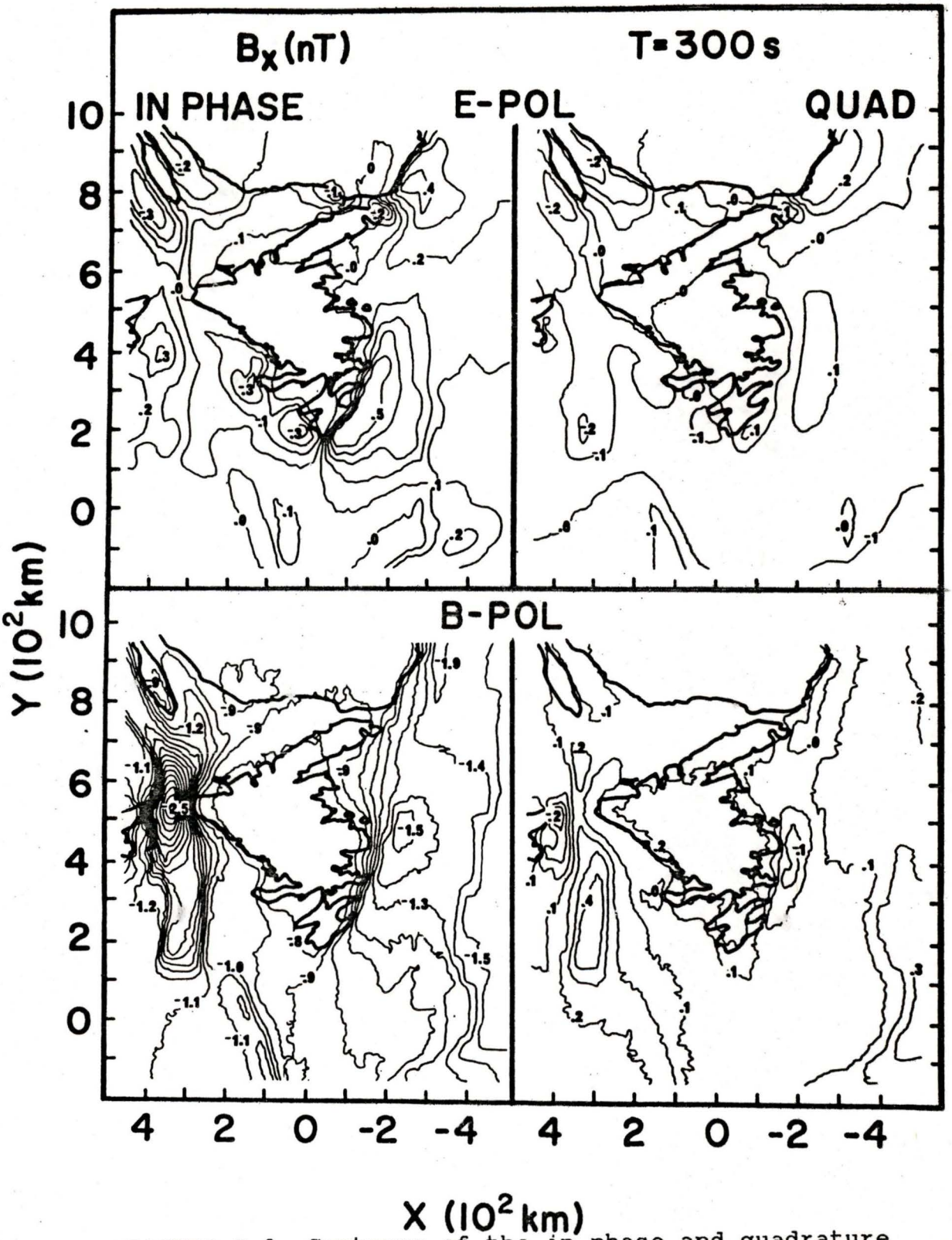

FIGURE C.2 Contours of the in phase and quadrature phase parts of B_x for a period of 300s and both polarizations.

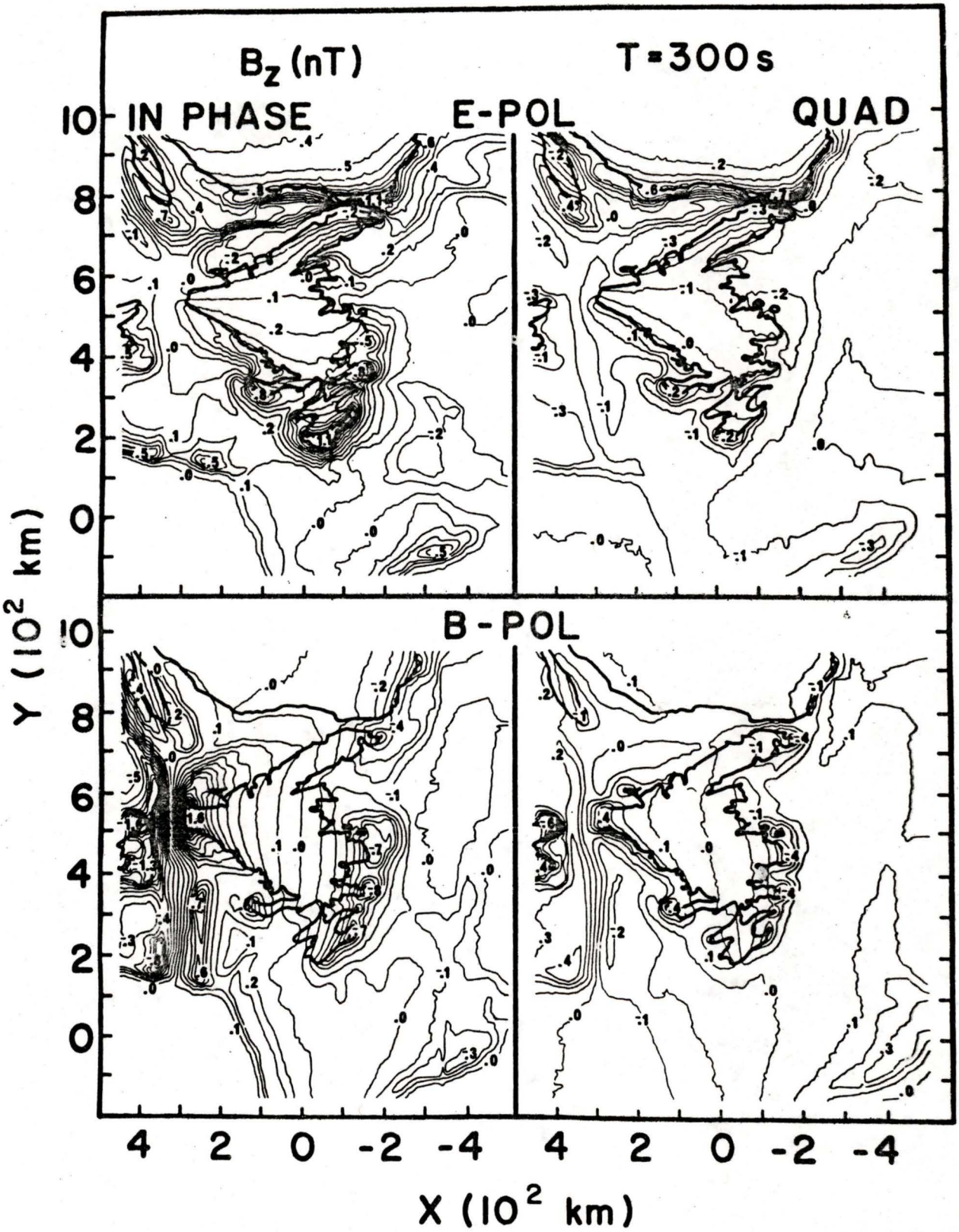

FIGURE C.3 Contours of the in phase and quadrature phase parts of B_z for a period of 300s and both polarizations.

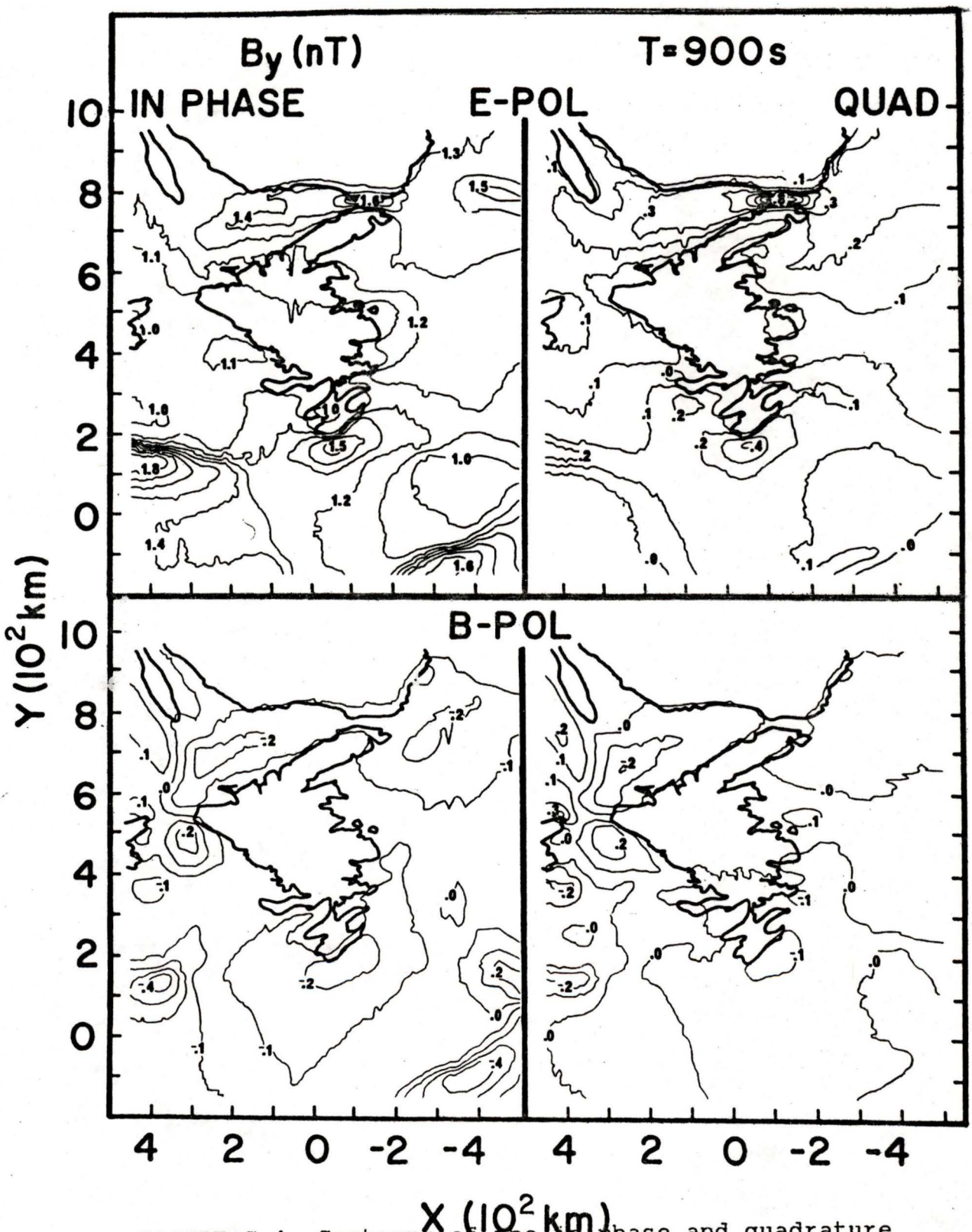

FIGURE C.4 Contours of the in phase and quadrature phase parts of B_y for a period of 900s and both polarizations.

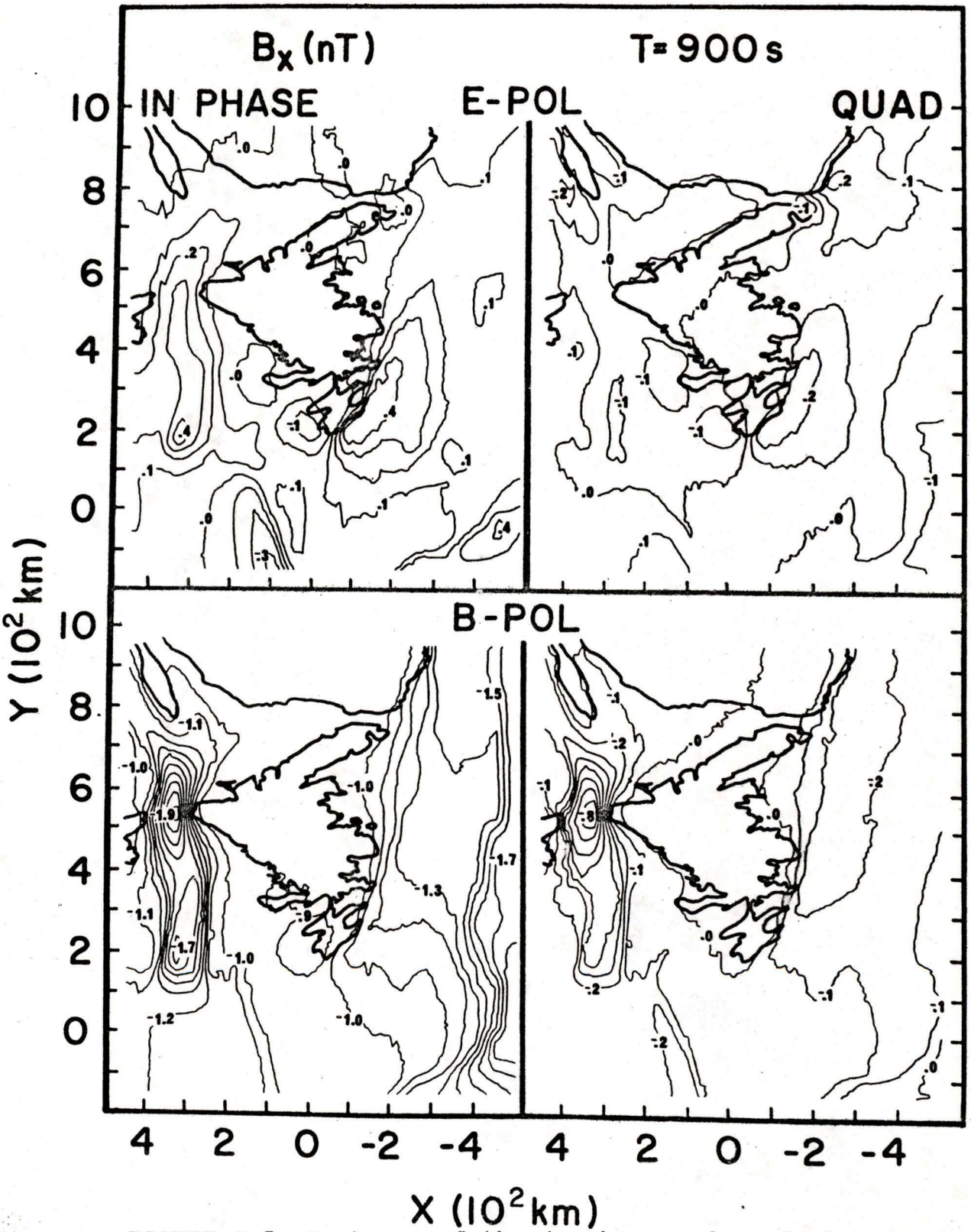

FIGURE C.5 Contours of the in phase and quadrature phase parts of B_x for a period of 900s and both polarizations.

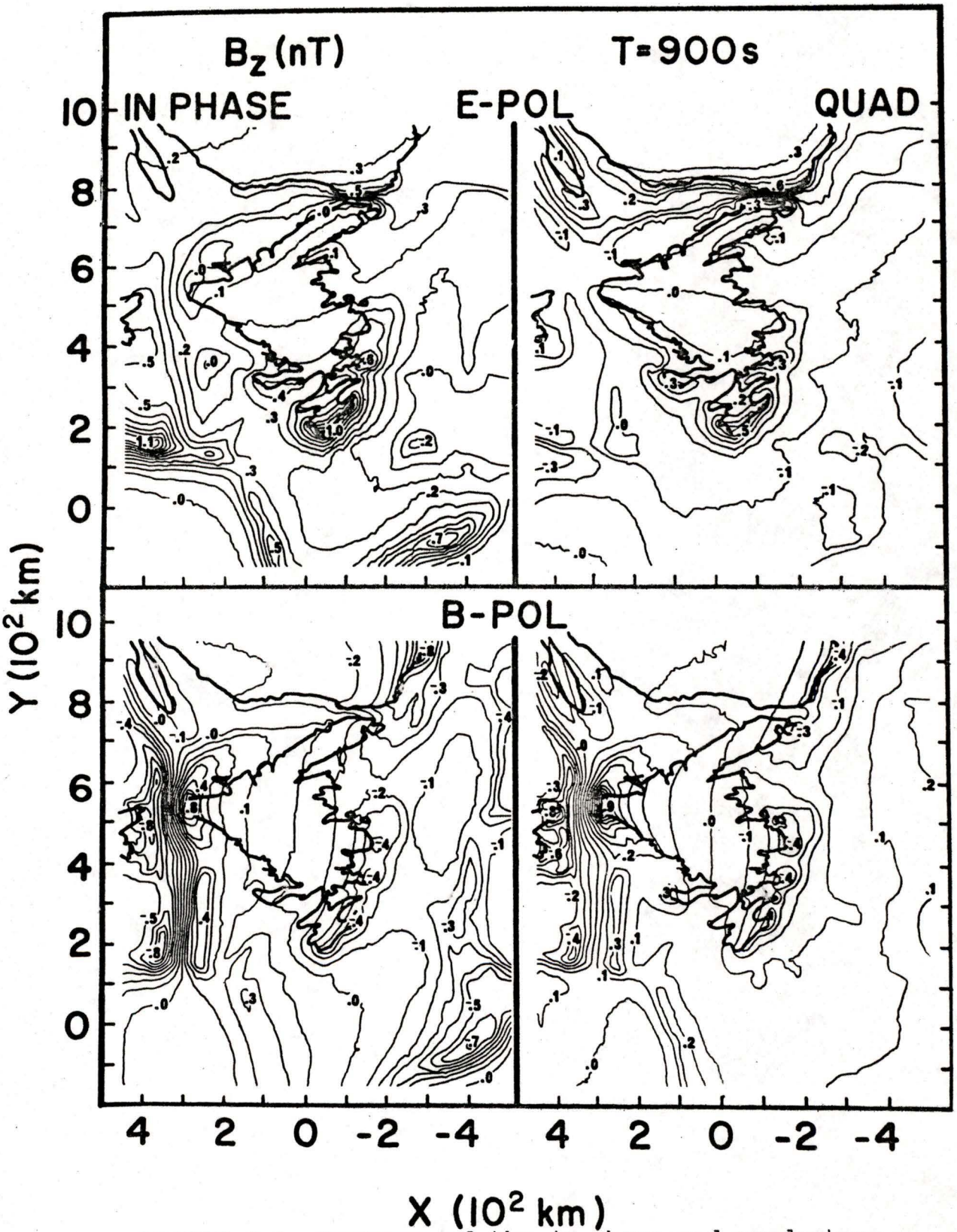

FIGURE C.6 Contours of the in phase and quadrature phase parts of B_z for a period of 900s and both polarizations.

APPENDIX D

INTER-STATION INDUCTION ARROWS FOR PERIODS OF 300s, 900s, AND 1800s

Inter-station induction arrows for periods of 300s, 900s, and 1800s are shown in Figs. D.1 - D.3.

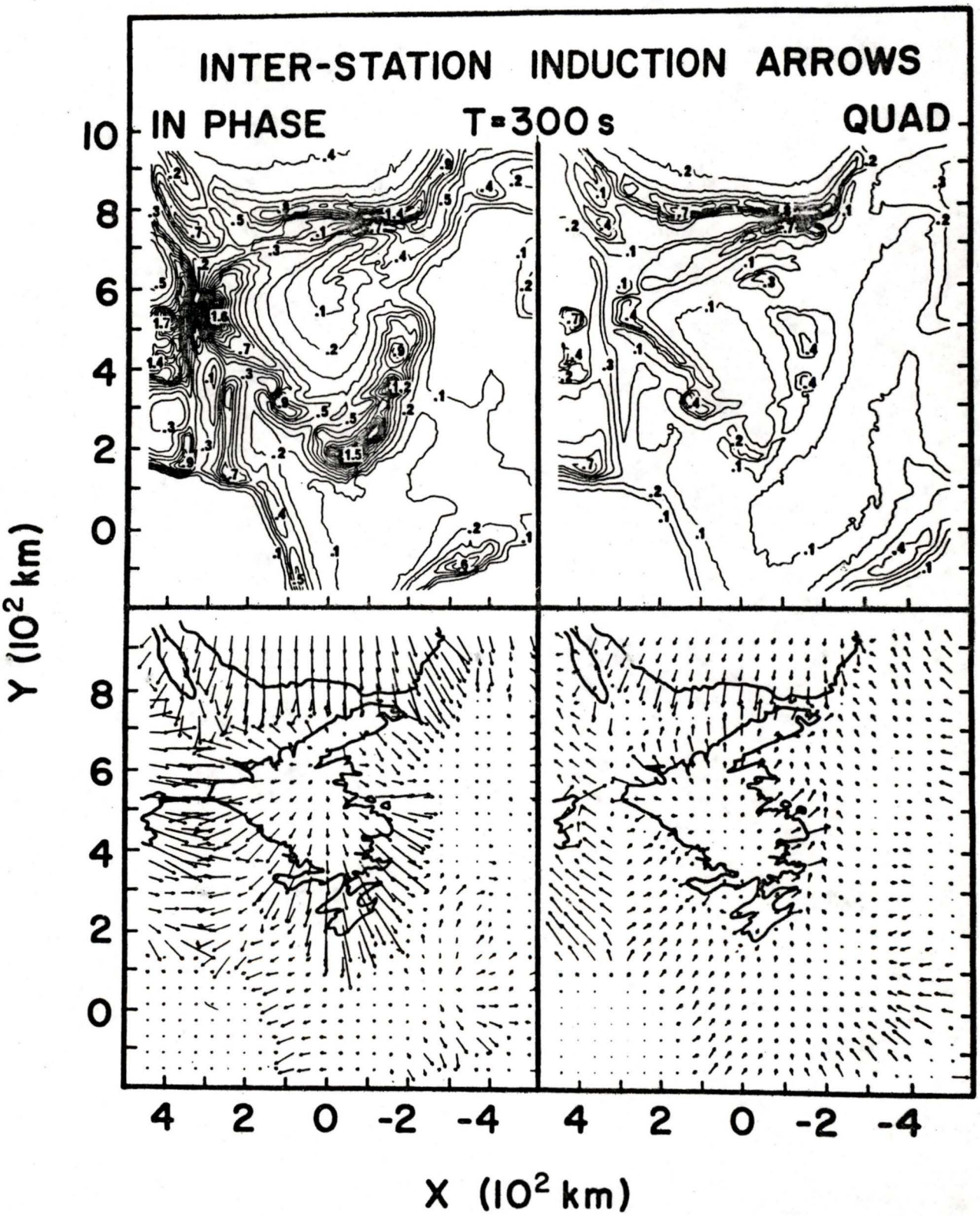

FIGURE D.1 Inter-station induction arrows for a period of 300s

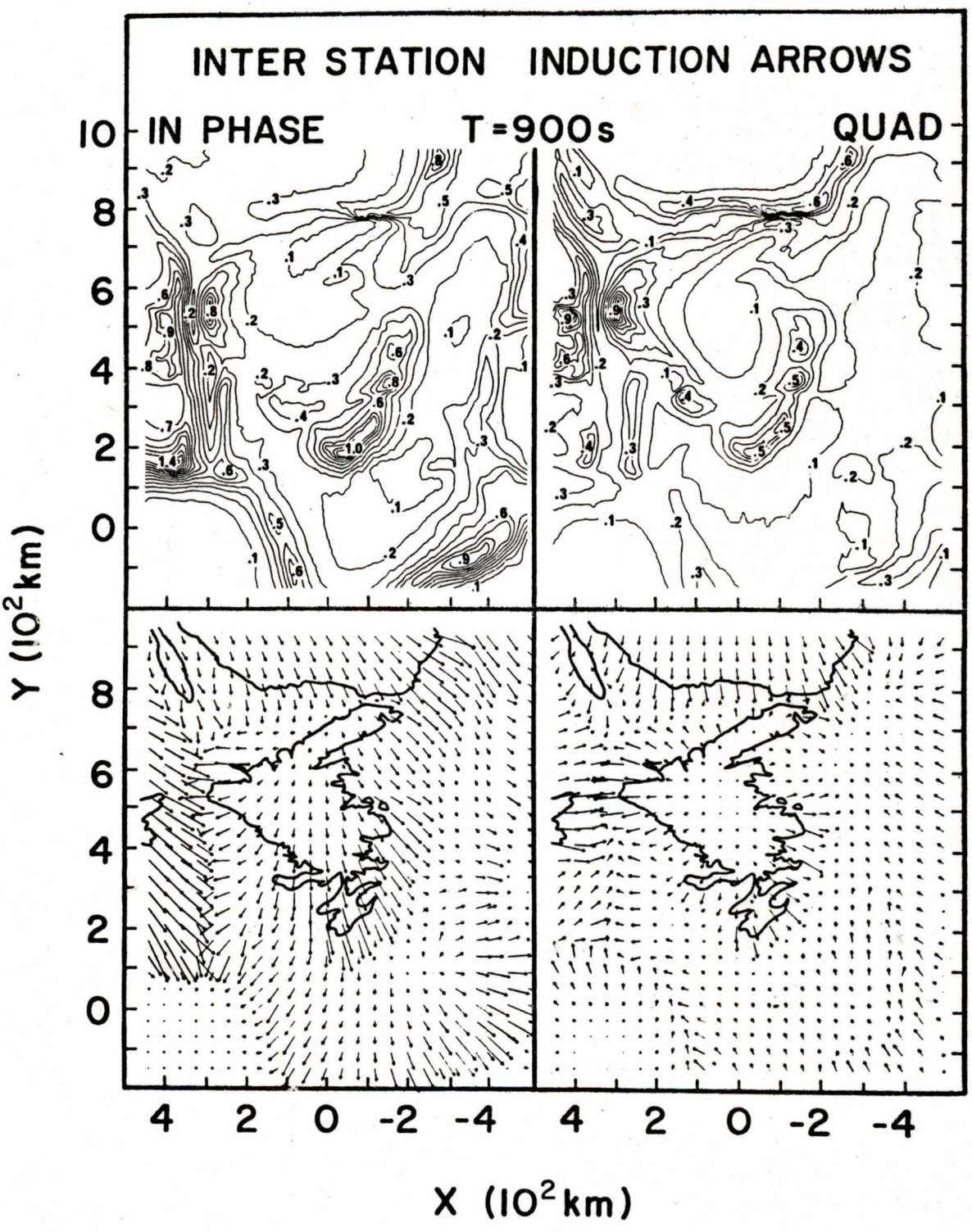

FIGURE D.2 Inter-station induction arrows for a period of 900s

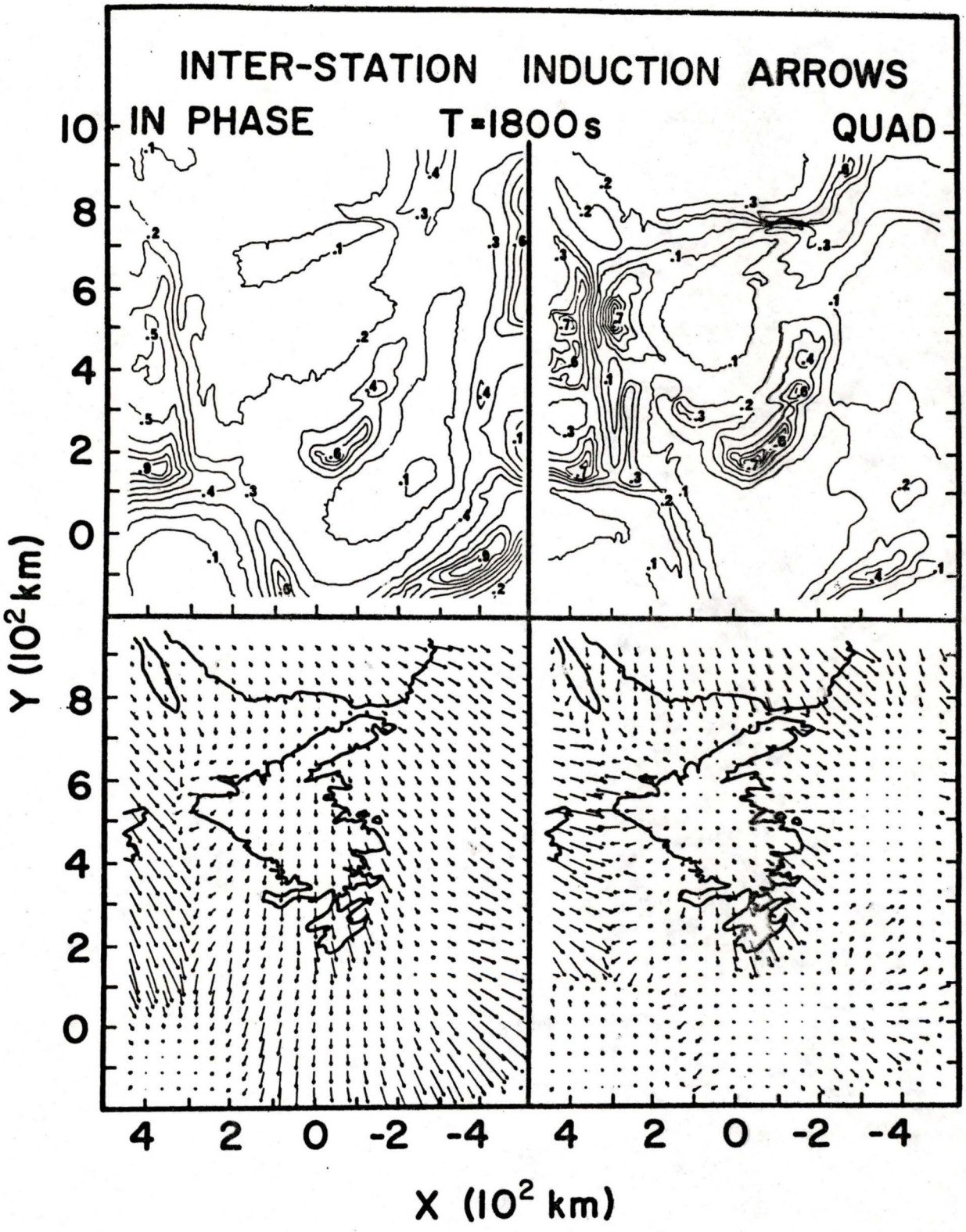

FIGURE D.3 Inter-station induction arrows for a period of 1800s

VITA

Surname: HEBERT Given Names: DAVID LAWRENCE

Place of Birth: Halifax, Nova Scotia

Date of Birth: 17 June, 1958

Educational Institutions Attended, with Dates of Entering and Leaving:

DALHOUSIE UNIVERSITY, HALIFAX, N.S.	1976 to 1980
UNIVERSITY OF VICTORIA, VICTORIA, B.C.	1980 to 1982

Degrees, Diplomas, Etc., Awarded, with Dates and Names of Institutions:

B. Sc. (Honours)	1980	Dalhousie Univeristy, Halifax

Honours and Awards:

Percy Bertram Jollota Scholarship	1977/78 and 1978/79
Burgess McKittrick Prize	1978
L. A. DeWolfe Memorial Scholarship	1979/80
University Medal (Physics)	1980
N. S. E. R. C. Postgraduate Scholarship	1980/81 and 1981/82

Papers Published:

Dave Hebert The frequency response of the horizontal magnetic field for a conducting channel, Geophys. J.R. astr. Soc. (in press)

Papers Presented:

Dave Hebert, H. W. Dosso, W. Nienaber, J. A. Wright An Elctromagnetic Analogue Model of the Newfoundland Region, American Geophysical Union, Fall Meeting, San Francisco, Dec. 1981.

PARTIAL COPYRIGHT LICENSE

I hereby grant the right to lend my thesis or dissertation (the title of which is shown below) to users of the University of Victoria, and to make single copies only for such users or in response to a request from the library of any other university, or similar institution, on its behalf or for one of its users. I further agree that permission for extentsive copying of this thesis for scholarly purposes may be granted by me or a member of the University designated by me. It is understood that copying or publication of this thesis for financial gain shall not be allowed without my written permission.

Title of Thesis/Dissertation:

AN ANALOGUE MODEL OF ELECTROMAGNETIC INDUCTION IN THE NEWFOUNDLAND REGION

Author: [redacted]

DAVID HEBERT

Date: August 5, 1982